Exploiting Structural Signal Information in Passive Emitter Localization

DISSERTATION

zur

Erlangung des Doktorgrades (Dr. rer. nat)

der

Mathematisch-Naturwissenschaftlichen Fakultät

der

Rheinischen Friedrich-Wilhelms-Universität Bonn

vorgelegt von

Dipl.-Inform. Christian Steffes

aus

Koblenz

Bonn, 2017

Angefertigt mit Genehmigung der Mathematisch-Naturwissenschaftlichen Fakultät
der Rheinischen Friedrich-Wilhelms-Universität Bonn

1. Gutachter: Priv.-Doz. Dr. Wolfgang Koch
2. Gutachter: Prof. Dr. Peter Martini

Tag der Promotion: 06.07.2017
Erscheinungsjahr: 2017

Abstract

The operational use of systems for passive geolocation of radio frequency emitters poses various challenges to single sensor systems or sensor networks depending on the measurement methods. Position estimation by means of direction finding systems often requires complex receiver and antenna technique. Time (Difference) of Arrival methods (TDOA, TOA) are based on measurements regarding the signal propagation duration and generally require broadband communication links to transmit raw signal data between spatially separated receivers of a sensor network. Such bandwidth requirements are particularly challenging for applications with moving sensor nodes. This issue is addressed in this thesis and techniques that use signal structure information of the considered signals are presented which allow a drastic reduction of the communication requirements.

The advantages of using knowledge of the signal structure for TDOA based emitter localization are shown using two exemplary applications. The first case example deals with the passive surveillance of the civil airspace (Air Traffic Management, ATM) using a stationary sensor network. State of the art airspace surveillance is mainly based on active radar systems (Primary Surveillance Radar, PSR), cooperative secondary radar systems (Secondary Surveillance Radar, SSR) and automatic position reports from the aircraft itself (Automatic Dependent Surveillance-Broadcast, ADS-B). SSR as well as ADS-B relies on aircrafts sending transponder signals at a center frequency of 1090 MHz. The reliability and accuracy of the position reports sent by aircrafts using ADS-B are limited and not sufficient to ensure safe airspace separation for example of two aircrafts landing on parallel runways. In the worst case, the data may even be altered with malicious intent. Using passive emitter localization and tracking based on multilateration (TDOA/hyperbolic localization), a precise situational awareness can be given which is independent of the content of the emitted transponder signals. The high concentration of sending targets and the high number of signals

require special signal processing and information fusion techniques to overcome the huge amount of data. It will be shown that a multilateration network that employs those techniques can be used to improve airspace security at reasonable costs.

For the second case, a concept is introduced which allows TDOA based emitter localization with only one moving observer platform. Conventional TDOA measurements are obtained using spatially distributed sensor nodes which capture an emitted signal at the same time. From those signals, the time difference of arrival is estimated. Under certain conditions, the exploitation of signal structure information allows to transfer the otherwise only spatial into a spatial and temporal measurement problem. This way, it is possible to obtain TDOA estimates over multiple measurement time steps using a single moving observer and to thus localize the emitter of the signals. The concept of direct position determination is applied to the single sensor signal structure TDOA scheme and techniques for direct single sensor TDOA are introduced.

The validity and performance of the presented methods is shown in theoretical analysis in terms of Cramér-Rao Lower Bounds, Monte-Carlo simulations and by evaluation of real data gained during field experiments.

Zusammenfassung

Der operationelle Einsatz von Systemen zur passiven Geolokalisierung von Funkemittern stellt je nach eingesetzten Messverfahren sehr unterschiedliche Anforderungen an Einzelsysteme oder Sensornetzwerke. Bei der Verwendung von Peilverfahren wird z.B. komplexe Empfänger- und Antennentechnik benötigt. Bei Time (Difference) of Arrival (TOA, TDOA) Methoden, die Messungen bezüglich der Signalausbreitungsdauer verwenden, wird in der Regel eine breitbandige Datenverbindung zwischen örtlich separierten Empfängern eines Sensornetzwerks benötigt. Nicht nur beim mobilen Einsatz solcher Systeme stellt eine derartige Bandbreite zur Übertragung von Signalrohdaten ein großes Problem dar. In der vorliegenden Arbeit werden daher Techniken hergeleitet, die, unter Ausnutzung von Vorwissen über die betrachteten Signale, eine erhebliche Reduktion der Kommunikationsanforderungen erlauben.

An zwei exemplarischen Anwendungen werden die Vorteile einer solchen Nutzung von Signalvorwissen bei der TDOA-basierten Emitterlokalisierung aufgezeigt. Das erste Fallbeispiel beschäftigt sich mit der passiven Überwachung des zivilen Luftraums (Air Traffic Management, ATM) mittels eines stationären Sensornetzwerks. Nach derzeitigem Stand der Technik basiert die Luftraumüberwachung auf aktiven Radaranlagen, sogenannten Primärradaren (Primary Surveillance Radar, PSR), kooperativen Sekundärradaren (Secondary Surveillance Radar, SSR) und auf automatischen Positionsmeldungen der Flugzeuge selbst (Automatic Dependent Surveillance-Broadcast, ADS-B). Sowohl beim Einsatz von SSR als auch bei ADS-B senden Flugzeuge Transpondersignale auf 1090 MHz. Die Zuverlässigkeit und Genauigkeit der bei ADS-B gemeldeten Eigenpositionen ist eingeschränkt und nicht ausreichend, um beispielsweise die Sicherheit bei Landungen auf parallelen Landebahnen zu gewährleisten. Die Daten können im schlimmsten Fall sogar mit böswilliger Absicht verändert werden. Mittels passiver Emitterlokalisierung und Tracking durch Multilateration (TDOA-/Hyperbelortung) kann ein genaues Lagebild unabhängig vom Inhalt der gesendeten

Transpondersignale bereitgestellt werden. Die hohe Dichte sowohl von sendenden Zielen als auch die große Anzahl an gesendeten Nachrichten erfordert spezielle Verfahren der Signalverarbeitung und Fusion, um das große Datenaufkommen zu bewältigen. Es wird gezeigt, dass ein Multilaterationsnetzwerk, welches solche Techniken verwendet, die Luftraumüberwachung bei relativ geringen Kosten verbessern kann.

Das zweite vorgestellte Verfahren zeigt die TDOA-basierte Emitterlokalisierung mit nur einer mobilen Plattform auf. Die übliche TDOA-Messung erfolgt mittels räumlich getrennten Sensoren, die zum gleichen Zeitpunkt ein gesendetes Signal erfassen und aus diesen Signalen Signallaufzeitdifferenzen bestimmen. Die Verwendung von Signalstrukturwissen erlaubt es, unter gewissen Voraussetzungen, das sonst rein räumliche in ein räumliches und zeitliches Messproblem zu verlagern. So ist es möglich mit nur einer mobilen Plattform TDOA-Messungen über mehrere Messzeitpunkte zu gewinnen und über die Bewegung der Beobachterplattform Emitter zu lokalisieren. Für dieses Szenario werden weiterhin Methoden vorgestellt, die Techniken der direkten Lokalisierung einsetzen und diese auf Einzelplattform-TDOA erweitern.

Die Gültigkeit und Performanz der entwickelten Verfahren werden jeweils durch theoretische Analysen (Cramér-Rao Schranken), Monte-Carlo Simulationen und durch die Auswertung von bei Messkampagnen gewonnenen Realdaten gezeigt.

Acknowledgments

I would like to express my sincere gratitude to my supervisor Priv.-Doz. Dr. Wolfgang Koch. I would like to thank him for providing perfect research and working conditions in his department at Fraunhofer FKIE, always having time for discussions and his support in the last years.

I thank Prof. Dr. Peter Martini for being the second supervisor and Prof. Dr. Rainer Manthey and Prof. Dr. Patrik Ferrari for their contribution to the examination committee.

I am grateful to Klaus Wild who gave me the opportunity to work on many interesting topics and projects in his research group during the time from 2010 to 2015.

My sincere thanks goes to Sven Rau, Dr. Marc Oispuu and Dr. Felix Govaers for hours of discussions, for supporting and motivating me during the work on this thesis and for their time spent proof reading papers, reports and this thesis. I also thank all (former) colleagues in the Sensor Data and Information Fusion Department, especially Manfred Okum and Lisa Meyer.

I thank Dr. Wolfgang Konle for many interesting and fruitful discussions on the topic of wide area multilateration in the last six years.

Finally, I am most grateful for the never ending support I receive from my wife and my parents.

Contents

CHAPTER I

Introduction

1.1 Passive Emitter Localization

The task of passive emitter localization and tracking is encountered in many civil and military applications. Determining the position of an emitter covertly and without emitting own signals has various advantages. In military reconnaissance applications, it is of highly strategic advantage not to reveal the own position or to give evidence of the own presence in an area. The clearance to use specific frequency bands is another important fact that needs to be taken into account and less additional electromagnetic pollution is emitted. At the least, it is a cost factor in civil applications that needs to be considered.

While traditional airspace radar systems provide a high level of accuracy, they are expensive, have a limited range and are often not easily accepted by the public due to the high amount of radiation. Secondary surveillance radar systems as well as ADS-B are techniques to fill this gap. For secondary surveillance systems, active polling from a ground radar is still needed. Also both techniques rely on a cooperative aircraft. While for SSR the aircraft answers a request of a ground station and the position is determined by the ground station using information provided by the aircraft, for ADS-B the aircraft actively and regularly transmits its own position, altitude, direction and other flight related parameters. Those messages somehow may be faulty due to technical reasons or even be maliciously altered. To overcome this surveillance gap and to be able to determine the positions of all aircrafts covering large areas, passive emitter localization techniques come into play. Complete airspace surveillance is not only a topic of security but may also improve flight times and fuel consumption. Aircrafts usually follow predefined routes and the possibility to reach a target destina-

tion is defined by the flight time in these corridors. This may result in additional fuel consumption that is also caused by holding patterns near the destination airport. To be able to improve flight path planning and thus save time and fuel, precise airspace surveillance is necessary.

The localization of emitters using small moving observer platforms with strong restrictions on the payload dimensions and weight demands for intelligent signal processing and localization approaches, especially for military reconnaissance tasks. Two main challenges arise from the application: The employed emitter location system (ELS) has to be light weight and small while enabling position estimation with high accuracy. The communication between observer and data fusion center or ground control station has to be reduced to a minimum.

The objective of this thesis is to address the problem of TDOA estimation and TDOA based localization by exploiting known signal structure information for a certain class of signals. Two use cases are considered. The first case is dealing with wide area multilateration for airspace surveillance, the second case is on the localization of emitters using small and mobile observer platforms.

1.2 Structure

This thesis is structured as follows. The fundamentals of passive emitter localization using TDOA/TOA measurements are described in Chapter 2.
Chapters 3 and 4 deal with the passive localization of aircrafts sending transponder signals. A TOA estimation method for ADS-B/Mode-S transponder signals is introduced in Chapter 3. Field experiments using a stationary sensor network to localize and track aircrafts using TOA estimates are conducted. The results of the evaluation of the obtained data is presented in Chapter 4.
In Chapter 5, methods for (direct) single sensor signal structure TDOA ((D)S^{4}TDOA*) are introduced. An analysis of (D)S^{4}TDOA* is given in Chapter 6. The performance of the presented methods is evaluated using the Cramér-Rao Lower Bound (CRLB) and Monte-Carlo simulations. The techniques are applied to measurement data gained during field experiments and an evaluation of the emitter localization accuracy is presented.
Summary and conclusion of the thesis are given in Chapter 7.

1.3 Contribution

Aspects related to this work have been published on various occasions [SKR11], [KSR+12], [SM16], [Ste15], [SO15], [SO16], [SM13], [Ste14], [SR12a], [SR12b]. Some of this work resulted from a cooperation with a Master student. Some results concerning the multilateration and tracking of aircrafts using ADS-B data (Chapter 3 and 4) have appeared in [SM16] and [Mey16]. Both publications are associated with our previously published methods [SKR11, KSR+12]. Chapters 5 and 6 are based on our previous publication [SO16] which relies on [Ste15, SO15].

The main contributions of the thesis can be formulated as follows:

1. Development of a novel method for the estimation of the Time of Arrival of transponder signals encountered in aviation using known signal structure information [SKR11]. A huge reduction (up to 99.2%, see Section 3.4.3) of the communication requirements is achieved using TOA estimation.
2. Evaluation of multilateration techniques for passive surveillance of the civil airspace using a distributed sensor network which generates TOA measurements for incoming transponder signals and allows the passive localization and tracking of aircrafts [KSR+12, SM16].
3. Introduction of a novel method (S^4TDOA) for TDOA estimation over time using a single sensor for signals with recurring signal structure [Ste15]. This technique allows TDOA based emitter localization with only one moving observer and may as well be used in a sensor network allowing drastic reduction of communication requirements.
4. Extension of the existing TDOA direct position determination scheme to the concept of S^4TDOA [SO15, SO16].
5. Localization of emitters with recurring signal structure using a small airborne sensor node [Ste15, SO15, SO16].
6. Comparison and evaluation of the performance of all introduced estimation methods using real data gained during field experiments, simulations and the Cramér-Rao Lower Bound.

CHAPTER II

Fundamentals

2.1 Scenario Description

A set of N observers is used to estimate the target state of Q RF emitters. Each observer is represented by a time-synchronized sensor node. The positions and velocities of the sensors are assumed to be known and given by $p_n = (x_n, y_n, z_n, \dot{x}_n, \dot{y}_n, \dot{z}_n)^T$, $n \in \{1, ..., N\}$. The unknown position and velocity of an emitter at a certain time step is given by the target state $\mathbf{x} = (x_e, y_e, z_e, \dot{x}_e, \dot{y}_e, \dot{z}_e)^T$. This emitter sends a signal $s(t)$ at unknown time t_e.

Simultaneously, each sensor collects a measurement. The received signal at some time step $i \in \{1, ..., I\}$ at sensor n is given by

$$z_{n,i}(t) = a_{n,i}\, s(t - t_{e,i} - t_{n,i}) \exp(j\nu_{n,i}t) + w_{n,i}(t)\,, \tag{2.1}$$

where $a_{n,i}$ represents the path attenuation, $t_{n,i}$ gives the time difference between signal emission time $t_{e,i}$ and signal reception, $\nu_{n,i}$ is the Doppler shift induced by the movement of the sensor and emitter and $w_{n,i}$ is additional receiver noise which is assumed to be uncorrelated and zero-mean Gaussian. The emitted continuous-time signal is represented by the complex envelope $s(t)$.

For a stationary sensor and a stationary emitter, $t_{n,i}$ is constant over the observation duration of the signal. If moving sensors and/or emitters are considered, it is assumed that the sampling rate is high enough that the sensor and emitter locations are approximately constant over the time of data collection. The reduced observer states

$p_n = (x_n, y_n, z_n)^T$ and emitter states $\mathbf{x} = (x_e, y_e, z_e)^T$ are used in the following. The time difference between signal emission and reception is given by

$$t_{n,i} = \frac{||\triangle p_n(\mathbf{x})||}{c}\,, \tag{2.2}$$

where c represents the propagation speed of the signal, $\triangle p_n(\mathbf{x}) = \mathbf{x} - p_n$ is the relative vector between sensor and emitter and $||\cdot||$ denotes the Euclidian distance. The propagation speed of RF waves corresponds approximately to the speed of light $c \approx 299792458\,\mathrm{m/s}$.

In practice, a sensor collects the signal data at a given sampling rate f_s. The time-discrete version of the received signal (2.1) is given by

$$z_{n,i}[k] = a_{n,i}\, s[k\triangle - \tau_{n,i}] + w_{n,i}[t]\,, \tag{2.3}$$

where $\triangle$ is the sampling interval and $\tau_{n,i} = t_{e,i} + t_{n,i}$ denotes the absolute TOA taking the local sensor clock into account.

2.2 The TDOA Measurement Problem

The TDOA measurement problem can be stated as follows. From the received digitized signals $z_a[k]$ and $z_b[k]$ of two spatially dislocated observers a and b, determine the TDOA $\tau_{(a,b)}$ of those signals. The resulting estimate $\hat{\tau}_{(a,b)}$ can then be used in a localization process to calculate the targets position. This TDOA measurement can either be done using both signals or by separately estimating a TOA $\hat{\tau}_n$ for each signal and then calculating the difference of those TOA measurements. In this thesis, known signal structure information is exploited to determine TOA measurements (see Chapter 3 and 5). However for most cases, TOAs can't be determined explicitly. In Section 2.5, classic methods for gaining TDOA measurements are described.

2.3 The TDOA/TOA Localization Problem

2.3.1 The classic TDOA Localization Problem

The TDOA based localization problem is stated as follows. From a set of TDOA measurements $\hat{\tau}_{(m)}$, $m \in \{1, ..., M_\tau\}$ taken at measurement step i and given the position information of the corresponding receivers, estimate the position $\mathbf{x}$ of the emitter.

The TDOA measurement $\tau_{(a,b),i}$ for a sensor pair (a, b) at time step i results from different distances between the receivers and the emitter. The time of arrival (TOA) of the emitted signal at sensor node n is given by

$$\tau_{n,i} = \frac{||\triangle p_n(\mathbf{x})||}{c} + t_{e,i}\,. \tag{2.4}$$

By calculating the TDOA of the signal received at two spatially separated sensors (a, b)

$$\tau_{(a,b),i} = \left(\frac{||\triangle p_a(\mathbf{x})||}{c} + t_{e,i}\right) - \left(\frac{||\triangle p_b(\mathbf{x})||}{c} + t_{e,i}\right) = \frac{||\triangle p_a(\mathbf{x})||}{c} - \frac{||\triangle p_b(\mathbf{x})||}{c}\,, \tag{2.5}$$

the unknown time of signal emission t_e is eliminated. Throughout this thesis, $\tau_{(m)} = \tau_{(a,b)}$ refers to a TDOA with measurement index m taken by a sensor pair (a, b), whereas τ_m denotes a TOA. In all cases, the additional index i refers to the time step of the measurement. An estimate of τ is denoted as $\hat{\tau}$. Since the time and range (difference) of arrival differ only by the constant propagation speed c, in practical applications, it is often beneficial to transform and process TOA and TDOA measurements in range domain.

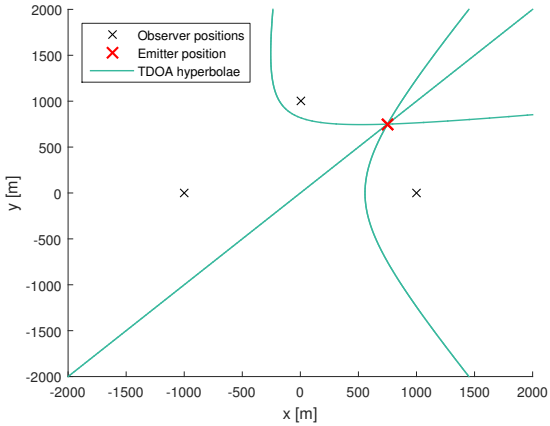

Figure 2.1: TDOA localization scenario.

A TDOA measurement of a sensor pair (a, b) can be interpreted as a hyperbola in 2-dimensional space or as a hyperboloid in 3D. The intersection of $m \in \{1, ..., M_\tau\}$ TDOA hyperbolae/hyperboloids yields the emitter position (see Figure 2.1).

For the emitter localization, different TDOA measurement sets can be considered. We refer to the measurement set consisting of measurements using a reference sensor (w.l.o.g. sensor 1) and all other sensors as the *measurement set using a reference sensor*. This set results in $M_\tau = N - 1$ TDOA measurements that are given by

$$\{\tau_{(1,n)}\},\ n \in \{2, ..., N\}\,. \tag{2.6}$$

The *full measurement set* consists of all possible combinations of TDOA pairings without repetition. The TDOA measurement set is then given by

$$\{\tau_{(a,b)}\},\ a \in \{1, ..., N-1\}, b \in \{a+1, ..., N\}\,. \tag{2.7}$$

The full measurement set thus consists of $M_\tau = \frac{N(N-1)}{2}$ TDOA measurements.

2.3.2 The TOA Localization Problem

From a set of TOA measurements $\hat{\tau}_n$, $n \in \{1, ..., N\}$ taken at measurement step i by N sensor nodes, estimate the unknown emitter position $\mathbf{x}$. If the time of emission is

known, a TOA measurement can be geometrically interpreted as a circle (see Figure 2.2) centered around the receivers position with radius

$$r = ||\triangle p_n(\mathbf{x})|| \,. \tag{2.8}$$

In 3-dimensional space, the TOA measurement results in a sphere of possible emitter positions. If the time of emission is unknown, which is the case for most applications e.g. for ADS-B/Mode-S signals, it has to be estimated along with the position of the emitter.

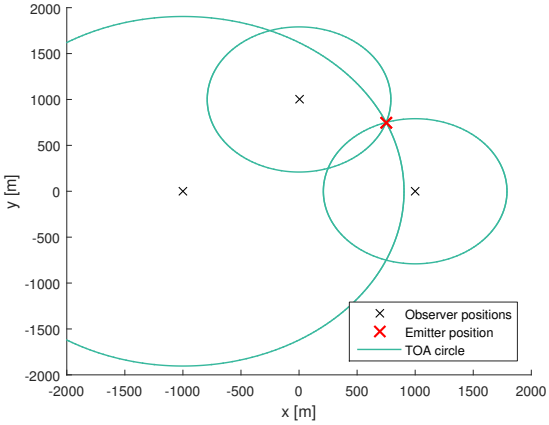

Figure 2.2: TOA localization scenario.

2.4 The Cramér-Rao Lower Bound

The Cramér-Rao Lower Bound (CRLB) (see for example [Kay93]) provides a lower bound on the estimation accuracy and its parameter dependencies reveal characteristic features of the estimation problem. The parameters to be estimated from the measurements $\mathbf{z} = (\mathbf{z}_1^T, ..., \mathbf{z}_M^T)^T$ are given in the vector $\mathbf{x}$. In this case, the CRLB is related to the covariance matrix $\mathbf{C}$ of the estimation error $\triangle\mathbf{x} = \mathbf{x} - \hat{\mathbf{x}}(\mathbf{z})$ of any unbiased estimator $\hat{\mathbf{x}}(\mathbf{z})$ as

$$\mathbf{C} = \mathrm{E}\left\{\triangle\mathbf{x}\,\triangle\mathbf{x}^T\right\} \geq \mathbf{J}^{-1}(\mathbf{x})\,, \tag{2.9}$$

where the inequality means that the matrix difference is positive semidefinite and $\mathbf{J}$ is the Fisher Information Matrix (FIM) given by

$$\mathbf{J}(\mathbf{x}) = \mathrm{E}\left\{\left(\frac{\partial\mathcal{L}(\mathbf{z};\mathbf{x})}{\partial\mathbf{x}}\right)\left(\frac{\partial\mathcal{L}(\mathbf{z};\mathbf{x})}{\partial\mathbf{x}}\right)^T\right\}, \tag{2.10}$$

where $\mathcal{L}$ denotes the log-likelihood function. If the estimator attains the CRLB then it is called *efficient*. The CRLB is given by the inverse Fisher Information.

In the following sections, CRLBs for the TDOA estimation (Section 2.6) as well as for the localization problems (Section 2.7) are described. Please note that the CRLB gives a lower bound on the attainable accuracy of an unbiased estimator. This bound may not be reached by estimators in real world systems. In this thesis, CRLBs are used as benchmark for newly developed localization approaches.

In the following, an example for the one-dimensional case is described (see [Kay93]). For the unknown parameter $\mathbf{x}$, the corresponding estimator $\hat{\mathbf{x}}(\mathbf{z})$ uses a measurement $\mathbf{z}$ given by

$$\mathbf{z} = \mathbf{x} + w\,, \tag{2.11}$$

where $w \sim \mathcal{N}(0, \sigma^2)$ denotes white Gaussian noise with variance σ^2. The corresponding probability density function (PDF) is

$$p(\mathbf{z};\mathbf{x}) = \frac{1}{\sqrt{2\pi\sigma^2}}\exp\left[-\frac{1}{2\sigma^2}(\mathbf{z}-\mathbf{x})^2\right]. \tag{2.12}$$

Clearly, when σ^2 is high, the estimate of the unknown parameter $\mathbf{x}$ becomes less accurate and for lower σ^2, the estimate becomes more precise. The PDF as a function of the unknown parameter $\mathbf{x}$ is called the *likelihood function*. The *log-likelihood function* is often used to eliminate the exponential term in the likelihood function. The "sharpness" of the likelihood function is directly connected to the accuracy of the estimation process. This sharpness can be quantified by the curvature of the log-likelihood function, the negative of the second derivative of the logarithm of the likelihood function at its peak, with the log-likelihood function being

$$\ln p(\mathbf{z};\mathbf{x}) = -\ln\sqrt{2\pi\sigma^2} - \frac{1}{2\sigma^2}(\mathbf{z}-\mathbf{x})^2\,. \tag{2.13}$$

The first derivative is

$$\frac{\partial \ln p(\mathbf{z};\mathbf{x})}{\partial \mathbf{x}} = \frac{1}{\sigma^2}(\mathbf{z}-\mathbf{x})\,, \tag{2.14}$$

and the negative of the second derivative

$$-\frac{\partial^2 \ln p(\mathbf{z};\mathbf{x})}{\partial \mathbf{x}^2} = \frac{1}{\sigma^2}\,. \tag{2.15}$$

In general, the average curvature of the log-likelihood function is then given by

$$-\,\mathrm{E}\left\{\frac{\partial^2 \ln p(\mathbf{z};\mathbf{x})}{\partial \mathbf{x}^2}\right\}. \tag{2.16}$$

We assume that the PDF $p(\mathbf{z};\mathbf{x})$ satisfies the "regularity" condition with the expectation taken with respect to $p(\mathbf{z};\mathbf{x})$

$$\mathrm{E}\left\{\frac{\partial \ln p(\mathbf{z};\mathbf{x})}{\partial \mathbf{x}}\right\} = 0,\ \forall \mathbf{x}\,. \tag{2.17}$$

The variance of any unbiased estimator $\hat{\mathbf{x}}$ is then bound by

$$\mathrm{var}(\hat{\mathbf{x}}) \geq -\frac{1}{\mathrm{E}\left\{\frac{\partial^2 \ln p(\mathbf{z};\mathbf{x})}{\partial \mathbf{x}^2}\right\}}\,, \tag{2.18}$$

where the derivative is evaluated at the true value of $\mathbf{x}$.

2.5 Methods for TDOA Measurement

The problem of estimating TDOAs from received signals has been analyzed and solutions were presented for example in [KV13, KC76, OBB12, UG99, YLX05, Ste81] and is often closely related to investigations concerning the achievable accuracy [Fri84, Qua81, Ste93, Wax82, VB16, DM12, Ste81, FH08, Yer10, YA11], see Section 2.6.

The standard technique relies on the cross correlation function (CCF) or the cross ambiguity function (CAF) for the joint estimation of TDOA and FDOA (Frequency Difference of Arrival). Both functions give a rate on the similarity of two input sequences with respect to the delay and, in case of the CAF, the Doppler-induced frequency shift.

The complex cross correlation function can be defined as (see [Lük92])

$$\mathrm{CCF}(\tau) = \int_{-\infty}^{\infty} z_a(t) z_b^*(t+\tau) dt\,, \tag{2.19}$$

where z_a and z_b are signals received by sensor a and b and z^* is the complex conjugate of z.

The maximum of the cross correlation function

$$\hat{\tau}_{(a,b)} = \arg\max_{\tau} |\mathrm{CCF}(\tau)|\,, \tag{2.20}$$

gives the Time Difference of Arrival estimate $\hat{\tau}_{(a,b)}$ of the two input signals. Fig. 2.3 depicts examples of the CCF for different signal bandwidths. Fig. 2.3a shows the CCF for 1 MHz, 100 kHz and 10 kHz at high SNR (signal-to-noise ratio). It can be observed, that the higher the signal bandwidth, the sharper the maximum. With lower bandwidth, the slope of the CCF becomes wider. Fig. 2.3b shows the same example for low SNR values. In this example, the peak of the signals with 1 MHz is still relatively distinct, whereas for the example with 10 kHz, more than one peak have approximately the same amplitude.

The CAF also takes the Doppler shift into account and describes a correlation in time and frequency domain. It can be defined by

$$\mathrm{CAF}(\tau, \nu) = \int_{-\infty}^{\infty} z_a(t) z_b^*(t+\tau) \exp(-j2\pi\nu t) dt\,. \tag{2.21}$$

The TDOA and FDOA are then given by the maximum of the CAF

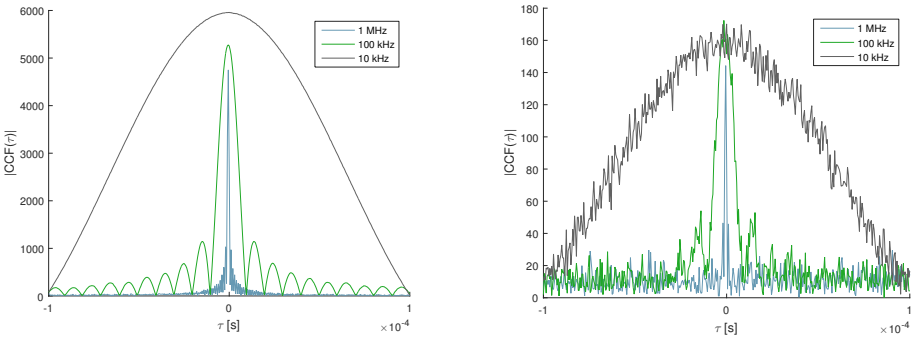

Figure 2.3: Examples of the cross correlation function for different signal bandwidths with (a) high SNR and (b) low SNR.

$$(\hat{\tau}_{(a,b)}, \hat{\nu}_{(a,b)}) = \arg\max_{\tau,\nu} |\mathrm{CAF}(\tau, \nu)| \,. \tag{2.22}$$

Since in most cases, TDOA based localization is performed using spatially separated observers, each sensor node has to transmit the received raw signal data to a reference sensor or a fusion center. Communication using data links is a key issue in real world applications, since a large amount of data needs to be transmitted. For military applications, wideband communication with long transmission times is a high strategic risk, since the communication can be used to detect or localize the observer which becomes an emitter itself. In civil applications with stationary sensor networks, wideband communication is a smaller issue, but nonetheless not trivial to solve. Wideband communication is at least a cost factor and when using mobile observers, bandwidth limitations and network coverage of mobile communication networks need to be taken into account as well.
In [Fow00, PF11] this problem is addressed with respect to data compression techniques for TDOA estimation. We present other solutions in this thesis, exploiting signal structure information to estimate TOAs. With these methods, only TOAs and message identifications have to be transmitted which allow a drastic reduction of communication requirements. Thus, a narrowband data link can be used.

2.6 CRLB on TDOA Measurement Accuracy

In this section, lower bounds for the estimation accuracy of TDOA measurements are presented. The section is structured as follows. In Section 2.6.1, a lower bound is introduced that relies on signal parameters like the signal bandwidth, SNR and the integration time. This bound was presented in the early 1980s by Stein [Ste81]. The observations that lead to the lower bound are based on the cross ambiguity and correlation functions. For example, signals with lower bandwidth tend to have a wider peak in the cross correlation than ones with higher bandwidth (see Fig. 2.3). For signals that are received with a low SNR, the amplitude of the peak is not as distinct.

Lower bounds on the estimation accuracy of TOA/TDOA measurements are a widely investigated field. Much research was done and publications dealing with this topic for generic signals and selected signal forms were published. [Fri84, Qua81, Ste93, Wax82, VB16, DM12, Ste81, FH08, Yer10, YA11].

In Section 2.6.2, lower bounds which use the received signals directly are presented. The CRLB for TDOA and FDOA estimation using the received signals were firstly introduced by Fowler et. al. [FH08] nearly three decades later. The work of Stein concerning the parameter based CRLB was mainly based on acoustic but was often applied to electromagnetic signals. However, Fowler states [FH08], that acoustic signals are usually wide-sense stationary (WSS) Gaussian processes and electromagnetic signals can be assumed to be deterministic. This may lead to incorrect results if the bound is applied to electromagnetic signals. In [Yer10], [YA11], the basis of the work of Fowler et. al. was picked up and enhanced to a more general case, where amplitude and phase shifts are unknown. The bound found in [YA11] is given in Section 2.6.2.

All presented lower bounds concerning the TDOA measurement accuracy also deal with a bound for FDOA estimation (also referred to as differential Doppler). This is due to the fact, that TDOA as well as FDOA estimation strongly depends on accurate knowledge of the respective center frequency and time delay. If the center frequency of the signal is not exactly known, the accuracy of the TDOA measurement degrades. The same applies to FDOA estimation if the time delay between the received signals is not estimated correctly.

2.6.1 Parameter based CRLB for TDOA Measurement Accuracy

One of the most cited publication dealing with CRLB on TDOA/FDOA measurement accuracy is the work of Stein [Ste81]. In this thesis, only TDOA measurement accuracy is of interest and Doppler induced frequency shifts are neglected. In the following, the CRLB derived by Stein in [Ste81] is presented.

The problem of estimating the TDOA $\tau_{(a,b),i}$ of received signals can be stated as follows. From a set of signals $z_{n,i}[k]$ received by sensors $n \in \{1, ..., N\}$ at measurement step i, estimate the corresponding TDOAs. A lower bound on the achievable accuracy of this estimation process is essential for the calculation of the achievable localization accuracy described in Section 2.7.

The emitted signal is characterized by multiple parameters. In this thesis, we use the following notation for these parameters. The signal bandwidth in [Hz] is given by B_s, the noise bandwidth in [Hz] by B, the duration of the signal in [s] (integration time) by T and the signals center frequency in [Hz] by f_0. We assume that the full signal is received at each sensor node. The influence of different signal forms and modulation techniques on the TDOA measurement estimation accuracy is not part of the investigation of Stein.

The signal-to-noise ratio (SNR) clearly has impact on the TDOA estimation accuracy. The SNR for sensor n at measurement step i is given by

$$\mathrm{SNR}_{n,i}[\mathrm{dB}] = \mathrm{P_R} - \mathrm{S_R}\,, \tag{2.23}$$

where P_R denotes the signal strength in [dBm] and S_R the receiver sensitivity given in [dBm].

The signal strength is given by

$$\mathrm{P_R} = \mathrm{P_E} + \mathrm{G_E} + \mathrm{G_R} + \mathrm{G_C} - \mathrm{PL}\,, \tag{2.24}$$

with P_E [dBm] being the transmission power of the emitter, G_E [dBi] the antenna gain of the emitter, G_R [dBi] the antenna gain of the receiver, G_C [dB] gain/loss resulting for example from cabling and PL [dB] the path loss due to the transmission from emitter position to receiver position. For Free Space Path Loss (FSPL) this loss is defined by

$$\mathrm{FSPL} = \left(\frac{4\pi r}{\lambda}\right)^2 = \left(\frac{4\pi r \mathrm{f_0}}{c}\right)^2\,, \tag{2.25}$$

where λ denotes the wave length and $r = ||\triangle p_n(\mathbf{x})||$ the distance between sensor and emitter. For r in [km], f_0 in [MHz] and $c \approx 299792458\,\mathrm{m/s}$ being the speed of light,

$$\mathrm{FSPL} = 20\lg(r) + 20\lg(\mathrm{f_0}) + 32.45\,. \tag{2.26}$$

The observations made by Stein rely on the cross ambiguity/correlation function for TDOA measurements. The influence of SNR, bandwidth and integration time results in more/less distinct peaks in the cross correlation function (see Section 2.5). All parameters mentioned above have influence on the TDOA measurements.

The CRLB (in this case the standard deviation) for the TDOA measurement of signals received by sensor a and b at time step i is given by

$$\sigma_{\tau_{(a,b),i}} = \frac{1}{\beta\sqrt{\mathrm{BT}\,\gamma}}\,, \tag{2.27}$$

where β is the "rms radian frequency" in the received signal spectrum and γ is the effective input SNR of both signals. This effective input SNR is defined by

$$\frac{1}{\gamma} = \frac{1}{2}\left(\frac{1}{\gamma_a} + \frac{1}{\gamma_b} + \frac{1}{\gamma_a\gamma_b}\right)\,, \tag{2.28}$$

where γ_a and γ_b give the SNRs for the received signals at sensor a and sensor b.

The rms radian frequency for a signal with rectangular spectrum is

$$\beta = \frac{\pi}{\sqrt{3}}\mathrm{B_s} \approx 1.8\,\mathrm{B_s}\,, \tag{2.29}$$

since

$$\beta = 2\pi\left[-\frac{\int_{-\infty}^{\infty}\nu^2 W_z(\nu)d\nu}{\int_{-\infty}^{\infty}W_z(\nu)d\nu}\right]^{1/2}\,, \tag{2.30}$$

where $W_s(\nu)$ is the power density spectrum of the signal.

Under the assumption that the spectrum of the received signals is rectangular, using (2.29) and (2.27), the standard deviation for the TDOA measurement accuracy is

$$\sigma_{\tau_{(a,b),i}} \approx \frac{0.55}{\mathrm{B_s}\sqrt{\mathrm{BT}\,\gamma}}\,. \tag{2.31}$$

An example of the lower bound for different bandwidths, integration times and effective SNRs is given. Using (2.31), the lower bound over bandwidth $\mathrm{B_s}$ (Figure 2.4a),

over integration time T (Figure 2.4b) and over effective SNR γ (Figure 2.4c) is depicted. When not variable, the bandwidth is set to $\mathrm{B_s} = \mathrm{B} = 1\,\mathrm{MHz}$, the integration time to $\mathrm{T} = 0.1\,\mathrm{s}$ and the effective SNR to $\gamma_{[dB]} = 10\,\mathrm{dB}$. We assume that the noise bandwidth B is equal to the signal bandwidth $\mathrm{B_s}$.

For the sake of completeness, the lower bound for FDOA estimation according to Stein is given in the following. Similar to TOA/TDOA measurements, $\nu_{a,i}$ denotes the FOA (Frequency of Arrival) of a signal received by sensor a at time step i, whereas $\nu_{(a,b),i}$ refers to the FDOA measurement of signals received by the sensors a and b at time step i.

For signals received by a sensor pair (a, b) at any time step i, the lower bound for the FDOA estimation is

$$\sigma_{\nu_{(a,b),i}} = \frac{1}{T_e\sqrt{\mathrm{BT}\,\gamma}}\,, \tag{2.32}$$

where T_e denotes the "rms integration time" which is defined as

$$T_e = 2\pi \left[\frac{\int_{-\infty}^{\infty} t^2 \left|s(t)\right|^2 dt}{\int_{-\infty}^{\infty} \left|s(t)\right|^2 dt} \right]^{1/2} . \tag{2.33}$$

For the ambiguity FDOA estimation of a constant energy signal over a finite duration T, the rms integration time is $T_e \approx 1.8\mathrm{T}$. This gives the standard deviation for the FDOA measurement estimation

$$\sigma_{\nu_{(a,b),i}} \approx \frac{0.55}{\mathrm{T}\sqrt{\mathrm{BT}\,\gamma}}\,. \tag{2.34}$$

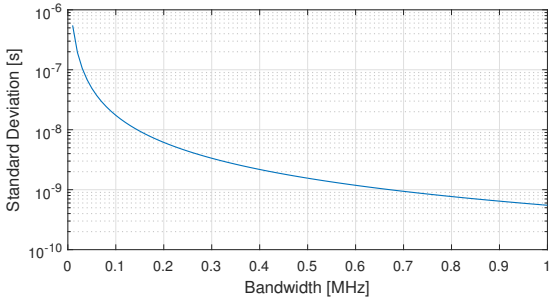

(a) Lower bound for the standard deviation of TDOA measurement over bandwidth. Integration time T = 0.1 s, $\gamma_{[dB]} = 10$ dB.

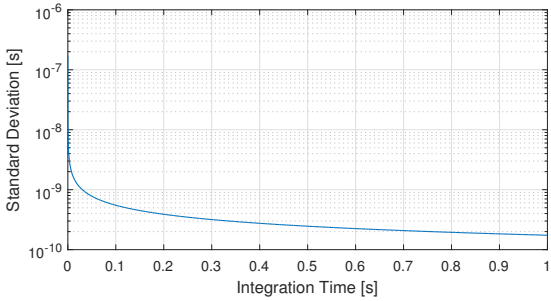

(b) Lower bound for the standard deviation of TDOA measurement over integration time. Bandwidth $B_s = 1$ MHz, $\gamma_{[dB]} = 10$ dB.

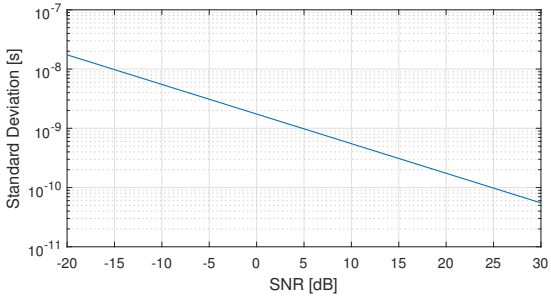

(c) Lower bound for the standard deviation of TDOA measurement over effective SNR. Bandwidth $B_s = 1$ MHz, integration time T = 0.1 s.

Figure 2.4: Parameter based lower bound for TDOA measurements.

2.6.2 Signal based CRLB for TDOA Measurement Accuracy

Although, the CRLB described in Section 2.6.1 is a widely used bound, some assumptions do not match the case of electromagnetic signals. Therefore, this bound will give too optimistic results (in general, estimators will not attain the bound) and should not be applied to the electromagnetic case. Acoustic or sonar signals are usually assumed to be wide-sense stationary Gaussian processes where electromagnetic signals, especially communication signals, can be assumed to be deterministic [FH08,Yer10,YA11]. A bound which is calculated based on the signals themselves instead of signal parameters has been introduced in [FH08]. Bounds for the deterministic as well as for the WSS case are derived and compared. Based on this work, Yeredor et. al. [YA11] extended the idea and presented a bound that does not assume the original signal and the phase difference to be known. This assumption gives a lower bound which is more realistic with respect to a real world system where neither the original signal nor the phase difference of received signals is known.

We use the bound of Yeredor et. al. [YA11] as benchmark for the evaluation of the presented DS^{4}TDOA$^{(*)}$ algorithms (see Chapter 5 and 6). The CRLB is therefore given here as described in [YA11]. We follow the same notation as [YA11] which is slightly different than the usual notation of this thesis.

The parameters $\triangle\tau$ and $\triangle\nu$ denote the TDOA and the FDOA, respectively. A sampled source complex signal $x[n]$ is received by sensor 1. Additional zero-mean, statistically independent complex circular Gaussian noise $v_1[n]$ is added. The received signals at sensor 1 and 2 are given by

$$\begin{aligned} r_1[n] &= x[n] + v_1[n], \quad -\frac{N}{2} \leq n \leq \frac{N}{2} - 1 \\ r_2[n] &= a e^{j\phi} e^{j\triangle\nu n} x_{\triangle\tau}[n] + v_2[n]\,, \end{aligned} \tag{2.35}$$

where $x_{\triangle\tau}$ is the time shifted version of $x[n]$ by $\triangle\tau$, a is the amplitude factor and ϕ is the phase shift.

The relation between the signal vectors $\mathbf{x}$ and $\mathbf{x}_{\triangle\tau}$ is approximated for $\triangle\tau \ll T$, where T is the observation duration, using the discrete Fourier transform (DFT) as $\mathbf{x}_{\triangle\tau} \approx \mathbf{F}^H \mathbf{D}_{\triangle\tau} \mathbf{F}\mathbf{x}$, with

$$\mathbf{F} = \frac{1}{\sqrt{N}} \exp\left(-j\frac{2\pi}{N}\mathbf{n}\mathbf{n}^T\right), \tag{2.36}$$

and

$$\mathbf{D}_{\triangle\tau} = \mathrm{diag}\left\{\exp\left(-j\frac{2\pi}{N}\mathbf{n}\triangle\tau\right)\right\}, \tag{2.37}$$

with

$$\mathbf{n} = \left[-\frac{N}{2} \; -\frac{N}{2}+1 \; ... \; \frac{N}{2}-1\right]^T. \tag{2.38}$$

When using $\mathbf{D}_{\triangle\nu}$ to represent the FDOA $\triangle\nu$ with $\mathbf{D}_{\triangle\nu} = \mathrm{diag}\left\{\exp\left(j\triangle\nu\mathbf{n}\right)\right\}$, the received signal vectors are given by

$$\begin{aligned}\mathbf{r}_1 &= \mathbf{x} + \mathbf{v}_1 \\ \mathbf{r}_2 &= ae^{j\phi}\mathbf{D}_{\triangle\nu}\mathbf{F}^H\mathbf{D}_{\triangle\tau}\mathbf{F}\mathbf{x} + \mathbf{v}_2\,.\end{aligned} \tag{2.39}$$

The parameter vector including the nuisance parameters amplitude a and phase shift ϕ is then given by $\theta = [a\;\pi\;\triangle\tau\;\triangle\nu]^T$. We define $\mathbf{Q}$ as

$$\mathbf{Q} = \mathbf{D}_{\triangle\nu}\mathbf{F}^H\mathbf{D}_{\triangle\tau}\mathbf{F}\,. \tag{2.40}$$

The concatenated signal vector $\mathbf{r} = [\mathbf{r}_1^T\;\mathbf{r}_2^T]^T$ has a mean of

$$\boldsymbol{\mu} = \begin{bmatrix}\boldsymbol{\mu_1}\\ \boldsymbol{\mu_2}\end{bmatrix} = \begin{bmatrix}\mathbf{x}\\ ae^{j\phi}\mathbf{Q}\mathbf{x}\end{bmatrix}. \tag{2.41}$$

The covariance matrix $\mathbf{C}$ of $\mathbf{r}$ only depends on the $N \times N$ covariance matrices $\mathbf{C}_i$ of the noise vectors $\mathbf{v}_i$ and is given by

$$\mathbf{C} = \begin{bmatrix}\mathbf{C}_1 & 0\\ 0 & \mathbf{C}_2\end{bmatrix}. \tag{2.42}$$

For the determination of the FIM, a delayed and frequency shifted version of $\mathbf{x}$ is introduced as $\tilde{\mathbf{x}} = \mathbf{Q}\mathbf{x}$ with its time derivative approximated by using the DFT

$$\mathbf{x}' = \frac{2\pi}{N}\mathbf{F}^H\mathbf{N}\mathbf{F}\mathbf{x}\,, \tag{2.43}$$

where $\mathbf{N}$ denotes a diagonal matrix containing the N time instances $\mathbf{N} = \mathrm{diag}\,\{\mathbf{n}\}$. The nuisance parameters a can be decoupled from the other parameters ϕ, $\triangle\tau$, $\triangle\nu$. The FIM is given by

$$\mathbf{J}_{\phi,\triangle\tau,\triangle\nu} = \frac{2}{\sigma_1^2 + \sigma_2^2/a^2}\begin{bmatrix} \mathbf{x}^H\mathbf{x} & -\mathbf{x}^H\mathbf{x}' & \tilde{\mathbf{x}}^H\mathbf{N}\tilde{\mathbf{x}} \\ -\mathbf{x}^H\mathbf{x}' & \mathbf{x}'^H\mathbf{x}' & -Re\{\mathbf{x}'^H\mathbf{Q}^H\mathbf{N}\tilde{\mathbf{x}}\} \\ \tilde{\mathbf{x}}^H\mathbf{N}\tilde{\mathbf{x}} & -Re\{\mathbf{x}'^H\mathbf{Q}^H\mathbf{N}\tilde{\mathbf{x}}\} & \tilde{\mathbf{x}}^H\mathbf{N}^2\tilde{\mathbf{x}} \end{bmatrix}, \tag{2.44}$$

where σ_1^2 and σ_2^2 are the noise variances. The CRLB on the parameters ϕ, $\triangle\tau$, $\triangle\nu$ is then given by $\mathbf{J}^{-1}_{\phi,\triangle\tau,\triangle\nu}$. The TDOA measurement accuracy is thus bound by $\sigma^2_{\triangle\tau} \geq \left[\mathbf{J}^{-1}_{\phi,\triangle\tau,\triangle\nu}\right]_{22}$

2.7 CRLB on TDOA based Emitter Localization

The choice of the CRLB has to be done in accordance with the investigated scenario. In this section, two bounds for TDOA based emitter localization are described. The main difference between those bounds is the way the TDOA measurements are obtained and the assumptions on the corresponding measurement errors.

The CRLB for the emitter localization problem depends on the measurements that are taken and thus on the information that is carried by those measurements with respect to the emitter position. The overall CRLB for the TDOA emitter localization problem does not depend on how the measurements are processed into a position estimate. There are also bounds that are associated to the used estimator but they may describe the behavior of the investigated estimator instead of the localization problem itself. Thus, the lower bounds presented in the section are universally valid and give the overall lower bound for the TDOA based emitter localization problem considering the assumptions on the scenario. If for example the TDOA measurement errors are correlated, a different bound applies than for uncorrelated measurement errors. Investigations dealing with the localization accuracy and the CRLB for TDOA based emitter localization can for example be found in [KHK11, Kau12, HC93, SHM10, ASG01, VKD14, PZJ15, Lee75b, Lee75a].

2.7.1 Uncorrelated Measurement Errors

Consider a scenario with two observers, each moving along a trajectory (see Fig. 2.5) and assuming a stationary emitter. At certain time steps i, each sensor simultaneously takes a measurement of the emitted signal. From this signal data, either TOA measurements are calculated and a TDOA is generated from the obtained TOAs or the TDOA is directly estimated from both received signals (f.e. by cross correlation). From a series of TDOA (TOA) measurements taken at different positions and time steps, the emitter position is estimated. We assume ideal conditions like error free knowledge of the observer positions and exact time synchronization. The TDOA measurement $\tau_{(a,b),i}$ can be assumed to be temporally and spatially uncorrelated. The Fisher Information matrix for a single TDOA measurement m obtained from a sensor pair (a, b) at a certain time step i with respect to the emitter location is given by

$$\mathbf{J}_{\mathrm{TDOA}_{(a,b),i}}(\mathbf{x}) = \left(\frac{\partial \tau_{(a,b),i}}{\partial \mathbf{x}}\right) \frac{1}{\sigma^2_{\tau_{(a,b),i}}} \left(\frac{\partial \tau_{(a,b),i}}{\partial \mathbf{x}}\right)^T, \tag{2.45}$$

where $\sigma^2_{\tau_{a,i}}$ denotes the variance of the TDOA measurement in range domain obtained by sensor a and sensor b at time step i. The variance is modeled by the variances of the TOA measurements $\sigma^2_{\tau_{a,i}}$ and $\sigma^2_{\tau_{b,i}}$ and is given by $\sigma^2_{\tau_{(a,b),i}} = \sigma^2_{\tau_{a,i}} + \sigma^2_{\tau_{b,i}}$.

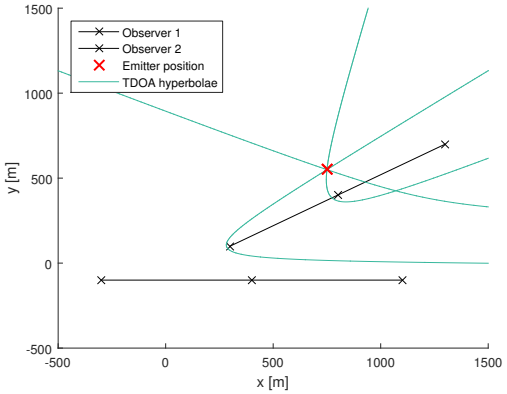

Figure 2.5: TDOA localization scenario with two moving observers.

For the TDOA of the sensor pair (a, b) in range domain and for better readability without the time index i:

$$\begin{pmatrix} \frac{\partial \tau_{(a,b)}}{\partial x_e} \\ \frac{\partial \tau_{(a,b)}}{\partial y_e} \\ \frac{\partial \tau_{(a,b)}}{\partial z_e} \end{pmatrix} = \begin{pmatrix} \frac{x_e - x_a}{||\triangle p_a(\mathbf{x})||} - \frac{x_e - x_b}{||\triangle p_b(\mathbf{x})||} \\ \frac{y_e - y_a}{||\triangle p_a(\mathbf{x})||} - \frac{y_e - y_b}{||\triangle p_b(\mathbf{x})||} \\ \frac{z_e - z_a}{||\triangle p_a(\mathbf{x})||} - \frac{z_e - z_b}{||\triangle p_b(\mathbf{x})||} \end{pmatrix} . \tag{2.46}$$

Since the emitter is stationary and the measurement errors are uncorrelated, the addition of FIMs of different time steps is possible and

$$\mathbf{J}_{\mathrm{TDOA}}(\mathbf{x}) = \sum_{i=1}^{\mathrm{I}} \mathbf{J}_{\mathrm{TDOA}_{(a,b),i}}(\mathbf{x}) \tag{2.47}$$

yields the FIM for the emitter localization after I time steps. The inverse of the Fisher Information matrix yields the CRLB. The CRLB for the position estimation accuracy in 3-dimensional space is then given by

$$\sigma_{\mathbf{x}}^2 \geq \mathrm{tr}\left(\mathrm{J}_{\mathrm{TDOA}}(\mathbf{x})^{-1}\right) . \tag{2.48}$$

2.7.2 Correlated Measurement Errors

In contrast to the previously described scenario, consider a sensor network with N spatially separated and stationary sensor nodes. Each observer takes a measurement either by estimating TOAs at each sensor node and using those to generate a TDOA measurement set or by directly measuring the TDOAs from the received signals (for example by cross correlation). When using 4 or more sensors for a 3D localization scenario (or 3 or more sensors for a 2D scenario), a position estimate can be calculated using only measurements from one time step. Different from the previous scenario, the measurements however have correlated errors. Again, the TDOA measurement errors are usually modeled using the TOA measurement variances of each sensor node. The TDOA variance is then given by $\sigma^2_{\tau_{(a,b),i}} = \sigma^2_{\tau_{a,i}} + \sigma^2_{\tau_{b,i}}$, where $\sigma^2_{\tau_{n,i}}$ is the TOA variance for sensor node n. Since only one time step is considered, for better readability the time index i is omitted in the following equations.

The Fisher Information matrix for the TDOA based emitter localization problem using a sensor network with N sensor nodes and correlated measurement errors is then given by

$$\mathbf{J}_{\mathrm{TDOA}}(\mathbf{x}) = \begin{bmatrix} \frac{\partial \tau_{(1,2)}}{\partial x_e} & \frac{\partial \tau_{(1,3)}}{\partial x_e} & \cdots & \frac{\partial \tau_{(1,N-1)}}{\partial x_e} \\ \frac{\partial \tau_{(1,2)}}{\partial y_e} & \frac{\partial \tau_{(1,3)}}{\partial y_e} & \cdots & \frac{\partial \tau_{(1,N-1)}}{\partial y_e} \\ \frac{\partial \tau_{(1,2)}}{\partial z_e} & \frac{\partial \tau_{(1,3)}}{\partial z_e} & \cdots & \frac{\partial \tau_{(1,N-1)}}{\partial z_e} \end{bmatrix} \mathbf{R}^{-1} \begin{bmatrix} \frac{\partial \tau_{(1,2)}}{\partial x_e} & \frac{\partial \tau_{(1,2)}}{\partial y_e} & \frac{\partial \tau_{(1,2)}}{\partial z_e} \\ \frac{\partial \tau_{(1,3)}}{\partial x_e} & \frac{\partial \tau_{(1,3)}}{\partial y_e} & \frac{\partial \tau_{(1,3)}}{\partial z_e} \\ \vdots & \vdots & \vdots \\ \frac{\partial \tau_{(1,N-1)}}{\partial x_e} & \frac{\partial \tau_{(1,N-1)}}{\partial y_e} & \frac{\partial \tau_{(1,N-1)}}{\partial z_e} \end{bmatrix}, \tag{2.49}$$

with $\mathbf{R}$ being the matrix of the measurement variances

$$\mathbf{R} = \begin{bmatrix} \sigma_{\tau_1}^2 + \sigma_{\tau_2}^2 & \sigma_{\tau_1}^2 & \cdots & \sigma_{\tau_1}^2 \\ \sigma_{\tau_1}^2 & \sigma_{\tau_1}^2 + \sigma_{\tau_3}^2 & \cdots & \sigma_{\tau_1}^2 \\ \vdots & \vdots & \ddots & \vdots \\ \sigma_{\tau_1}^2 & \sigma_{\tau_1}^2 & \cdots & \sigma_{\tau_1}^2 + \sigma_{\tau_{N-1}}^2 \end{bmatrix}, \tag{2.50}$$

For the sake of completeness, the corresponding Fisher Information matrix for the TOA based emitter localization problem with unknown time of emission is given. The unknown time of emission t_e is regarded as nuisance parameter which results in a constant in the FIM. The FIM is given by

$$\mathbf{J}_{\mathrm{TOA}}(\mathbf{x}) = \begin{bmatrix} \frac{\partial \tau_1}{\partial t_e} & \frac{\partial \tau_2}{\partial t_e} & \cdots & \frac{\partial \tau_N}{\partial t_e} \\ \frac{\partial \tau_1}{\partial x_e} & \frac{\partial \tau_2}{\partial x_e} & \cdots & \frac{\partial \tau_N)}{\partial x_e} \\ \frac{\partial \tau_1}{\partial y_e} & \frac{\partial \tau_2}{\partial y_e} & \cdots & \frac{\partial \tau_N}{\partial y_e} \\ \frac{\partial \tau_1}{\partial z_e} & \frac{\partial \tau_2}{\partial z_e} & \cdots & \frac{\partial \tau_N}{\partial z_e} \end{bmatrix} \mathbf{R}_{\mathrm{TOA}}^{-1} \begin{bmatrix} \frac{\partial \tau_1}{\partial t_e} & \frac{\partial \tau_1}{\partial x_e} & \frac{\partial \tau_1}{\partial y_e} & \frac{\partial \tau_1}{\partial z_e} \\ \frac{\partial \tau_2}{\partial t_e} & \frac{\partial \tau_2}{\partial x_e} & \frac{\partial \tau_2}{\partial y_e} & \frac{\partial \tau_2}{\partial z_e} \\ \vdots & \vdots & \vdots & \vdots \\ \frac{\partial \tau_N}{\partial t_e} & \frac{\partial \tau_N}{\partial x_e} & \frac{\partial \tau_N}{\partial y_e} & \frac{\partial \tau_N}{\partial z_e} \end{bmatrix}, \tag{2.51}$$

with $\mathbf{R}_{\mathrm{TOA}}^{-1}$ being the measurement covariance matrix:

$$\mathbf{R}_{\mathrm{TOA}} = \begin{bmatrix} \sigma_{\tau_1}^2 & 0 & \cdots & 0 \\ 0 & \sigma_{\tau_2}^2 & \cdots & 0 \\ \vdots & \vdots & \ddots & \vdots \\ 0 & 0 & \cdots & \sigma_{\tau_N}^2 \end{bmatrix}, \tag{2.52}$$

When using the inverted matrix $\mathbf{J}_{\mathrm{TOA}}^{-1}$

$$\mathbf{A} = \begin{bmatrix} [\mathbf{J}_{\mathrm{TOA}}^{-1}]_{22} & [\mathbf{J}_{\mathrm{TOA}}^{-1}]_{23} & [\mathbf{J}_{\mathrm{TOA}}^{-1}]_{24} \\ [\mathbf{J}_{\mathrm{TOA}}^{-1}]_{32} & [\mathbf{J}_{\mathrm{TOA}}^{-1}]_{33} & [\mathbf{J}_{\mathrm{TOA}}^{-1}]_{34} \\ [\mathbf{J}_{\mathrm{TOA}}^{-1}]_{42} & [\mathbf{J}_{\mathrm{TOA}}^{-1}]_{43} & [\mathbf{J}_{\mathrm{TOA}}^{-1}]_{44} \end{bmatrix}, \tag{2.53}$$

it can be shown that $\mathbf{A} = \mathbf{J}_{\mathrm{TDOA}}^{-1}$ (see [SHM10]).

2.7.3 Choosing the adequate CRLB

Investigations concerning the CRLBs and the comparison of TDOA and TOA based emitter geolocation with unknown time of emission are for example conducted by [SHM10, Kau12]. Both papers seem to use different assumptions concerning the measurements that are taken. Since the goal of both is to compare TDOA and TOA based emitter localization, the measurement errors are modeled like described in the

previous section with $\sigma^2_{\tau_{(a,b)}} = \sigma^2_{\tau_a} + \sigma^2_{\tau_b}$. In all cases, the TOA measurement errors $\sigma^2_{\tau_n}$ are assumed to be uncorrelated $\forall n \in N$.

The CRLB on emitter localization depends on the measurements that are actually taken and not on how the measurements are processed into a localization result. Therefore, when gaining TDOAs by using TOA measurements, it is not important if the measurement set using a reference sensor (see Eq. (2.6)) or the full measurement set (see Eq. (2.7)) is used by the estimator. The overall lower bound for the estimation problem in both cases is as described in Section 2.7.2. For the CRLB, the measurement $\tau_{(2,3)}$ does not carry any further information on the emitter location, if the measurements $\tau_{(1,2)}$ and $\tau_{(1,3)}$ are already considered, since they all depend on the same three TOA measurements τ_1, τ_2 and τ_3. Thus, $\tau_{(2,3)}$ does not introduce any new information. The estimator however will profit from using the full measurement set.

While both papers come to the conclusion that the theoretical bounds of TDOA and TOA localization are identical, the TDOA models and the results of Monte-Carlo simulations differ. In [SHM10], it is shown that the CRLBs are identical. The employed bound for TDOA based localization is like described in Section 2.7.2. In [Kau12], it is shown that the choice of the reference sensor does not influence the CRLB if the measurement noise $\sigma^2_{\tau_{(m)}}$ is the same for all $m \in M$. Additionally, a CRLB using the full measurement set is presented. This bound is smaller than the one using a reference sensor. However, we believe that this bound is not applicable for this scenario under the assumptions that were taken since $\tau_{(2,3)}$ does not introduce any new information if $\tau_{(1,2)}$ and $\tau_{(1,3)}$ are used and the measurements are calculated using the same TOA estimates. For other scenarios, this bound might be valid.

The Monte-Carlo simulations in both papers differ. While in [SHM10], TOA outperforms TDOA based localization, in [Kau12], both methods achieve results of similar accuracy. This is probably due to the fact, that in [SHM10], the TDOA estimator only relies on the measurement set using a reference sensor, while in [Kau12], the full measurement set is used. An estimator that uses the full set outperforms an estimator using the measurement set with a reference sensor. Solving the localization problem using only the TDOA set with a reference sensor only means using an inefficient estimator. We believe the main theses and results concerning the comparison of TOA and TDOA based localization of both papers to be absolutely valid.

In conclusion, TOA and TDOA based geolocation are shown to have the same CRLB and both estimation problems can be solved with very similar performance. To reach the same performance as a TOA estimator, a TDOA estimator should use the full

measurement set.

2.7.4 Comparison of the CRLB to Monte-Carlo Simulations

2.7.4.1 Correlated Measurement Errors

To show the validity of the CRLBs presented in the previous sections and the applicability to the investigated localization scenarios of this thesis, the bounds are compared to Monte-Carlo simulations.

As stated in Section 2.7.3, the current research on the comparison of TOA and TDOA based geolocation seems a bit vague concerning the choice of the bound which is valid for a given scenario. This probably is due to the assumptions on measurement error correlation. Let us assume a scenario, where TOA measurements are gained. Those measurements τ_n, $n \in \{1, ..., N\}$ are defined by Eq. (2.2). Usually, additive zero-mean Gaussian distributed noise is assumed. Thus a TOA measurement of observer n at time step i is given by

$$\hat{\tau}_{n,i} = \frac{||\triangle p_n(\mathbf{x})||}{c} + v_{n,i}, \quad v_{n,i} \sim \mathcal{N}(0, \sigma^2_{\tau_{n,i}}), \tag{2.54}$$

where v is zero-mean Gaussian noise with variance $\sigma^2_{\tau_{n,i}}$. The TOA measurement errors of different observers and different time steps can be assumed to be uncorrelated. If a TDOA measurement set is generated on the basis of a TOA measurement set, the TDOAs are clearly not uncorrelated. Additionally, some TDOA measurements may not carry any new information on the emitter location if they are based on two TOAs that are already considered in other TDOA measurements. For example, if the two TDOA measurements $\hat{\tau}_{(1,2)} = \hat{\tau}_1 - \hat{\tau}_2$ and $\hat{\tau}_{(1,3)} = \hat{\tau}_1 - \hat{\tau}_3$ are used, the TDOA $\hat{\tau}_{(2,3)} = \hat{\tau}_2 - \hat{\tau}_3$ is only composed of information that is already available and used. In our opinion, the CRLB cannot make use of all three TDOAs since this would result in a bound that relies on assumptions that are not valid for the investigated scenario.

The CRLB using the full measurement set (which should not exist in this scenario setup) is compared to the CRLB with a reference sensor described in Section 2.7.2. A Monte-Carlo simulation using two TDOA and a TOA estimator is implemented to show the validity of the CRLB using a reference sensor. A two-dimensional scenario with 8 sensor nodes is investigated. A signal is emitted by an unknown target, and is received by each sensor node which estimates a corresponding TOA $\hat{\tau}_n$, $n \in \{1, ..., N\}$. Zero-mean Gaussian noise is added to the error free TOA measurements. From those TOAs, the TDOA measurement set using a reference sensor (w.l.o.g. sensor 1) and

the full TDOA measurement set are generated. The corresponding CRLB for the full measurement set, as well as for the set using a reference sensor are calculated as described by [Kau12].

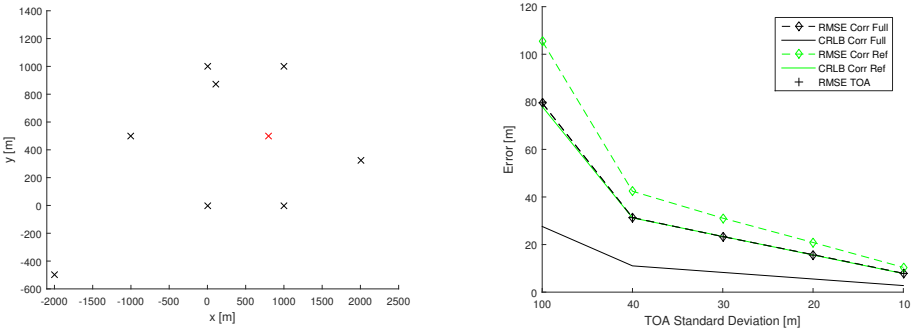

(a) **(b)**

Figure 2.6: (a) Scenario with 8 observers (black cross) and emitter position 1 (red cross). (b) Simulation results.

Two emitter positions (see red cross Fig. 2.6a and Fig. 2.7a) are chosen to exemplary show the comparison of the CRLB to the results of the corresponding Monte-Carlo simulations. One target position lies outside of the sensor network geometry, the other on the inside. The TOA of the signal at each sensor node is calculated according to Eq. (2.2). Zero-mean Gaussian noise with standard deviation σ_{τ_n} is added to the true TOA values. The standard deviation is constant and the same for all sensor nodes $\sigma_{\tau_n}\ \forall n \in \{1, ..., N\}$. Therefore, the resulting TDOA measurements are correlated. Five different values for the TOA measurement standard deviation are considered: $\sigma_{\tau_n} \in \{10, 20, 30, 40, 100\}$ m. For each emitter position and standard deviation, 5000 Monte-Carlo runs are conducted.

Figures 2.6b and 2.7b depict the results of the simulation versus the CRLB for target position 1 and 2, respectively. The CRLB of the reference sensor set is shown as a green line, the CRLB using the full set using a black line. The RMSE (root mean square error) of the Monte-Carlo simulation is plotted in dashed lines. Additionally, the simulation results using a TOA estimator are given by black +.

Both, the TOA and the TDOA estimator using the full measurement set are almost identical and are close to the CRLB using the reference sensor. The TDOA estimator that uses the measurement set using a reference sensor shows worse performance. The

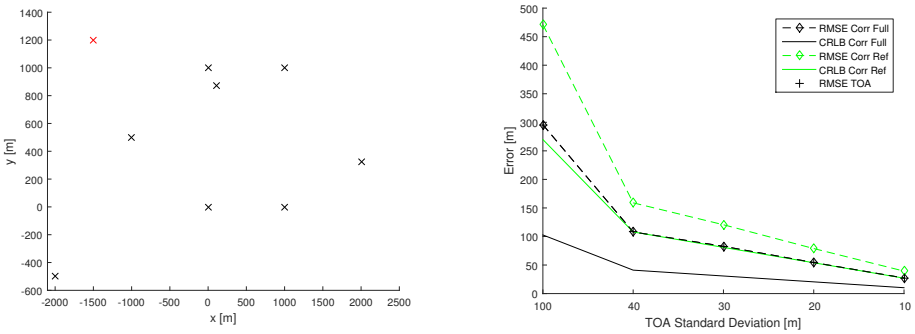

(a) **(b)**

Figure 2.7: (a) Scenario with 8 observers (black cross) and emitter position 2 (red cross). (b) Simulation results.

CRLB that is based on the full measurement set is way lower and is not reached by any of the estimators.

The results support the theory concerning the above made assumption on the TDOA based CRLB when TDOAs are generated from TOAs. The CRLB using a reference sensor is to be used in this kind of scenario. Using an estimator that is based on the TDOA measurement set using a reference sensor yields worse results than an estimator that uses the full set whose accuracy is of the same magnitude or even identical as the one of a TOA estimator. Thus, to solve the localization problem, either a TDOA estimator using the full TDOA measurement set or a TOA estimator which estimates the time of emission along with the position of the target is to be used.

2.7.4.2 Uncorrelated Measurement Errors

To show the impact of the TDOA measurement correlation, the same simulations are performed for uncorrelated TDOA measurements. The CRLB for the measurement set with a reference sensor as well as the full set are calculated. Monte-Carlo simulations using the corresponding estimators were conducted.

The TDOA measurements are generated by calculating the true TDOA according to Eq. (2.5) and adding zero-mean Gaussian noise. The measurement variance for a sensor pair (a, b) is given by the corresponding TOA variances $\sigma^2_{\tau_{(a,b)}} = \sigma^2_{\tau_a} + \sigma^2_{\tau_b}$.

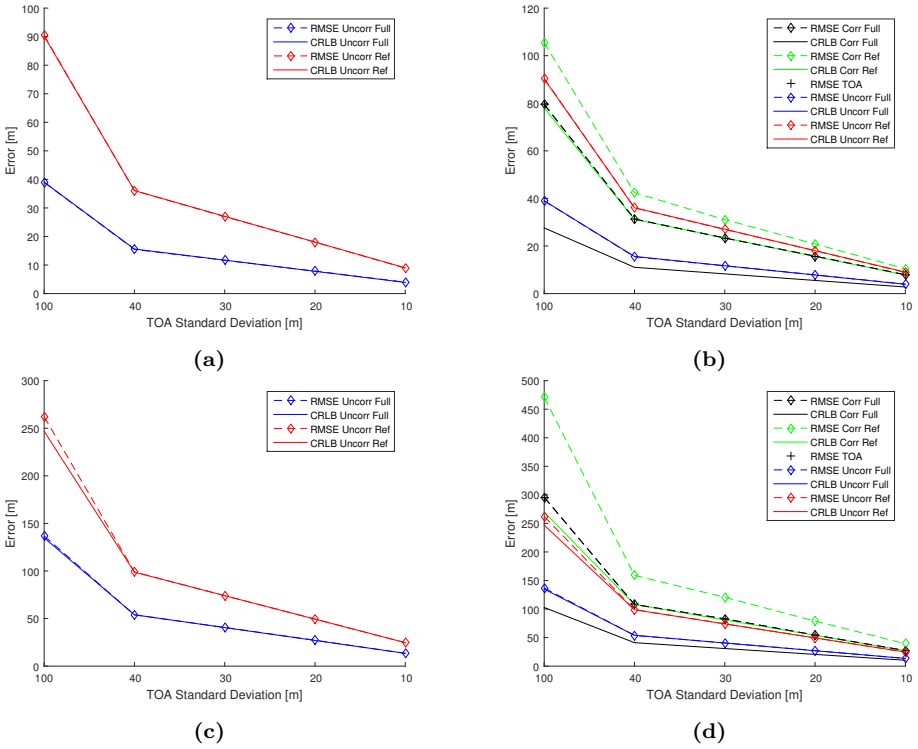

Figure 2.8: Simulation results for emitter position 1 showing (a) uncorrelated and (b) all measurements and for emitter position 2 showing (c) uncorrelated and (d) all measurements.

Since the independent noise is added directly to each TDOA measurement $\hat{\tau}_{(a,b)}$, the measurement errors of $\hat{\tau}_{(1,2)}$, $\hat{\tau}_{(1,3)}$ and $\hat{\tau}_{(2,3)}$ are now uncorrelated.

In a real world application, a scenario with stationary sensors and these error assumptions is highly unlikely if not nonexistent. However, it is useful to investigate the scenarios to verify the bounds and employed estimators. A valid scenario would be for example using two moving emitters and taking TOA/TDOA measurements over time.

Fig. 2.8a and Fig. 2.8c show the results for emitter position 1 and 2, respectively. The used estimators attain the corresponding CRLB. Fig. 2.8b and Fig. 2.8d depict the comparison of the results using the reference sensor and full measurement set

including correlated and uncorrelated measurements.

The results suggest, that the implemented estimators are efficient and reach the CRLB. Because all estimators use identical methods to solve the non-linear estimation problem, again the theoretical assumptions concerning the full measurement set seem valid. It should not be used in the CRLB calculation for TDOA based emitter localization since in the case of correlated TDOA measurements gained from TOA measurements, the full set suggests more information on the emitter location than it really contains.

2.8 Position Estimation Methods for TDOA based Emitter Localization

Usually, the TDOA localization problem is solved in a two step approach. The first step is to measure the TDOA of a signal received at two dislocated sensor positions. This can be done by either determining a TOA for each sensor and then subtracting those TOAs or by directly measuring the TDOA of the received signals. In the second step, a set of TDOA measurements (at least two measurements for 2D localization and three measurements for 3D localization) is used to estimate the location of the emitter.
The classic technique is to estimate the TDOA of two received signals by determination of the maximum of the cross correlation or cross ambiguity function (see Section 2.5). In some cases, it is possible to measure the time of arrival (TOA) of a received signal and to generate a corresponding timestamp in reference to a common clock (for example sensors synchronized to UTC using GPS). The TDOA measurement is then given by the difference of those TOAs. The TDOA measurement problem is discussed in Section 2.2.

Only in the ideal case without measurement uncertainty, the TDOA hyperbolae will have an intersection at the location of the emitter. When dealing with measurement noise, the hyperbolae will most probably not meet at a single point. With further distance from the observers and geometrical influences, even small errors induce a high position uncertainty (see Fig. 2.9). The emitter location now has to be estimated by determining the most probable position that best fits all measurements.

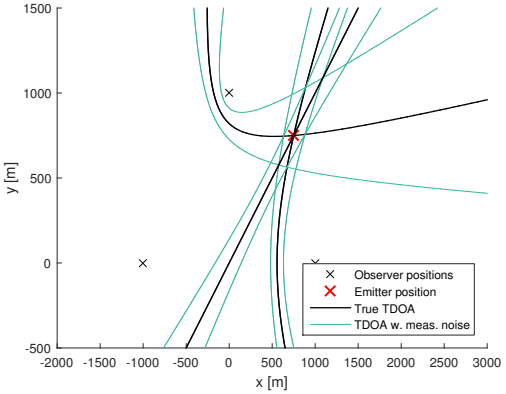

Figure 2.9: TDOA localization scenario with TDOA measurement errors.

There are several methods for TDOA based geolocation (step two) once a set of TDOA measurements is generated [CH94, Fri87, SA87, GS08, HC93]. An example for a closed-form solution is given in [GS08] which will be used in the evaluation of the field experiments given in Chapter 4. This closed-form algorithm is described in Section 2.8.1. Other techniques [Tor84] include maximum likelihood estimation or a diversity of filtering algorithms like Kalman filters [Koc14,MKK10]. The initialization of a bank of Kalman filters using Gaussian Mixtures is for example investigated in [DK10].

The TDOA measurement set can consist of measurements using a reference sensor or by using a full measurement set as described in Section 2.3.1. The resulting TDOA sets may include uncorrelated or correlated errors. The impact on the geolocation accuracy was discussed in Section 2.7.

When using for example the full TDOA measurement set which is given in Eq. 2.7, minimizing the squared error function with respect to the unknown emitter position $\mathbf{x}$ yields the most probable emitter location

$$\hat{\mathbf{x}} = \arg\min_{\mathbf{x}} \mathrm{TDOA}_{\mathrm{ML}}(\mathbf{x}) \,, \tag{2.55}$$

with

$$\mathrm{TDOA}_{\mathrm{ML}}(\mathbf{x}) = \sum_{m=1}^{M} \frac{\left(\tau_{(m)}(\mathbf{x}) - \hat{\tau}_{(m)}\right)^2}{\sigma^2_{\tau_{(m)}}} \,, \tag{2.56}$$

where $\tau_{(m)}(\mathbf{x})$ gives the TDOA that would have been measured by sensors a and b for an emitter being located at position $\mathbf{x}$ and the corresponding known sensor positions p_a and p_b.

The localization using TOA measurements with unknown time of emission could be interpreted as a special case of TDOA based localization (or vice versa). The achievable accuracy according to the CRLB of both approaches is identical as described in Section 2.7. Along with the emitter state (in this case the position $\mathbf{x} = (x_e, y_e, z_e)^T$), the unknown time of emission has to be estimated. For the CRLB analysis, it is considered a nuisance parameter and is not of direct interest for the results of the position estimation process.

For the TOA measurements collected by M observers, the most probable emitter location is given by the least squares function of

$$(\hat{\mathbf{x}}, \hat{t}_e) = \arg\min_{\mathbf{x}, t_e} \mathrm{TOA}_{\mathrm{ML}}(\mathbf{x}, t_e)\,, \tag{2.57}$$

with

$$\mathrm{TOA}_{\mathrm{ML}}(\mathbf{x}, t_e) = \sum_{m=1}^{M} \frac{\left(\tau_m(\mathbf{x}) - \hat{\tau}_m - t_e\right)^2}{\sigma^2_{\tau_m}}\,. \tag{2.58}$$

2.8.1 Closed-Form Solution

In this section, the closed-form TDOA position estimation algorithm presented in [GS08] is introduced. This method is used for the first step of the position estimation given in Chapter 4. A system of equations is used which additionally to the emitter state $\mathbf{x}$ involves the unknown distance $D_n = ||\triangle p_n(\mathbf{x})||$ between the observer n and the emitter.

The measurement set with reference sensor 1 can be used to give the following solution for the position estimation problem

$$\mathbf{A}\mathbf{x}_s = \mathbf{w}\,. \tag{2.59}$$

The matrix $\mathbf{A}$ is given by

$$\mathbf{A} = \begin{bmatrix} x_1 - x_2 & y_1 - y_2 & z_1 - z_2 & \hat{\tau}_{(1,2)} \\ x_1 - x_3 & y_1 - y_3 & z_1 - z_3 & \hat{\tau}_{(1,3)} \\ x_1 - x_4 & y_1 - y_4 & z_1 - z_4 & \hat{\tau}_{(1,4)} \\ \vdots & \vdots & \vdots & \vdots \\ x_1 - x_N & y_1 - y_N & z_1 - z_N & \hat{\tau}_{(1,N)} \end{bmatrix}, \tag{2.60}$$

where the emitter state with the additional unknown distance between emitter and reference sensor is

$$\mathbf{x}_s = \begin{bmatrix} x_e \\ y_e \\ z_e \\ D_1 \end{bmatrix}, \tag{2.61}$$

and the vector $\mathbf{w}$

$$\mathbf{w} = \begin{bmatrix} w_{(1,2)} \\ w_{(1,3)} \\ w_{(1,4)} \\ \vdots \\ w_{(1,N)} \end{bmatrix}, \tag{2.62}$$

with

$$w_{(a,b)} = \frac{1}{2}\left(\hat{\tau}_{(a,b)} - x_a^2 + x_b^2 - y_a^2 + y_b^2 - z_a^2 + z_b^2\right). \tag{2.63}$$

If the rows of $\mathbf{A}$ are linearly independent and $\mathbf{A}$ has at least the same rank as $\mathbf{x}_s$ has entries, the pseudo inverse of $\mathbf{A}$ is given by

$$\mathbf{A}^{\dagger} = \left(\mathbf{A}^T\mathbf{A}\right)^{-1}\mathbf{A}^T. \tag{2.64}$$

Using (2.59) and applying (2.64), the position of the emitter (along with the distance between observer and emitter) is estimated by

$$\mathbf{x}_s = \mathbf{A}^{\dagger}\mathbf{w}. \tag{2.65}$$

2.8.2 Direct Localization

For the TDOA geolocation technique, single step approaches have been introduced. Those methods are commonly called direct position determination (DPD). The location of the emitter is directly estimated from the raw signal data without explicitly calculating intermediate measurements [WA06, AW09, VKD14]. These techniques have also been applied to single moving observer scenarios for AOA measurements [ON10, Ois09] and will be described in Chapter 5 for the TDOA based localization [Ste15, SO15, SO16]. The key idea of direct position determination is to postpone the decision of a TDOA measurement into the localization step. For example in multipath environments, a wrong value for the TDOA might be chosen since the true TDOA is only the second probable TDOA value. However, when information from all sensor pairs is fused, this measurement does not fit the location of the

emitter. By linking the received signal data to the range domain and interpreting the data as likelihood function for the emitter location, the second probable TDOA (in this example the true TDOA) still adds information in the fused likelihood of all sensor data and thus improves the emitter location estimate.

The conventional two step localization approach requires a measurement and a localization step. In the measurement step, a TDOA measurement set is calculated by for example determining the maximum of the cross correlation function (see Section 2.5). Using this set, the emitter position is estimated by optimizing Eq. (2.55) with respect to $\mathbf{x}$. In the case of direct position determination, the determination of the maximum of the cross correlation function is omitted. Instead, the cross correlation functions of all considered sensor pairings are evaluated w.r.t. the emitter position in a single step.

Using the CCF (see Section 2.5)

$$\mathrm{CCF}_{(a,b)}(\mathbf{x}) = \sum_{k=1}^{K} z_a^*[k] z_b^{(\tau_{(a,b)}(\mathbf{x}))}[k]. \,, \tag{2.66}$$

with the conjugate complex $f^*[k]$ of the function $f[k]$, the time-shifted sampled version $f^{(\tau)}[k]$ of $f(t-\tau)$ and

$$\tau_{(a,b)}(\mathbf{x}) = \frac{||\triangle p_a(\mathbf{x})|| - ||\triangle p_b(\mathbf{x})||}{c} \,. \tag{2.67}$$

The localization problem is then stated by

$$\hat{\mathbf{x}} = \arg\min_{\mathbf{x}} \sum_{\substack{a=1 \\ a \neq b}}^{N} -|\mathrm{CCF}_{(a,b)}(\mathbf{x})| \,. \tag{2.68}$$

Example

The idea of direct position determination is illustrated using the following example. A scenario with 4 observers is considered. The emitted signal is recorded simultaneously by all sensors, only one measurement time step is considered. A chirp signal with a duration of 10 ms and a bandwidth of 1 MHz is digitized at a sampling rate of 2 MHz. The received signals are delayed by the propagation time of the signal between the corresponding sensor node and the emitter (see Eq. (2.1)) and zero-mean Gaussian noise is added. To show the benefit of using direct position estimation techniques,

the received signal of sensor 3 is overlain by a second delayed version of the emitter signal, simulating multipath propagation. The amplitude of the multipath signals is set to be higher than the line of sight (LOS) version. The localization process with and without the received multipath signal is evaluated.

For the two step approach, the full TDOA measurement set (see Eq. (2.7)) is calculated determining the maximum of the corresponding CCFs. The direct position estimation method uses the same CCFs in Eq. (2.68). The CCFs of the received signals z_1 and z_3 with and without the additional multipath signal are depicted in Fig. 2.10. As can be seen, the multipath signal causes a second peak in the CCF. Since the amplitude of the delayed signal was chosen to be higher than the LOS signal, this peak is the maximum of the CCF. If the conventional two step localization approach is used, one TDOA measurement is generated from each CCF. In this case, a wrong TDOA is selected. The information that the CCF shows a second prominent peak is discarded in this way. Using direct position determination, this information is preserved and takes effect in the localization.

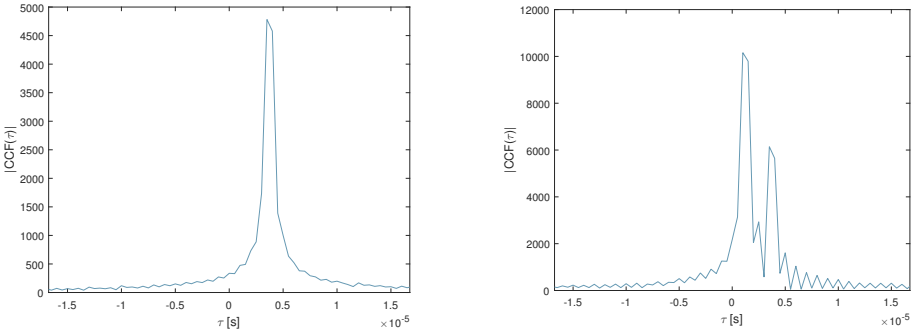

(a) **(b)**

Figure 2.10: Cross correlation function of signal z_1 and z_3. (a) without and (b) with additional multipath signal.

The results of the emitter localization are depicted in Fig. 2.11. The normalized localization cost functions (Eq. (2.55) and Eq. (2.68)) are evaluated over the plotted area. Figures 2.11a and 2.11b show the results for the scenario without multipath propagation. As can be seen, the TDOA hyperbolae (representing the TDOA measurements of the 2-step approach) intersect close to the true emitter position where the cost function has its minimum. Therefore, both methods give approximately the same localization result very close to the true emitter position.

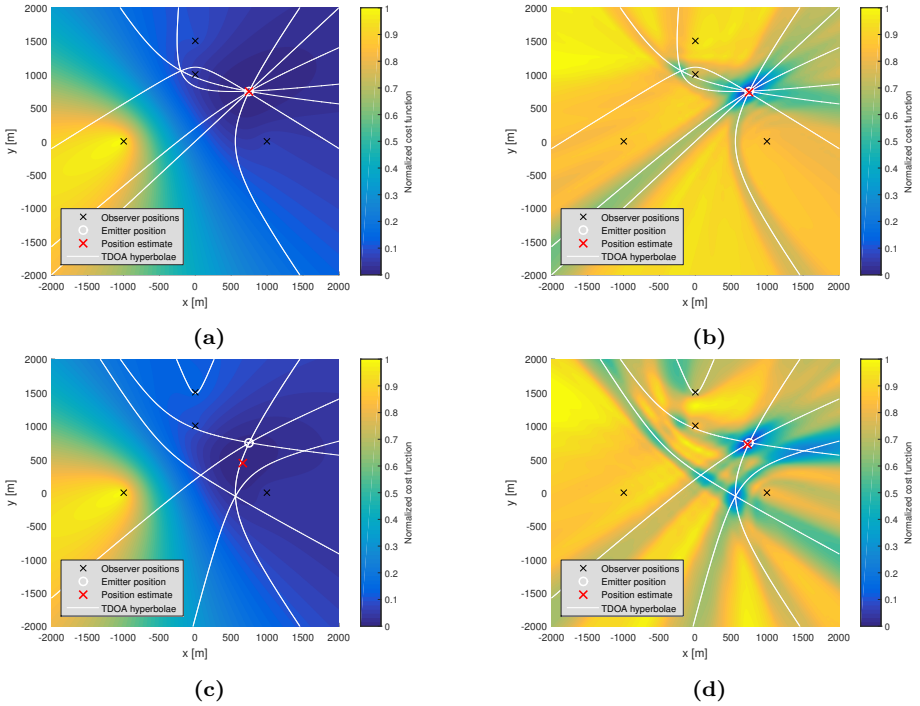

Figure 2.11: Localization cost functions and results. (a) 2-step localization without multipath (b) DPD-localization without multipath (c) 2-step localization with multipath (d) DPD-localization with multipath.

The evaluation of the scenario with multipath propagation at sensor 3 is depicted in Figures 2.11c and 2.11d. The TDOA hyperbolae no longer intersect in a single location. It can be observed, that the minimum of the cost function and thus position estimate of the 2-step approach is located between two intersection points. The advantage of direct position determination can clearly be seen in Fig. 2.11d. The multipath signal also causes lower values of the cost function at the intersection of the hyperbolae resulting from the maximums of the CCFs involving sensor 3. However, the second peak of the CCF (see Fig. 2.10b) also adds information to the localization process. Therefore, the minimum of the localization cost function (and the position estimate) is still close to the true emitter position.

2.9 Real World Error Sources

Real world emitter localization systems are subject to many sources of error which have impact on the accuracy of the position estimates. As already stated in the previous sections, the TDOA measurement is one error source in the process of passive emitter localization. The localization accuracy suffers from other faulty parameters as well.

One key factor for TDOA based geolocation is the synchronization of the sensor nodes. Radio frequency waves propagate at approximately speed of light in vacuum. Thus, a synchronization in the range of nanoseconds is required. Precise time synchronization of spatially separated sensor nodes can for example be achieved by using GPS, broadband reference signals with known emitter position or highly accurate local clocks. In the case of GPS loss at the sensor nodes for ADS-B airspace surveillance, stationary ADS-B transponders could be easily used as reference signal to adjust the local clocks. The precision of GPS based synchronization using oven controlled crystal oscillators (OCXO) of 20 ns or better is achievable. The 1 pulse per second (PPS) signal of the GPS receiver is used to discipline the local oscillator of the receiver. It was shown, that accuracies of the 1PPS signal between two flying platforms of 40 ns seem feasible [MH95]. For this analysis, cesium time standards were used as reference (which are also error prone to a certain degree).
The accuracy of synchronization using reference signals depends on the employed signals and the resulting SNR at the receiver nodes. Especially for applications in a small area of interest with high localization accuracy, extreme precise time synchronization is required which cannot always be implemented by receiver nodes which are synchronized using cabled references. Very high synchronization accuracy can be achieved with high sampling rates and suitable signals.

Another important topic with respect to the localization accuracy is the observer position uncertainty. For stationary sensor networks that are deployed for long use (for example monitoring stations that are permanently installed systems), the location of the sensor nodes can be determined very precisely. However, if the sensor nodes are moving or stationary for short time periods, the position of the observer has to be measured as well. For outdoor applications, GPS is often used to gather this information. However, uncertainties in the observer position also influence the position estimates of passive emitter localization systems [VGS10, HLK07]. This applies to almost all localization techniques like AOA, TDOA, TOA, FDOA or RSS (received signal strength).

CHAPTER III

Wide Area Multilateration using Signal Structure TOA Estimation

3.1 Motivation

Accurate knowledge of position information of aircrafts is mandatory for airspace surveillance and air traffic management (ATM). The state of the art technique consists mainly of three different systems:

1. Primary Surveillance Radar (PSR) where the position of the aircraft is determined using an active radar system on ground without the assistance of the aircraft in question.
2. Secondary Surveillance Radar (SSR) which uses a ground station to interrogate aircrafts to transmit their current altitude. The angle between ground station and the aircraft is then determined by the ground station and used along with the transmitted altitude to locate the aircraft.
3. Automatic Dependent Surveillance-Broadcast (ADS-B) where the aircraft automatically and periodically broadcasts its own position (determined by using an on-board GPS system and a barometer for the altitude information) to other planes and ground stations.

All three systems have advantages and drawbacks. To motivate this work, only some of them are mentioned here. The main disadvantage of PSR and SSR is that they are expensive, suffer from objections from the surrounding population and to achieve an area-wide airspace surveillance, a dense network resulting in high costs and a heavy usage of radar frequency bands is necessary.

ADS-B lacks of reliability since systems like GPS or barometric sensors may fail, position information may be incomplete or faulty and in the worst case, may even be actively spoofed. However, ADS-B telegrams can be used to determine the aircrafts position using multilateration methods without even considering the content of the broadcasted messages.

Therefore, by employing localization techniques that are based on a sensor network and the duration of signal wave propagation from emitter to receiver, the location of the plane emitting an ADS-B, Mode-S, Mode-A/C telegram can be estimated independently of the transmitted position information. Two methods that are suitable for such emitter geolocation are based on Time of Arrival (TOA) and Time Difference of Arrival (TDOA) estimation. Those techniques are referred to as passive emitter localization/tracking (PET) and multilateration (MLAT) and enable passively estimating the geolocation of an emitter. Because of parameters like signal bandwidth, modulation method and the known message structure, ADS-B is well suited for content-independent TOA/TDOA based aircraft position determination.

Employing TOA/TDOA based geolocation techniques as an expansion of PSR/SSR systems for airspace surveillance allows for a gap-free and not deceivable surveillance using a network of low cost sensor nodes. This kind of reliability concerning the knowledge of aircraft positions can enable a more flexible route planning and thus a time and fuel saving navigation at a very high security level.

Some of the work presented in this chapter and Chapter 4 was part of a project conducted by Fraunhofer FKIE which itself is based on our previous work given in [SKR11, KSR+12]. The results can be found in [SM16]. Some of this work resulted from a cooperation with a Master student and has appeared in [Mey16].

Very recently, TDOA based geolocation (multilateration) of aircrafts using ADS-B transponder signals has attracted much attention. Analysis concerning the localization of aircrafts or UAS using multilateration techniques are for example given in [NKGG16, NAK+16, JNB12, PMH11, DM03]. One key task is to detect aircrafts that send faulty position information by using multilateration [MBK+15b, MBK+15a] or AOA measurements [RRJS11]. A sensor network for research purposes has been set up to evaluate ADS-B data [SSL+14]. In other applications, the transmitted position of ADS-B messages is used to calibrate direction of arrival sensors or tracking radar systems [RBSS09, TX15, ZWLZ16].

Integrating UAS into the civilian airspace introduces many challenges such as sense and avoid. ADS-B is one technology to enable secure UAS flights [LS15, ZZL15].

Therefore, it is extremely important to have reliable position information of all airborne aircrafts.

ADS-B is subjected to many security concerns. The main concerns lie in spoofing, jamming and error prone position transmission due to faulty equipment. The reliability and security of ADS-B is thus also an investigated topic with ongoing research [BHB+16, Coo15, AOS+15].

An overview of the status of ADS-B integration into airspace surveillance and SESAR (Single European Sky ATM Research Programme) is for example given in [SMV11, Rek14].

3.2 Airspace Surveillance using Automatic Dependent Surveillance-Broadcast

The automatic and periodic transmission of position information by aircrafts is an extension to Secondary Surveillance Radar Mode-S communication. ADS-B messages are transmitted at the same center frequency of 1090 MHz like Mode A/C or Mode-S telegrams. In this section, only ADS-B telegrams which transmit *Airborne Position Messages* (APM) are described as an example. The process of measuring TOAs of received ADS-B, Mode-S and Mode-A/C data is valid for all transmitted telegrams.

The information that can be communicated using ADS-B are radar-independent data like the position of the aircraft (determined by the aircraft using GPS satellite navigation), the altitude (determined using an altimeter, see Section 3.3), the flight number or the ICAO (International Civil Aviation Organization) address of the aircraft. Those signals are broadcasted using a transponder to ground control stations and other planes that are equipped with an ADS-B-IN compatible transponder. ADS-B telegrams are divided into different message types. One type described in this section is the Airborne Position Message (see for example [Int13], [Int14]).

An ADS-B/Mode-S signal is always composed of two parts: a 8 μs long preamble and a data block. The data block is either 56 or 112 pulse time slots long. All pulses have a duration of 1 μs. This results in a data rate of 1 Mbit/s. ADS-B, Mode-S, Mode-A/C signals are modulated using pulse position modulation (PPM). A rising edge is used to modulate a transmitted bit with value 0 and a falling edge characterizes a bit with value 1. Figure 3.1 depicts a message telegram showing the duration of preamble, data block and pulse lengths.

The duration of the preamble is 8 μs. In this time, four pulses are sent at specified times. The time between the rising edge of the first pulse and the rising edge of the

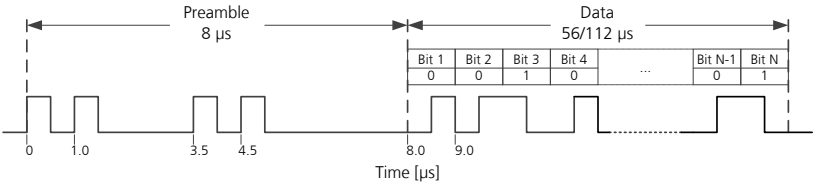

Figure 3.1: Signal structure of Mode-S/ADS-B communication using pulse position modulation according to [Int14].

Bit 1 - 5	Bit 6 - 8	Bit 9 - 32	Bit 33 - 88			Bit 89 - 112
DF	CA	AA ICAO	Airborne Position Message			PI
			41 - 52	55 - 71	72 - 88	
			Altitude	Latitude	Longitude	

Table 3.1: Message structure of a DF17 Airborne Position Message.

second pulse is 1 μs, between the first and the third pulse 3.5 μs and 4.5 μs between the first and the fourth pulse.

The data packet (valid for 56 μs and 112 μs long data blocks) starts with 5 bit downlink format (DF) information. Some of these formats are reserved for military purposes. The format number for ADS-B 1090ES (Extended Squitter), which includes the Airborne Position Message, is DF17. The following description applies to DF17 only and can be different for other downlink formats. The DF field is followed by a 3 bit CA (capability) field. The ICAO address of the aircraft is then transmitted using the 24 bit long AA (aircraft address) field. The message field for extended squitter is 56 bit long and in the case of APM includes CPR-encoded (Compact Position Reporting) latitude, longitude and altitude information. The last field is the 24 bit long parity information (PI) field which includes a checksum for error detection and will be described later. Table 3.1 gives an overview of the bit structure of an APM message.

Compact Position Reporting

To save transmission time, latitude and longitude position information in ADS-B messages are coded using Compact Position Reporting (CPR). This allows data reduction in the broadcast of the aircrafts position without losing accuracy. The position information (lat, lon) is transmitted according to the parity of the corresponding second, this position was measured in. The parity information is given in bit 54. If this bit is set to 1, the position data was gained during an odd second (*odd format*), if this bit is set to 0, a position in the *even format* related to an even second is transmitted. To be able to unambiguously determine the reported position, an ADS-B message in even and in odd position format is required. The temporary delay between those two messages should be small because some position information is assumed not to change over short periods of time (for example the information if the plane is located on the northern or southern hemisphere). Airborne Position Messages are 17 bits long which results in a position resolution of approximately 5 m [Radb].

When using CPR, the earth is divided into zones. There are $NZ = 15$ geographical latitude zones. This parameter sets the maximal range of the APM to 360 NM.
The number of longitude zones NL depends on the latitude given in degrees. It can be calculated using

$$NL(lat) = \text{floor}\left(2\pi\left[\arccos\left(1 - \frac{1-\cos\left(\frac{\pi}{2\cdot NZ}\right)}{\cos^2\left(\frac{\pi}{180^\circ}\cdot lat\right)}\right)\right]^{-1}\right), \tag{3.1}$$

where the number of NL lies between 59 ($lat = 0^\circ$) and 1 ($lat < -87^\circ$). The value is always rounded to the next smaller integer.

To calculate the geographical latitude, the size $DLat_i$ of the latitude zone in north-south direction is calculated using

$$DLat_i = \frac{360^\circ}{4\cdot NZ - i}. \tag{3.2}$$

The index i is given by bit 54 of the ADS-B message (odd format $i = 1$, even format $i = 0$).

The value YZ_i gives the Y-coordinate inside the current zone and is stated by

$$YZ_i = \text{floor}\left(2^{17}\cdot\frac{\text{mod}(lat, DLat_i)}{DLat_i} + \frac{1}{2}\right), \tag{3.3}$$

where mod denotes the modulo operation.

The reported latitude is then given by

$$RLat_i = DLat_i \cdot \left(\frac{YZ_i}{2^{17}} + \text{floor}\left(\frac{lat}{DLat_i} \right) \right) . \tag{3.4}$$

For the computation of the geographical longitude, at first, the size of the longitude zone in east-west direction is calculated using

$$DLon_i = \begin{cases} \frac{360^\circ}{NL(RLat_i)-i} & \text{,if } NL(RLat_i) - i > 0 \\ 360^\circ & \text{,if } NL(RLat_i) - i = 0 \end{cases} , \tag{3.5}$$

where $NL(RLat_i)$ is given in (3.1).

The X-coordinate XZ_i in the calculated longitude zone is

$$XZ_i = \text{floor}\left(2^{17} \cdot \frac{\text{mod}(lon, DLon_i)}{DLon_i} + \frac{1}{2} \right) . \tag{3.6}$$

The resulting decoded position information is finally given by

$$\begin{aligned} XZ_i &= \text{mod}(XZ_i, 2^{17}) \\ YZ_i &= \text{mod}(YZ_i, 2^{17}) . \end{aligned} \tag{3.7}$$

Along with the location of the aircraft in latitude and longitude direction (see (3.7)), the altitude is also encoded in the APM. This altitude information in feet is encoded using the 12 bit long altitude field. Bit 48 of the telegram contains the Q-bit which gives the multiplication factor for the decoded altitude (Q-bit = 1, factor = 25, Q-bit = 0, factor = 100). The remaining altitude bits are binary-coded with order most significant bit first. From the decoded decimal altitude, 1000 ft have to be subtracted to obtain the reported altitude in feet.

An example for the altitude decoding is given in the following. The altitude bits of the telegram are 110000111000 which results in a reported altitude of

$$
\begin{aligned}
Q &= 1 \\
A &= 1100001\ 1000 => 1560 \\
Alt_{[ft]} &= A \cdot 25 - 1000\,\text{ft} = 1560 \cdot 25 - 1000 = 38000\,\text{ft} \\
Alt_{[m]} &= 38000\ \text{ft} \cdot 0.3048 = 11582.4\,\text{m}\,.
\end{aligned} \tag{3.8}
$$

The decimal value of the binary coded altitude is 1560. Using the multiplication factor 25 according to Q-bit = 1 and subtracting 1000, the resulting altitude is 38000 ft $\approx$ 11.6 km.

A decoding of CPR-coded position information with only one received message is also possible. Instead of using an odd and an even format messages, a reference position is needed to determine in which latitude and longitude zone the computation is to be performed. This calculation is not described in this report but can be found in [Radb].

Cyclic Redundancy Check

Cyclic Redundancy Check (CRC) is a method to detect errors in digital communication which uses polynomial division to create a checksum of a bit sequence. The message content, that shall be transmitted, is used as a binary polynomial which is divided by a generator polynomial. The checksum that is gained in this way is attached to the message itself. By dividing this whole transmitted bit sequence with the generator polynomial, errors in the transmission of the data can be detected.

In the case of ADS-B, the CRC checksum that is attached to the ADS-B message data is 24 bits long. The used generator polynomial is given by

$$
\begin{aligned}
G(x) &= 1 + x^3 + x^{10} + x^{12} + x^{13} + x^{14} + ... + x^{23} + x^{24} \\
&= 1111111111111010000001001\,.
\end{aligned} \tag{3.9}
$$

To check if the telegram was transmitted correctly, the whole data is divided by the CRC generator polynomial. If the rest of this division equals zero, the signal transmission is error free.

3.3 Coordinate Systems and Altitude in Aviation

The established standard coordinate system used in navigation (for example GPS) or geodesy for global positioning is the World Geodetic System 1984 (WGS84). The input position information from the received ADS-B messages (and usually also from secondary surveillance radar systems) are given in WGS84. However, for the geolocation estimation, a local Cartesian coordinate system is much better suited. Thus, all input coordinates are transformed to a local ENU (East-North-Up) coordinate system using a given reference position. This is done using a transformation from WGS84 to an Earth-Centered, Earth-Fixed (ECEF) coordinate system and from ECEF to ENU. For the data evaluation presented in this report, the position of the reference sensor (see Section 4.3.1) is used as origin of the ENU coordinate system. The emitter localization and tracking is performed in the local coordinate system and afterwards, all results are transformed back to WGS84. The WGS84 coordinate system uses the WGS84 geoid to describe the gravitational equipotential surface of the earth which defines the mean sea level.

When referring to "altitude" or "height" information, especially in aviation applications, a clear distinction of the nomenclature is mandatory. In general, the term "true altitude" refers to the elevation of an object above the mean sea level (MSL), whereas the "absolute altitude" gives the height of the aircraft over the terrain below it (above ground level, AGL).

In aviation, height information is given in barometric altitudes which are characterized by three-letter Q-codes. The "QNH altitude" is the altitude information of the altimeter in the aircraft when set to local barometric pressure at MSL. The altitude at MSL is then 0 ft or m. If the altimeter is set and adjusted to "QFE altitude", the altitude 0 ft/m refers to the altitude of the airfield the altimeter was adjusted to. QFE altitudes can be used when flying in the proximity of the departure airfield at low altitudes. "QNE altitude" refers to the pressure altitude above a standard datum air pressure plane and is used in aviation after reaching a certain height (this height varies for different continents/countries) to give the flight level (FL) of the aircraft.

All mentioned Q-code altitudes are only accurate to a certain degree, since the assumed pressure models do not reflect real air pressure especially when dealing with different weather conditions. However, altitude separation of aircrafts is unproblematic because all planes at a certain FL will have the same barometric altitude offset compared to the true altitude when set to standard pressure altitude QNE.

ADS-B uses barometric altitude information and thus may induce an offset between the transmitted and the true altitude over MSL. For the position estimation of the

aircraft using TOA/TDOA based geolocation, all sensor positions are given in WGS84 and the calculations are performed in a local ENU coordinate system. The estimated altitude will then always refer to altitude over geoid or true altitude. The evaluation in the following chapters concerning the localization accuracy of TOA/TDOA position estimates with respect to the altitude is only possible to a certain degree since the true 3-dimensional position of the aircraft is unknown. The ADS-B position which is used as ground truth is error prone due to the described deviations of the barometric altitude information. This matter will be addressed in the corresponding chapters.

3.4 TOA Determination of ADS-B Transponder Signals

To reduce the communication requirements in a multilateration sensor network, one could either compress the received raw signal data or determine TOA timestamps and only transmit those timestamps and a message identification. The estimation of an accurate TOA and a corresponding message ID is not possible for arbitrary signals but is the preferable solution if applicable since it allows a drastic reduction of communication requirements. ADS-B transponder communication is perfectly suited to be used in a multilateration sensor network with TOA estimation. The signals have a high bandwidth, which promises a precise time resolution, and can easily be decoded and thus a message ID can be generated.

In [SKR11], we introduced a highly accurate TOA estimation method for ADS-B transponder signals which makes use of the known signal structure. In the following, this technique is described and an evaluation of the approach is given. For the field experiments and the evaluation of TDOA/TOA based geolocation of aircrafts sending ADS-B transponder signals given in Chapter 4, the presented TOA estimation could not be used, since a sensor system with no accessibility to the signal processing needed to be used. However, in [KSR+12], we showed that with the use of this TOA estimation method, the localization and tracking of aircrafts sending ADS-B messages using a sensor network with four sensor nodes is feasible and a good localization performance was achieved. These studies paved the way for the work presented in Chapter 4. The comparison of the accuracy of our TOA estimation method (see Section 3.4.2) to the TOA accuracy of the employed sensor network in Chapter 4 (see Section 4.2) indicates, that our approach allows even more precise timestamping than the Radarcape sensors used in Chapter 4.

3.4.1 Method Description, Signal Processing

The key idea of the approach is to use the known signal structure and modulation of ADS-B/Mode-S telegrams (described in Section 3.2) to estimate a highly precise time of arrival for each received message. At first, messages are detected in the raw signal data using a moving average filter. If a message candidate is found (see Fig. 3.2), the corresponding subset of the signal data is correlated with a simulated preamble (see Fig. 3.3), thus giving a raw estimate of the start of the message preamble. In a second step, the samples corresponding to the message itself are shifted over a simulated synchronization clock making use of the signal modulation technique (pulse position modulation). Taking the local clock of the sensor, which is used to relate the received samples to a common time (for example UTC), into account, a timestamp for the

message arrival at the sensor node is calculated. The accuracy of the TOA estimation process can further be increased by using signal interpolation which technically doesn't add information but gives finer time resolution of the sampled signal data.

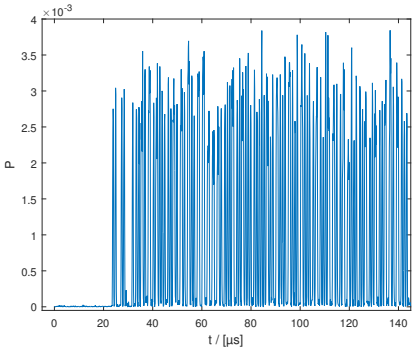

Figure 3.2: Absolute value of a digitized ADS-B signal (112 μs long data block).

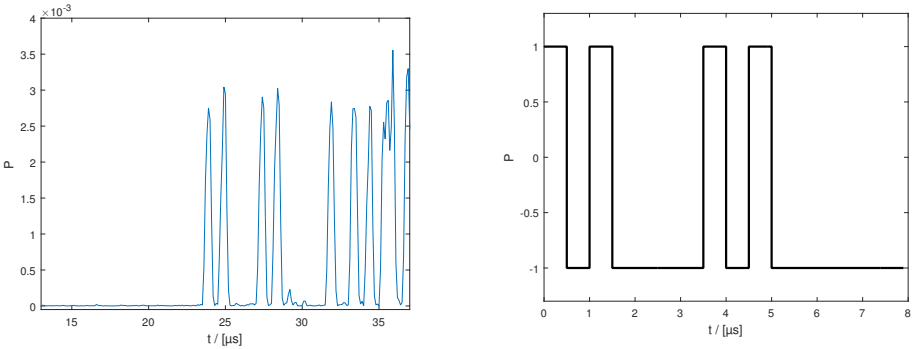

Figure 3.3: (a) Absolute value of the preamble of a received signal and (b) simulated ADS-B preamble.

3.4.1.1 Correlation with the preamble

Each ADS-B message starts with the same preamble to indicate the arrival of a new message. To determine the first edge of the message the signal is correlated with the simulated ideal preamble shown in Fig. 3.4.

Over the interval of $[0; 8\,\mu s[$ the ideal preamble can be described [1] by

$$p[t] = 2\left[\text{rect}(\frac{t-t_0}{T}) + \text{rect}(\frac{t-t_1}{T}) + \text{rect}(\frac{t-t_2}{T}) + \text{rect}(\frac{t-t_3}{T})\right] - 1 \tag{3.10}$$

with

$$T = 0.5\,\mu s,\ t_0 = 0.25\,\mu s,\ t_1 = 1.25\,\mu s,\ t_2 = 3.75\,\mu s,\ t_3 = 4.75\,\mu s,$$

where T is the pulse duration and the t_i, $i = 0, \ldots, 3$, are the displacements of the pulses in t-direction.

The discrete correlation function $\text{CCF}(\tau)$ is defined as

$$\text{CCF}(\tau) = \sum_{k=1}^{K} z_1^*[k] z_2^{(-\tau)}[k]\,, \tag{3.11}$$

i.e. from the correlation of the two signals $z_1[k]$ and $z_2[k]$ in time domain, $z^*[k]$ denotes the conjugate complex of the function $z[k]$.

To determine the first sample of the preamble,

$$\text{CCF}(\tau) = \sum_{k=1}^{K} z^*[k] p^{(-\tau)}[k]\,, \tag{3.12}$$

is evaluated, where z denotes the discrete time signal segment and p the simulated preamble respectively.

The estimate for the TOA of the preamble is calculated by detecting the peak in the CAF:

$$\hat{\tau} = \arg\max_{\tau} |\text{CCF}(\tau)|\,. \tag{3.13}$$

Fig. 3.4a depicts the correlation process. In Fig. 3.4b, the resulting correlation function is shown.

The argument at the maximum of the correlation function gives the required sample number. Division by the sampling rate f_s yields the time in seconds where the preamble of the ADS-B message begins relative to the start of the recorded signal. As defined in [Radb], the message starts $8\,\mu s$ after the begin of the preamble. Therefore, the time measurement $\hat{\tau}_{\text{preamble}}$ of the first edge of the signal is defined as

$$\hat{\tau}_{\text{preamble}} = \frac{\arg\max_{\tau} |\text{CCF}(\tau)|}{f_s} + 8\,\mu s. \tag{3.14}$$

[1] For the definition of the rect function see [OL02]

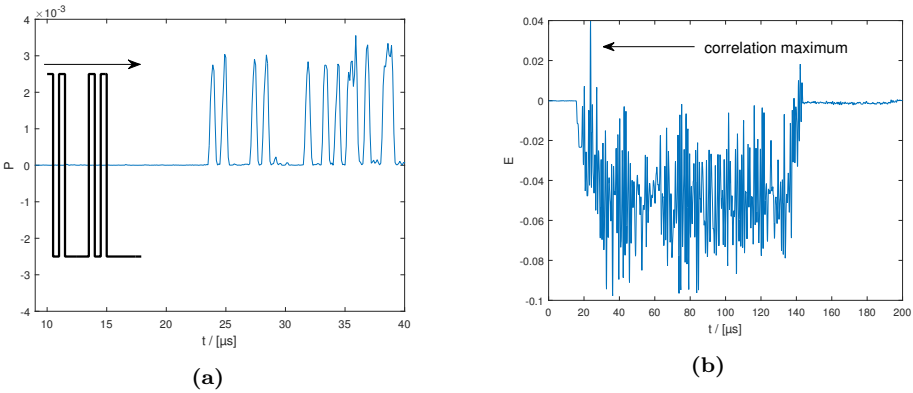

(a) **(b)**

Figure 3.4: (a) Simulated preamble and signal segment and (b) correlation function of signal and preamble.

3.4.1.2 Timestamp generation

Alignment of a synchronization clock with the beginning of the message is essential to get an accurate TOA measurement and to decode the message. To determine a more precise timestamp for the beginning of the message and to decode the messages bit string, the signal is shifted samplewise over a simulated 1 Mbit/s synchronization clock. Since an approximate sample index of the start of the message can be derived from Eq. (3.14), only a shift by a small number of samples is needed to identify the exact message start. After each shift, the absolute values of the derivative of the signal power during positive clock cycles are summed up. The maximum of these sums gives the optimal envelope of falling and rising edges in positive clock cycles. It characterizes the best alignment of message and clock and yields the sample shift for synchronization. A rising edge of the signal corresponds to a bit with value 0 whereas a falling edge characterizes the bit 1. Therefore, the derivative of the signal is positive during a rising edge and negative for falling edges. Fig. 3.5 shows the signal and the first derivative of the signal plotted over the synchronization clock.

Let n_{start} denote the number of samples the signal needs to be shifted to best match the clock. The TOA timestamp $\hat{\tau}_{a,i}$ of the message received by sensor a at measurement step i is then defined as

$$\hat{\tau}_{a,i} = \hat{\tau}_{\text{preamble}} + \frac{n_{start}}{f_s}. \tag{3.15}$$

The evaluation of the presented method is given in Section 3.4.2.

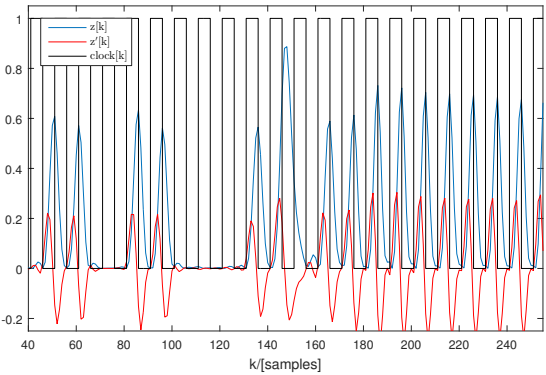

Figure 3.5: Absolute value of the signal and its first derivative over synchronization clock.

3.4.2 Method Evaluation

The goal of our trials is to determine the accuracy of gaining TOA measurements, the precision of timestamp generation for incoming ADS-B messages. Two different measurement trials are performed. In the first measurement setup, two sensors share one RF antenna to determine the error which results from GPS time synchronization and our timestamp generation without having to deal with different (maybe unknown) signal propagation delay.

The expectation of the TDOA $\tau_{(a,b)}$ is given by

$$\mathrm{E}\left[\tau_{(a,b)}\right] = 0\,. \tag{3.16}$$

Since the errors of the TOA measurements themselves cannot be determined, the variance error of the TDOA measurement, which is defined by $\sigma^2_{\tau_{(a,b)}} = \sigma^2_{\tau_a} + \sigma^2_{\tau_b}$, at least allows a conclusion on the behavior of the sensors when used in a TDOA sensor network. The TDOA measurement error for this setup including other systematic errors like GPS time synchronization is directly given by the TDOA measurement $\hat{\tau}_{(a,b)}$ itself.

In a second trial, each sensor is equipped with an own RF antenna. These second experiments are performed in order to show that our results are not constrained by the factor that both sensors share one reception antenna. The sensors and antennas were built up at very narrow distances to each other so that $\mathrm{E}\left[\tau_{(a,b)}\right] \approx 0$.

The variance of the TDOA measurement is given by

$$\sigma^2_{\tau_{(a,b)}} = \sigma^2_{\tau_a} + \sigma^2_{\tau_b}\,, \tag{3.17}$$

where $\sigma^2_{\tau_n}$ denotes the variance of the TOA estimation of sensor n. As already stated in Section 2.3, $\tau_{(m)} = \tau_{(a,b)}$ refers to a TDOA with measurement index m taken by a sensor pair (a, b), whereas τ_m denotes a TOA. The variances are denoted accordingly.

For the evaluation of the timestamp accuracies, the mean and standard deviation of the TDOA measurements are given by

$$\mu_{\hat{\tau}_{(M),i}} = \frac{1}{IM} \sum_{i=1}^{I} \sum_{m=1}^{M} \tau_{(m),i} - \hat{\tau}_{(m),i}\,. \tag{3.18}$$

and

$$\sigma_{\hat{\tau}_{(M),i}} = \sqrt{\frac{1}{IM} \sum_{i=1}^{I} \sum_{m=1}^{M} ((\tau_{(m),i} - \hat{\tau}_{(m),i}) - \mu_{\hat{\tau}_{(m),i}})^2}\,, \tag{3.19}$$

where M is the number of TDOA measurements, the ground truth $\tau_{(m),i} = 0$, $\forall m \in \{1, ..., M\}\,, i \in \{1, ..., I\}$ and $\hat{\tau}_{(m),i}$, $m \in \{1, ..., M\}$ denotes the TDOA measurement set at time step i (here, a time step equals one received ADS-B message). In this case, the TDOA measurement sets are given by pairing the measurements taken by a reference sensor (w.l.o.g. sensor 1) with all other sensors measurements, resulting in the measurement set $\{(1, 2), (1, 3), ..., (1, N)\}$, thus $M = N - 1$. This yields the TDOA measurement standard deviation for the whole measurements that were taken.

The root mean square error (RMSE) is given by

$$\mathrm{RMSE}_{\hat{\tau}_{(M),i}} = \sqrt{\frac{1}{IM} \sum_{i=1}^{I} \sum_{m=1}^{M} (\tau_{(m),i} - \hat{\tau}_{(m),i})^2}\,. \tag{3.20}$$

3.4.2.1 Measurement Setup A

Two sensors, each equipped with a GPS antenna for time synchronization and position determination, are connected through a power splitter to one RF antenna (see Fig. 3.6a). Both sensors simultaneously start the signal reception of ADS-B signals at 1090 MHz center frequency. The output of the sensors is a time discrete, quantized

baseband signal and a corresponding timestamp for the first captured sample. This timestamp is generated using a GPS synchronized clock.

In three sessions, a set of 100 measurement pairs $(z_{1,i}, z_{2,i}) \in Z_A$, where $z_{n,i}$ denotes the $i-$th measurement from sensor n, is recorded. Each signal measurement has a duration of 1 second and most likely contains multiple ADS-B messages which are selected. The messages are decoded and checked for errors by calculating the ADS-B checksum. Messages with errors are discarded. For the remaining ones a time of arrival timestamp is calculated using the methods described in Section 3.4.1.

Subsequently, messages extracted from $z_{(1,i)}$ are compared to messages from $z_{(2,i)}$ $\forall i = 1..100$ in order to identify the corresponding ones. For corresponding pairs of ADS-B messages, the difference of their timestamps, the TDOA measurement, is calculated. Due to the fact that sensors share one RF antenna, they receive the signal at the same position and the same time. Therefore, the TDOA in an ideal system without errors should be zero. Non-zero values could be caused by synchronization errors or inaccurate determination of the TOA measurements.

The time resolution of the timestamps strongly depends on the sample rate f_s. For our trials, a sample rate $f_s = 10$ MS/s is used, therefore only a time resolution of 100 ns is possible. Better time resolution and more robust message decoding is achieved by interpolating the signals before determining the exact timestamp.

3.4.2.2 Experimental Results A

Fig. 3.6b shows the time differences between corresponding messages from sensor one and sensor two calculated using the original data without interpolation. From the set Z_A, 1521 pairs of messages from both sensors are decoded correctly with a mean TDOA of $\mu = 4.5108$ ns, a standard deviation of $\sigma = 41.7658$ ns and a maximum time difference of 163 ns. The sample rate $f_s = 10$ MS/s only gives a time resolution of 100 ns between two samples, this quite good result already indicates a good time synchronization and reliable timestamp generation. Outliers with TDOA values larger than 1 ms are discarded, since they probably result from repeated identical ADS-B status messages.

By signal interpolation with factor 10, 1561 messages from both sensors are decoded correctly with $\mu = -2.8386$ ns and $\sigma = 17.1384$ ns, as shown in Fig. 3.6c. As depicted in Fig. 3.6d, further interpolation does not much improve the results. $\mu = -3.3105$ ns and $\sigma = 16.8774$ ns for 1504 messages is achieved. Nonetheless, if the signals are recorded at $f_s = 10$ MS/s, interpolation by factor 100 is needed in a sensor network

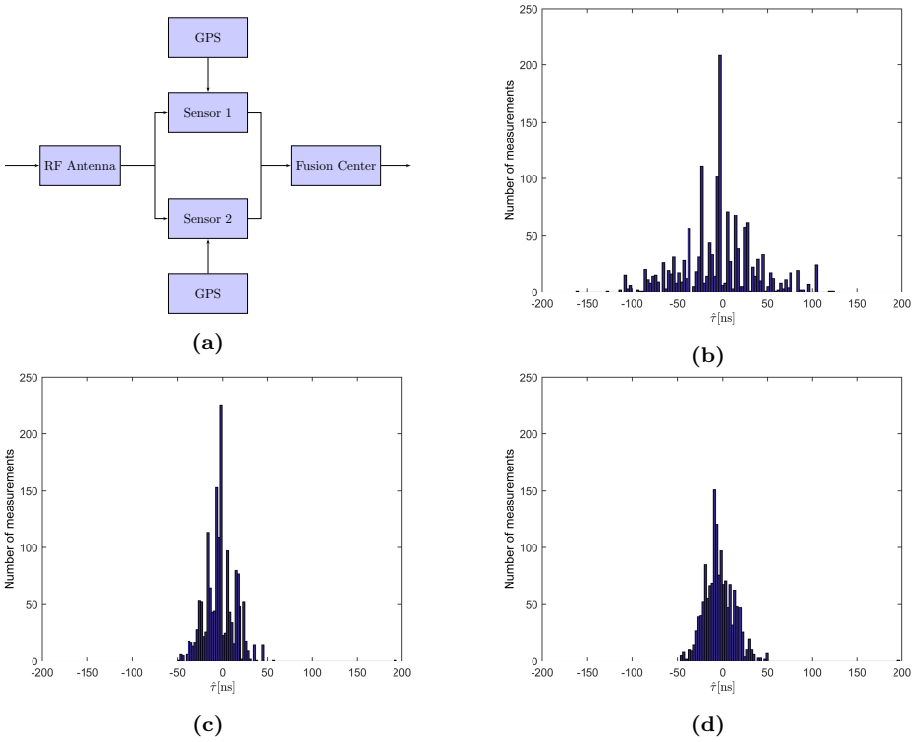

Figure 3.6: (a) Measurement setup A, results with (b) no interpolation, (c) interpolation by factor 10 and (d) interpolation by factor 100.

with multiple sensors at different positions for accurate TDOA localization. Since the sensors in our trials use the same RF antenna, the resulting error between the two sensors is due to GPS time synchronization and timestamp generation inaccuracy. The results are also given in Table 3.2.

3.4.2.3 Measurement setup B

In addition to our trials with one RF antenna as described in Section 3.4.2.1, a second set consisting of 50 measurements $(z_{1,i}, z_{2,i}) \in Z_B$ is recorded using one RF antenna for each sensor. In this setup, both sensors are completely independent and do not share any sort of hardware (see Fig. 3.7a) but are placed closely to each other.

Interpolation factor	# meas	μ [ns]	σ [ns]	RMSE [ns]
1	1521	-4.5	41.8	42
10	1561	-2.8	17.1	17.4
100	1504	-3.3	16.9	17.2

Table 3.2: TDOA errors for measurement setup A.

The RF antennas and sensors are separated by a distance of approximately 1 meter. Depending on the position of the emitter, the signal propagation delay between the antennas may vary. In free space, signals propagate at speed of light $c \approx 3 * 10^8$ m/s. With a distance of 1 meter between the antennas, the delay may differ between 0 ns and $\frac{1 \text{ m}}{3*10^8 \text{ m/s}} \approx 3.3$ ns.

3.4.2.4 Experimental Results B

Fig. 3.7 shows the results of this trial. Without signal interpolation, 596 messages are decoded with a time difference between timestamps of $\mu = 6.4597$ ns and $\sigma = 50.0302$ ns. By interpolating the signal by factor 10, 564 messages are decoded with $\mu = 5.2447$ ns and $\sigma = 26.9964$ ns. With further interpolation, the timestamp generation accuracy is given by $\mu = 4.9967$ ns and $\sigma = 25.8131$ ns. The results are given in Table 3.3.

Interpolation factor	# meas	μ [ns]	σ [ns]	RMSE [ns]
1	596	6.5	50	50
10	564	5.2	27	27.5
100	610	5.0	25.8	26.3

Table 3.3: TDOA errors for measurement setup B.

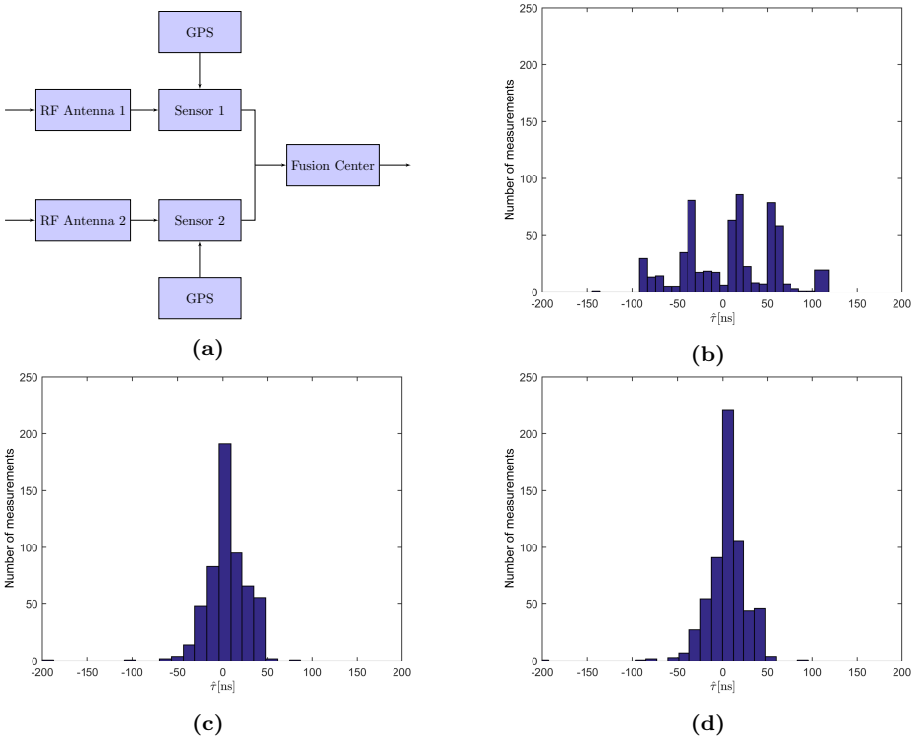

Figure 3.7: (a) Measurement setup B, results with (b) no interpolation, (c) interpolation by factor 10 and (d) interpolation by factor 100.

3.4.3 Reduction of communication requirements

The possible reduction of communication bandwidth is shown using the example of multilateration of ADS-B transponder signals investigated in this chapter. Common RF receivers digitize the received signals using an ADC (analog-to-digital converter) with a resolution of 14 bit. Since computers use multiples of 8 bits (1 byte) to store data, each sample takes 16 bit of storage space. The Nyquist-Shannon sampling theorem states that when digitizing a continuous-time into a discrete-time signal, a sample rate of at least the double of the signals bandwidth is needed to represent the signal without information loss. In the case of ADS-B, a sample rate of 2 MHz when using complex valued samples is needed. One complex sample requires 4 bytes of storage space (2 bytes for the real and 2 bytes for the imaginary part). Therefore, a signal with a duration of one second has $2,000,000 \times 4\,\text{bytes} = 8,000,000\,\text{bytes}$. The common TDOA estimation approach would have to transmit this amount of data every second from each sensor to a reference node or data fusion center. If the signal processing and a TOA estimation can be performed independently by each sensor node, only a timestamp and the decoded message are transmitted. Each message is either 56 or 112 bits (7 or 14 byte) long and a corresponding timestamp takes additional 8 bytes.

During our experiments (see Chapter 4), the average value of correctly received messages per second over all sensor nodes during the observation interval of 30 minutes was approximately 257. The data that needs to be transmitted by each sensor node (if only long ADS-B frames are received) per second is $257 \times (14+8)\,\text{bytes} = 5654\,\text{bytes}$. Assuming TCP/IP as transmission protocols and that each message is sent directly in a separate TCP packet (TCP/IP header 40 bytes), a transmission rate of 15,934 byte/s is needed. For a MTU of 1460 byte (maximum transmission unit, 1500 byte - TCP/IP header), the standard approach requires $8,000,000 + \lceil \frac{8,000,000}{1,460} \rceil \times 40\,\text{byte/s} = 8,219,200\,\text{byte/s}$. Therefore, less than 0.2% of the bandwidth is needed when using signal structure information compared to the common TDOA estimation.

Consider a scenario where received messages are perfectly aligned after each other without pauses between them. Taking the ADS-B preamble duration into account, 15625 messages are received per second. The data to be transmitted including TCP/IP overhead (one message per TCP packet, worst case only short ADS-B frames) is $15625 \times (7+8+40)\,\text{byte/s} = 859,375\,\text{bytes/s}$. In the considered case, less than 10.5% of the bandwidth is needed when using signal structure information compared to the common TDOA estimation. In the worst case, messages could overlap. However the previous scenario is already highly improbable since ADS-B does not use a channel access method.

In the considered example, a reduction of the communication requirements by up to 99.8% is possible. Additionally, a decrease of the required processing power of the data fusion center is achieved by processing the received signals directly at each sensor node. Clearly, scenarios are imaginable with no reduction at all, in the worst case even an increase. In this case, the TOA method should not be applied. But when considering other scenarios (like the one investigated in Chapter 5 and 6), an even higher reduction is possible, depending for example on the bandwidth and duration of the observed signals.

3.4.4 Conclusion

The presented method allows precise TOA determination of ADS-B/Mode-S transponder signals. The main advantage of this technique is that only a message ID consisting of the messages bit string (112 bit for long ADS-B messages, see Section 3.2) and the corresponding TOA timestamp need to be transmitted to a data fusion center. The requirements on the communication channel between sensor nodes and a central processing center could be drastically reduced.

The accuracy of TOA estimation was shown in two field experiments with different experimental setups. It can be observed, that a good timestamping performance could be achieved. The error values that were given include GPS synchronization inaccuracy. The amount of error induced by the synchronization cannot easily be determined.

Although this exact method could not be used for the field experiments described in Chapter 4 due to technical sensor system reasons, it was used for field experiments described in [KSR+12] to localize and track aircrafts and its validity could be confirmed.

CHAPTER IV

Wide Area Multilateration - Evaluation

In this chapter, field experiments for TDOA based wide area multilateration using ADS-B/Mode-S transponder signals are described, the results are presented and discussed. This chapter is structured as follows. In Section 4.1, the employed sensor system based on Radarcape nodes is described. The accuracy of the TOA estimation process of the sensor network is evaluated. Experiments are described and the results are evaluated with respect to the achieved TDOA measurement accuracy (Section 4.2). In Section 4.3, field experiments for the localization and tracking of aircrafts are described and analyzed. A summary in given in Section 4.4.

4.1 Radarcape System Description

Field experiments for wide area multilateration were conducted using a sensor network consisting of 10 Radarcape sensor nodes (Planevision Systems GmbH). The requirements on each sensor node were commercial off-the-shelf with short delivery time, real-time signal processing and accurate timestamping of received ADS-B/Mode-S messages. The sensors should have the possibility to store all received data on a storage device but also to stream the data using a network connection. To achieve more accurate timestamping, the standard Radarcape sensors (Planevision System GmbH) were enhanced by GPS disciplined Oven Controlled Crystal Oscillators (OCXO).

The system architecture of the Radarcape sensor is given in Fig. 4.1. The main component of each sensor node is a BeagleBone single board computer (SBC) which runs a Linux operating system. The signal processing is done on a receiver/FPGA board which is attached to the SBC. The algorithms used for signal processing, message decoding and timestamp calculation are closed source. A Trimble GPS receiver is used

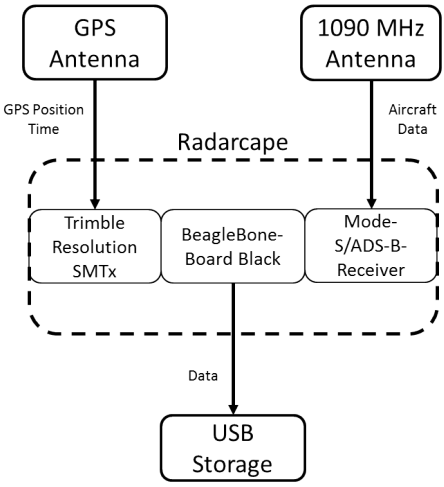

Figure 4.1: Radarcape System Architecture.

for the determination of the sensors position and time. The OCXO is disciplined using the 1PPS signal (1 pulse per second) of the GPS receiver.

The front and back side of the Radarcape sensor are depicted in Fig. 4.2. To stream the received data to a fusion center, the sensors can be connected to a network. The data for this project was recorded using a local storage device attached to the front USB port of the sensor. A software was developed by Fraunhofer FKIE to store the decoded messages including the corresponding timestamps of the Radarcape along with position and time information from the GPS receiver into separate files (see Section 8.1). The timestamps are given in nanosecond resolution.

4.2 Timestamp Accuracy Evaluation

A key requirement for precise TOA/TDOA based geolocation is the accuracy of the time synchronization/timestamps of the sensor nodes. A synchronization accuracy of stationary sensors in the range of $\approx 20\,\text{ns}$ is achievable using GPS. The accuracy of the timestamps of the received signals depend on the synchronization of the sensor nodes to a common reference (for example UTC) as well as on the accuracy of the TOA determination for the received signals to the local sensor clock. This TOA/TDOA estimation strongly depends on signal parameters like the signal bandwidth, the

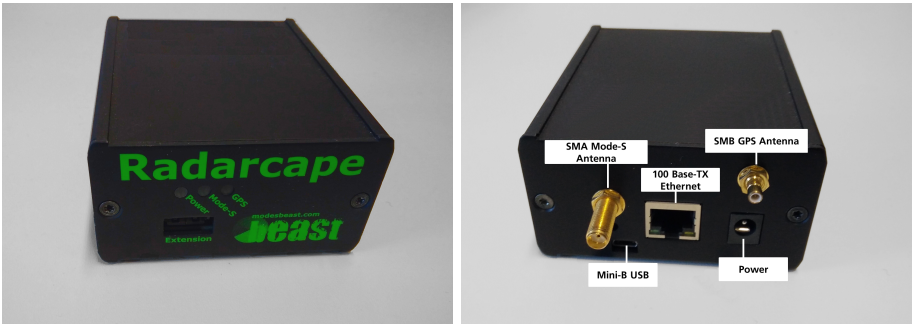

(a) **(b)**

Figure 4.2: Radarcape Sensor.

message duration and the signal-to-noise ratio (see Section 2.6). ADS-B messages are well suited for TOA/TDOA estimation since the signal bandwidth is comparatively high and the integration time with 56 or 112 μs is long enough. The SNR naturally decreases with higher distance between emitter and observer. However, a line of sight condition can almost always be assumed. Additional factors in the signal processing chain may degrade the TOA accuracy.

In this section, the accuracy of the message timestamping and the sensor clock synchronization of the Radarcape system is experimentally determined. Since the time of emission of the signals is unknown, this accuracy cannot be determined directly. We thus use the fact that when placing multiple sensor nodes at the same location, the TDOA $\tau_{(a,b)}$ of received messages at sensor nodes a and b should be 0.

The expectation of the TDOA $\tau_{(a,b)}$ is

$$\mathrm{E}\left[\tau_{(a,b)}\right] = 0\,. \tag{4.1}$$

Therefore, the error of the TDOA measurement process is directly given by the TDOA measurement $\hat{\tau}_{(a,b)}$ itself. This error also includes system dependent errors like the time synchronization or errors induced by the signal processing chain. The magnitude of these additional errors cannot be determined, but the resulting error of the TDOA measurement process gives the wanted overall system TDOA timestamping performance.

The mean, standard deviation and RMSE are calculated according to Eq. (3.18),

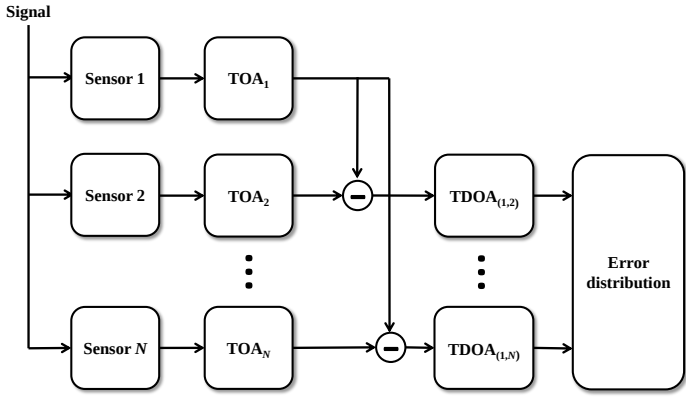

Figure 4.3: Block diagram for the timestamp accuracy evaluation.

(3.19) and (3.20) given in Section 3.4.2. To evaluate possible clock drifts, the measurements are also evaluated over short periods of time $I_\epsilon \subset I$ or even only for one measurement step i. Also, the standard deviations are calculated for each sensor pairing $(m) = (a, b)$ separately.

A block diagram representing the processing chain to experimentally determine the TDOA measurement accuracy is given in Fig. 4.3.

4.2.1 Experimental Setup

To be able to determine the timestamp accuracy of the system, all 10 sensor nodes were built up at the same position. The roof of a building at Fraunhofer FKIE was chosen for the experiments due to good line of sight conditions in almost all directions and to avoid multipath signal propagation effects.

The Radarcape sensors including GPS and 1090 MHz antennas were mounted on a small trolley. The largest distance between two reception antennas is approximately 1 m (signal propagation time $\approx 3.3\,\text{ns}$). The experimental setup is depicted in Fig. 4.4. Before starting the data recording, all sensors were running for at least 30 minutes to ensure good GPS positioning and timing information.

4.2.2 Results

Sensor 1 was chosen as reference sensor. A data set with a duration of 20 minutes was extracted from the recorded data. For all messages that were received by the

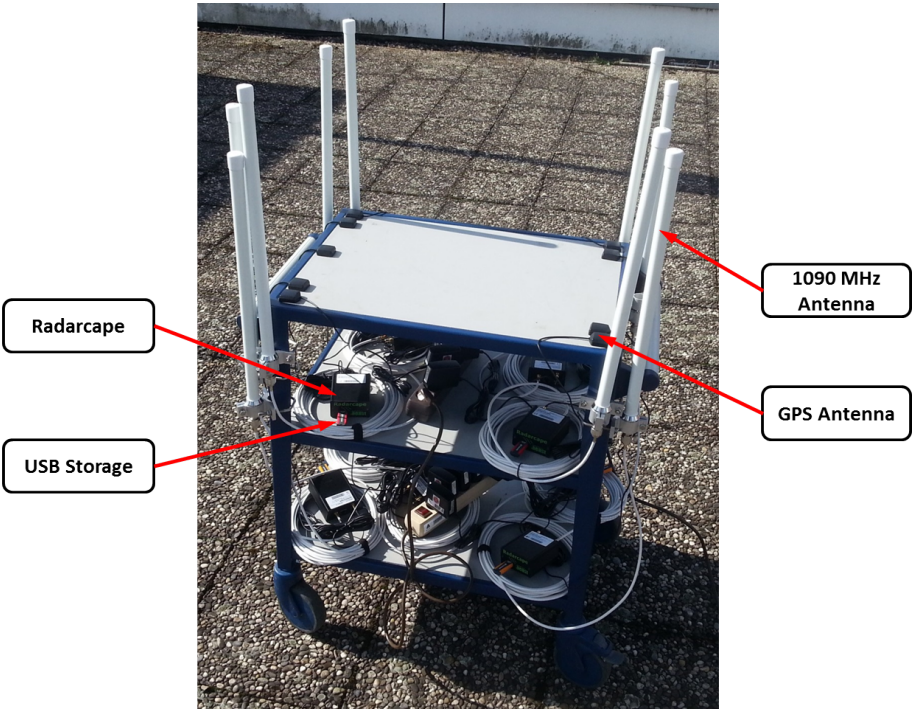

Figure 4.4: Experimental setup.

reference sensor, the corresponding messages received by all other sensors are searched. Subtraction of the associated TOA timestamps yield the TDOA measurements and, according to the experimental setup, the TDOA measurement error.

From the 20 minute data set, between 75589 (sensor pair (1,7)) and 98834 (sensor pair (1,3)) TDOA measurements were evaluated. For each sensor pairing, the mean, the standard deviation and the RMSE are determined. The results are given in Table 4.1. The first column of each sensor pair gives the corresponding values for all TDOA measurements of the sensor pair. Since very few outliers with high TDOA errors exist, outliers with TDOAs larger than 5000 ns were filtered. Less than 0.08 % of the measurements were discarded in this way. The errors for the resulting TDOA measurements are given in the second column for each sensor pair.

The error distributions for all sensors pairs are depicted in Fig. 4.5. For better

readability, only TDOA measurements lying between −300 ns and 300 ns are shown.

Along with the received messages and timestamps, status data is recorded by the Radarcape sensors. One information of this status data is the amount of time difference between the local sensor time and the 1PPS signal of the GPS receiver. This information is given once per second and the value is given in multiples of 15 ns. Since the Radarcape sensors used by Fraunhofer FKIE include an OCXO, which is much more stable than the standard Radarcape oscillators, the status data never showed a time deviation. This is due to the fact that the resolution of the time correction status data is only 15 ns.

To analyze the data with respect to time synchronization or oscillator drifts, the TDOA errors are plotted over time. A moving average filter is applied to the data. The results are given in Fig. 4.6. The blue lines indicate the TDOA error over time using a moving average filter with a duration of 1 s. The red lines show the TDOA error using a moving average filter of 10 s. Time drifts in the range of 20 ns can be observed. To get an idea of how much error is induced by the reference sensor, all nine sensor pairings are compared in Fig. 4.7. Here, only the results of a 10 s moving average filter are depicted. As can be observed, the different sensor pairings show a noticeable mean difference of up to 100 ns. It can be assumed that this bias is resulting from the time synchronization of the sensor nodes and is thus a system-inherent error. The mean error compensated TDOA errors are depicted in Fig. 4.7 (b).

Estimating and compensating the usually unknown synchronization bias would give better TOA measurement accuracy with respect to a reference time (in this case UTC) and thus enable a more accurate emitter localization performance of the multilateration system. The localization accuracy would also benefit from compensating the much smaller amount of error induced by clock drifts. Both errors could be estimated over multiple messages received from multiple targets in a data fusion/tracking step. Nevertheless, the achieved TDOA measurement accuracy of the sensor network is already very good and well suited for TOA/TDOA based emitter geolocation. The mean errors (after discarding outliers) are lying between -60 ns and 9 ns with standard deviations between 45 ns and 56 ns.

Sensor pair	# meas	μ [ns]	σ [ns]	RMSE [ns]
(1,2)	76953	31	2130	2131
(1,2), no outliers	76899	9	50	51
(1,3)	98834	-12	1240	1240
(1,3), no outliers	98816	-21	48	53
(1,4)	80015	-22	2157	2157
(1,4), no outliers	79950	-27	56	63
(1,5)	92773	-49	1596	1597
(1,5), no outliers	92745	-60	45	75
(1,6)	78490	28	1945	1946
(1,6), no outliers	78455	9	52	53
(1,7)	75589	11	2307	2307
(1,7), no outliers	75526	-5	56	56
(1,8)	89154	-29	1462	1462
(1,8), no outliers	89127	-39	47	61
(1,9)	78444	-59	2048	2049
(1,9), no outliers	78398	-47	48	88
(1,10)	89339	-33	1284	1284
(1,10), no outliers	89310	-42	47	63

Table 4.1: TDOA errors with and without filtered outliers.

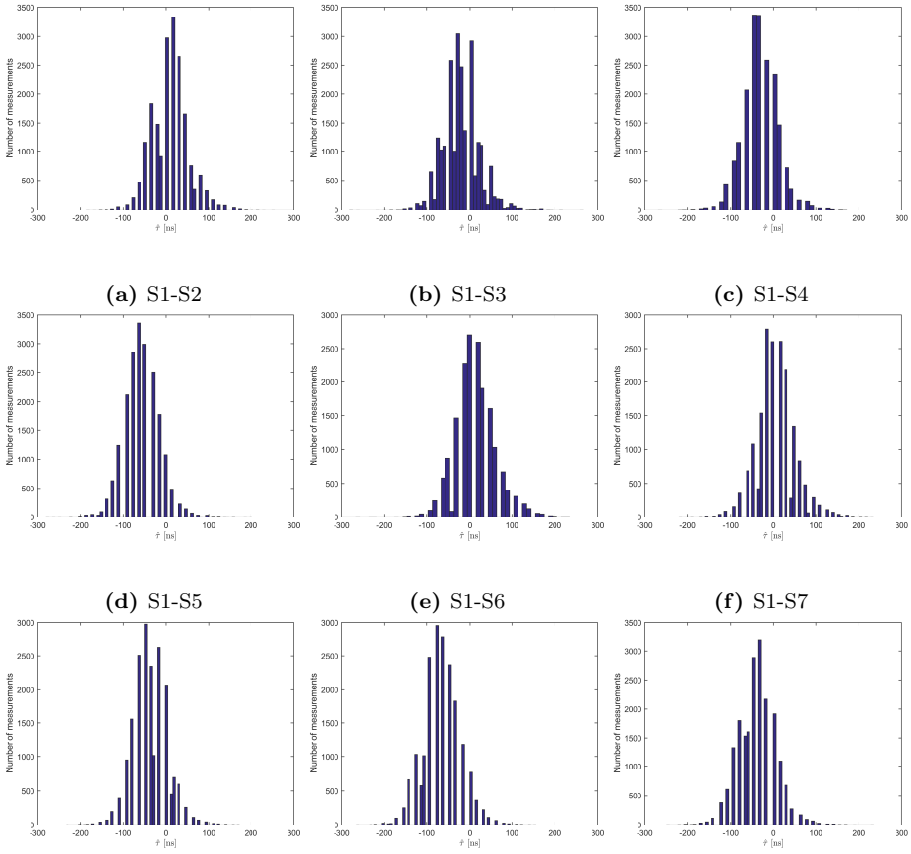

(a) S1-S2 **(b)** S1-S3 **(c)** S1-S4

(d) S1-S5 **(e)** S1-S6 **(f)** S1-S7

(g) S1-S8 **(h)** S1-S9 **(i)** S1-S10

Figure 4.5: TDOA measurement error distribution.

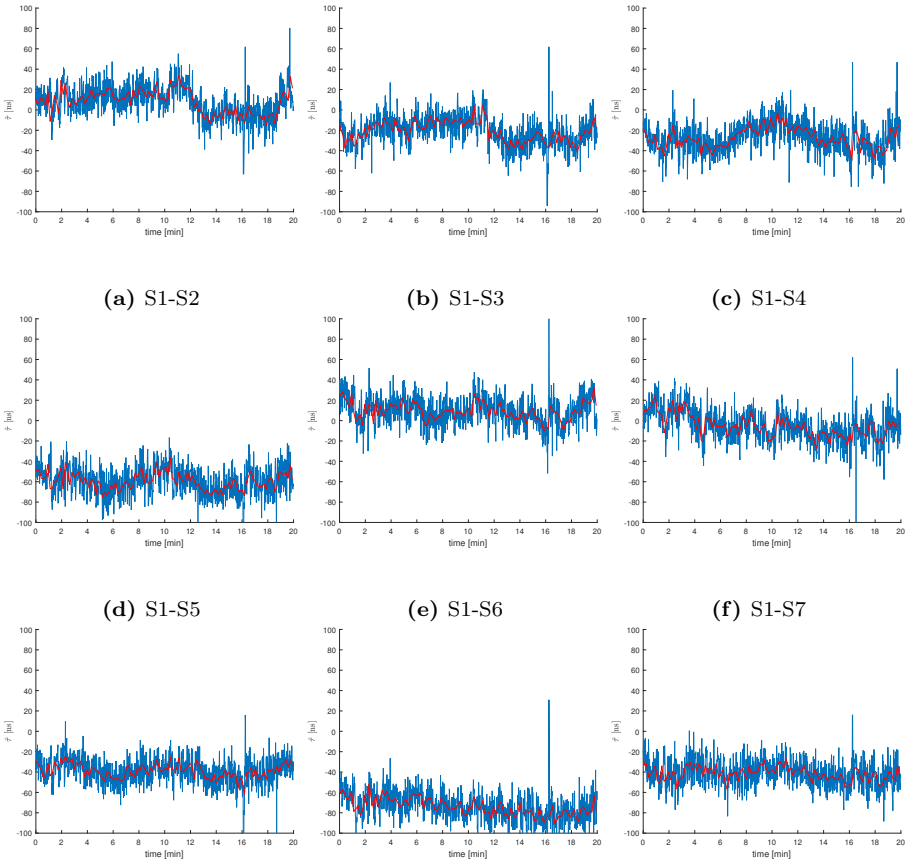

(a) S1-S2 **(b)** S1-S3 **(c)** S1-S4

(d) S1-S5 **(e)** S1-S6 **(f)** S1-S7

(g) S1-S8 **(h)** S1-S9 **(i)** S1-S10

Figure 4.6: TDOA error over time using a moving average filter over 1 s (blue line) and 10 s (red line) of data.

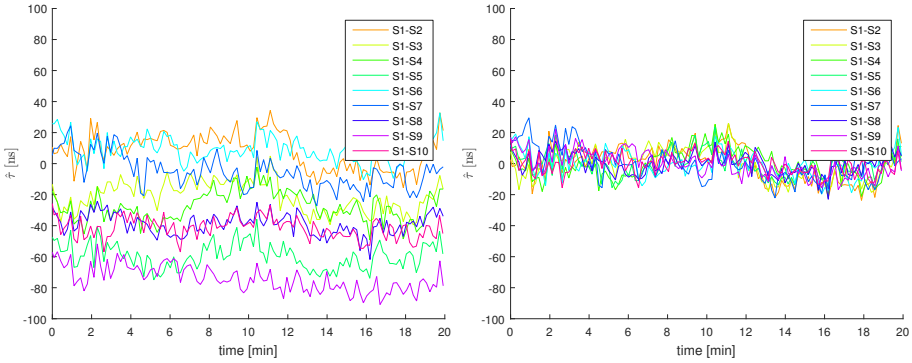

Figure 4.7: Comparison of TDOA error over time (moving average filter over 10 s of data). (a) without and (b) with compensated mean error.

4.2.2.1 Annotation

For the described evaluation, all sensor nodes were placed approximately at the same position. This yields a very similar or even identical GPS satellite view. With a spatially distributed sensor network with long distances between the sensor nodes, the time synchronization quality to UTC reference using GPS may somewhat degrade.

From the obtained TDOA measurement variance $\sigma^2_{\tau_{(a,b)}}$, it is not possible to determine the amount of error induced by each sensor node, see Eq. (3.17). Since the results of all sensor pairings showed very similar error distributions, we assume that the TOA variances for all sensors are of similar magnitude.

4.2.3 Conclusion and Comparison to the method presented in [SKR11]

Although our developed TOA estimation technique presented in Section 3.4 and [SKR11] could not be used for the following field trials, the method was used in [KSR+12] to localize aircrafts using a sensor network. The TDOA measurement accuracy compared to the accuracy of the Radarcape system seems to be higher. Due to technical reasons, the method could only be evaluated for a small number of ADS-B messages whereas for the TDOA measurement accuracy of the Radarcape system, a much larger number of messages was taken into account. The results indicate that a RMSE of approximately 25 ns is achievable using our TOA estimation technique with signal interpolation. The RMSE for the Radarcape system lies between 51 and 88 ns.

4.3 Field Experiments for Aircraft Localization and Tracking

To evaluate the geolocation performance of the described multilateration system (Section 4.1) based on TOA/TDOA measurements of ADS-B messages, field experiments were conducted. In Section 4.3.1, the experimental setup is described. The employed localization and tracking methods are described in Section 4.3.2. The results are given in Section 4.3.3.

4.3.1 Setup

A network of 10 Radarcape sensor nodes was deployed in the area around Wachtberg, Bonn and Cologne. The center of the network was approximately in the area of Wachtberg. The "reference sensor" was mounted on the roof of a building at Fraunhofer FKIE in Wachtberg. All other 9 sensors were built up in private homes of Fraunhofer FKIE employees. The sensor positions are shown in Fig. 4.8. The largest distance between two sensor nodes is nearly 60 km (sensor 3 - sensor 5).

The sensors were configured to record all received data telegrams which are sent by aircrafts at a center frequency of 1090 MHz. This includes ADS-B as well as Mode-S and Mode-A/C data. ADS-B messages are pre-checked for correct reception using CRC (see Section 3.2). The complete data is saved on a USB storage device attached to the sensor. Although a direct data transmission using for example a TCP/IP Internet connection would have been possible, this feature was not used during this campaign.

Data was recorded by the sensor network for the duration of one week, starting in the evening of 29.10.2015 and ending on 05.11.2015. Unfortunately, due to technical issues, one sensor node failed recording data after three days. From the whole recorded data, two data sets were extracted for detailed evaluation. The first data set was recorded on 30.10.2015 during 10:00 UTC to 12:00 UTC. Data set 2 is composed of the data recorded on 29.10.2015 between 21:30 UTC and 22:30 UTC. A description of the Radarcape data format and Fraunhofer FKIE meta data format can be found in Section 8.1.

Depending on the site, each sensor did record between 3 and 20 GB of data. This is due to mounting positions, line of sight conditions, antenna altitude, terrain profile and shadowing effects from buildings. For example, one reception antenna was mounted on the wall of a house. In this case, there are no line of sight conditions to aircrafts flying on the other side of the house.

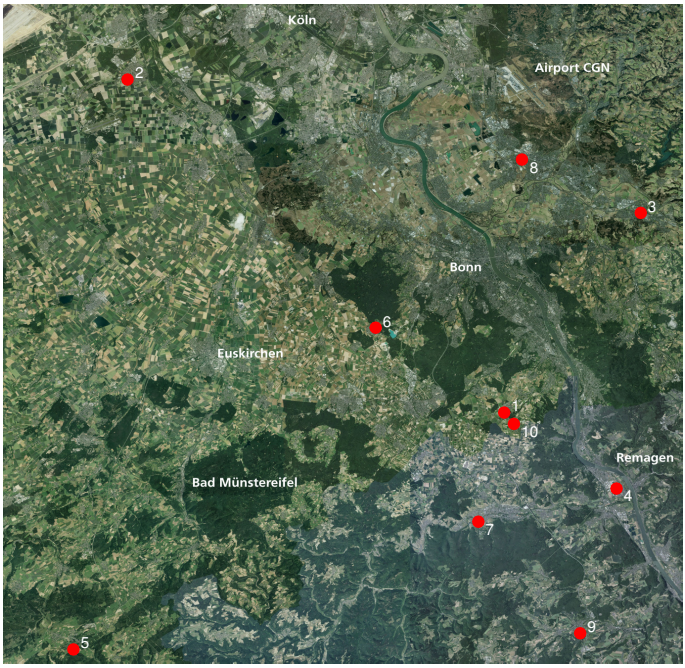

Figure 4.8: Experimental setup. Sensor positions projected over satellite image. (Map Data: ©GeoBasis-DE/BKG 2016).

Some of the Radarcape sensors could be installed inside the building with the GPS and 1090 MHz reception antennas mounted on the roof. Other sensor nodes were placed outside, thus being subject to much higher temperature differences. Although the Radarcape sensors are equipped with OCXOs, an influence of the environmental conditions on the timestamp accuracy can not be ruled out. The mounting positions of the sensors are depicted in Fig. 4.9 and Fig. 4.10.

(a)

(b)

Figure 4.9: Mounting position of (a) the reference sensor 1 and (b) sensor 9.

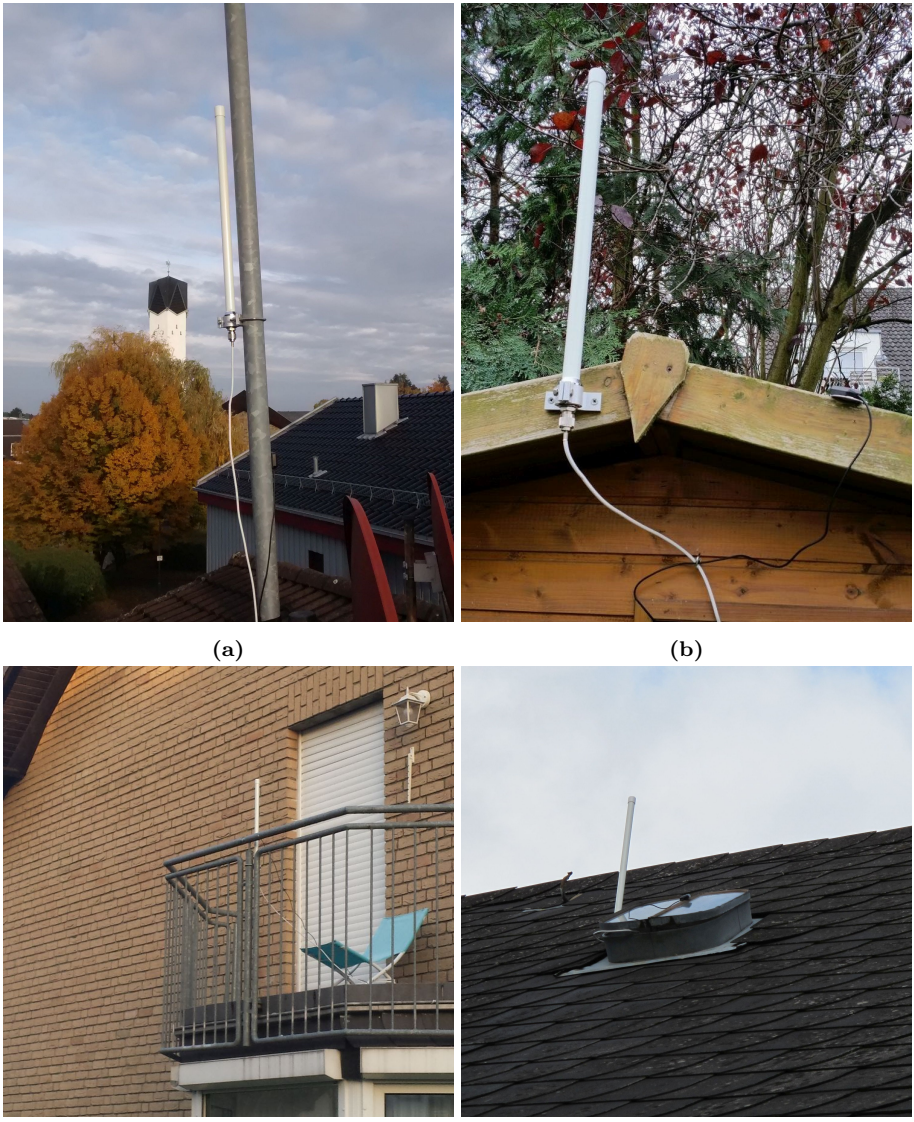

(a) **(b)**

(c) **(d)**

Figure 4.10: Mounting positions of (a) sensor 6, (b) sensor 8, (c) sensor 3 and (d) sensor 5.

4.3.2 Evaluation

From the whole data of each data set, one sensor node was chosen as reference sensor. We chose the sensor which was installed at Fraunhofer FKIE site due to its good line of sight conditions in all directions and for being located in the center area of the sensor network.

For all message telegrams received by the reference sensor, corresponding messages are searched in the data sets of all other sensor nodes. If at least 5 sensors did receive the same signal, the aircrafts location is calculated. The position estimate is determined in three steps. In the first step, a TDOA closed-form solution (described in Section 2.8.1) is used to get a rough emitter position. This estimate is used as initialization for a least squares algorithm (see Section 2.8). If multiple messages are received from one aircraft, the resulting position estimates are then Kalman filtered. The entire processing chain from the received signal to the resulting multilateration track is depicted in Fig. 4.11.

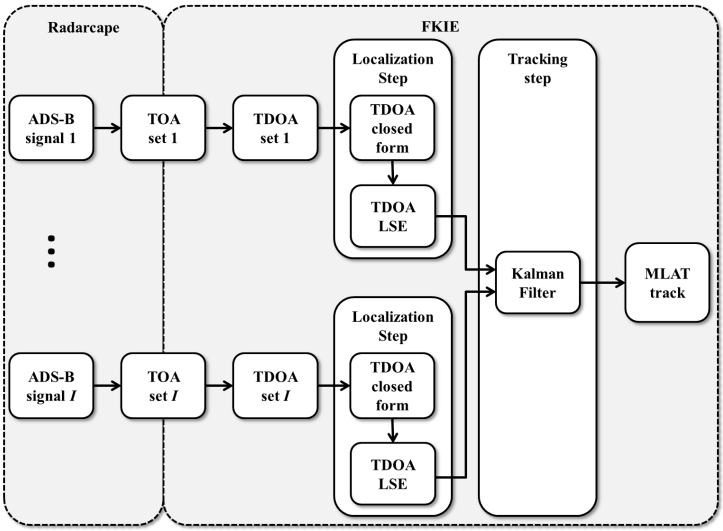

Figure 4.11: Processing chain from the received ADS-B messages to the MLAT track.

4.3.2.1 ADS-B Message Association

To reduce the processing time during the message association step, knowledge of the sensor network's geometry is used. The largest possible TDOA results if emitter and

both sensors that are used for the TDOA measurement lie on one line. The maximum possible TDOA is then given by

$$\tau_{(a,b)}^{max} = \frac{||p_a - p_b||}{c}\,, \tag{4.2}$$

where $||\cdot||$ denotes the Euclidian distance. This maximum possible TDOA remains constant for all received messages, as long as a stationary sensor network is used.

The TOA of message i received by the reference sensor a is known and given by the measurement $\hat{\tau}_{a,i}$. When looking for matching messages received by a sensor b, the search can be reduced to messages with timestamps $\hat{\tau}_{b,i}$ lying between

$$\hat{\tau}_{a,i} - \tau_{(a,b)}^{max} - \tau_{noise} \leq \hat{\tau}_{b,i} \leq \hat{\tau}_{a,i} + \tau_{(a,b)}^{max} + \tau_{noise}\,, \tag{4.3}$$

where τ_{noise} denotes additional uncertainty which takes timestamp imprecision into account.

The resulting processed data set includes the received messages with index i and the corresponding TOAs $\hat{\tau}_{n,i}$ for each sensor node n that received the message. In the same step, the ADS-B information (ICAO address, position, altitude) is decoded from the received message bit string as described in Section 3.2 and stored along with the TOAs.

As already described, the choice of the reference sensor was made because of the good signal reception conditions at the sensor location and also because the sensor lies in the center of the sensor network. Thus, the probability of receiving the same messages by as much other sensors as possible is high.

4.3.2.2 Position Estimation

If a message was received simultaneously by at least 5 sensor nodes, a corresponding multilateration position estimate is calculated. The obtained data set (see Section 4.3.2.1) includes I received messages that can be used in this way. From the stored TOAs, the TDOAs are given by

$$\hat{\tau}_{(a,b),i} = \hat{\tau}_{a,i} - \hat{\tau}_{b,i}\,. \tag{4.4}$$

The position estimation is then performed based on a set of TDOAs in two steps. The corresponding methods are described in Section 2.8. In the first step, the closed-form

TDOA solution described in [GS08] is used to get an initial position estimate. For a 3D localization, this algorithm uses the 4 non-redundant TDOA measurements from 5 sensor nodes. For the sensor nodes 1 to 5, this TDOA measurement set would be $\left(\hat{\tau}_{(1,2)}, \hat{\tau}_{(1,3)}, \hat{\tau}_{(1,4)}, \hat{\tau}_{(1,5)}\right)$.

In the second step, a least squares cost function is optimized using Nelder/Mead simplex optimization [NM65]. The initialization point for this cost function is the position estimate obtained from the closed-form solution that uses only 5 sensors nodes and the TDOA measurement set using a reference sensor. The cost function is given by Eq. (2.55). We use the full TDOA measurement set according to Eq. (2.7).

The result of this optimization yields the position estimate for the aircraft. If multiple messages from one aircraft were received, a Kalman filter is used to track this aircraft along its flight path (see Section 8.2). The aircrafts ICAO address is used to assign single position estimates to the corresponding tracks. When using ADS-B signals, the ICAO address is included in all message formats. Therefore, it is always clear which measurement corresponds to which track.

For TOA based geolocation with unknown time of signal emission t_e, the cost function given in Eq. (2.57) is used.

4.3.2.3 Localization Accuracy Evaluation

To assess the localization accuracy of the multilateration system, the true aircrafts location is needed to compare the position estimates to. For the results given in Section 4.3.3, we mainly use the ADS-B position information transmitted by the aircraft. As already mentioned, this information may be error prone and for some examples, we show that the multilateration tracks differ from the ADS-B positions (see Section 4.3.5). Thus, we also use track information obtained from a radar network (*Reference Tracking Radar Network*, RTRN) with up to 30 radars (not available for all aircrafts) for the error determination.

The localization error for each received message $i \in \{1, ..., I\}$ is given by

$$||\hat{\mathbf{x}}_i - \mathbf{x}_i||\,, \tag{4.5}$$

where $\hat{\mathbf{x}}_i$ denotes the position estimate and $\mathbf{x}_i$ the ground truth obtained from ADS-B or the RTRN. For the evaluation of the localization accuracy, the root mean square error (RMSE) is used.

The RMSE is given by

$$\mathrm{RMSE}_{\mathbf{x}} = \sqrt{\frac{1}{I}\sum_{i=1}^{I} ||\hat{\mathbf{x}}_i - \mathbf{x}_i||^2}\,. \tag{4.6}$$

Additionally, we define the signed difference $\Delta\hat{\theta}_i$ where $\hat{\theta}_i$ is an estimate of the parameter θ (for example the deviation in x-, y-, or z-direction separately) as

$$\Delta\hat{\theta}_i = \hat{\theta}_i - \theta\,. \tag{4.7}$$

The mean signed difference is then given by

$$\mu_{\hat{\theta}} = \frac{1}{I}\sum_{i=1}^{I} \Delta\hat{\theta}_i\,. \tag{4.8}$$

Annotation: The altitude information sent by the aircraft using ADS-B or Mode-S usually relies on an on-board barometric altitude measurement. This altitude however is not the true altitude of the aircraft over geoid. All calculations and position estimations described in this report are done in a Cartesian or the WGS84 coordinate system. Thus the MLAT altitude is always given over geoid. The true altitude of the aircraft over geoid is unknown and thus the error evaluation will often show an offset in z-direction (between barometric pressure altitude and altitude over geoid). This offset may vary due to changing weather conditions. See also Section 3.3.

4.3.2.4 Discussion

For the results described in Section 4.3.3, only ADS-B telegrams including the aircrafts position are evaluated. This is done since the ground truth used for the determination of the TOA/TDOA estimation errors is given by the transmitted ADS-B positions. The developed algorithms are applicable to all ADS-B message types (including for example altitude or velocity messages). The used Kalman filter tracking relies on the knowledge, which position estimate belongs to which aircraft. This measurement assignment is based on the ICAO address included in all ADS-B telegrams. For Mode-S and Mode-A/C messages, the localization algorithms remain the same. Only the Kalman filter tracking step would need to be adapted since in a fully passive scenario, the aircraft emitting Mode-S and Mode-A/C data is not known to the sensor network. Thus, a tracking filter with measurement to track assignment would be used. In

Section 4.3.5 we show that the ADS-B position information is not always reliable. For those examples, track data generated by the RTRN is also used as ground truth.

The localization accuracy using TDOA or TOA is very similar. The data was evaluated using both methods but no significant difference in position estimation precision could be observed. Thus, mainly the results of TDOA based emitter geolocation are presented in Section 4.3.3. A comparison of TDOA and TOA based localization for the field experiments data is given in Section 4.3.6. Theoretical analysis based on the Cramér-Rao Lower Bounds for both techniques (see Section 2.7) and the results of earlier field experiments conducted by Fraunhofer FKIE and Cassidian [KSR+12] also point towards this direction.

4.3.3 Results

Both data sets are evaluated using the techniques described in the previous sections. Only to give an impression of the amount of aircrafts tracked during these time intervals, the results of the evaluation of data set 1 using all measurements are depicted in Fig. 4.12. The reference sensor is located in the origin of the coordinate system. In this figure, single aircrafts and the corresponding tracking accuracies cannot be identified. However, it is shown that a MLAT network with 10 sensor nodes distributed over an area of less than $50 \times 50\,\text{km}$ is able to detect, localize and track aircrafts in an observation area of approximately $350 \times 350\,\text{km}$.

The achieved tracking accuracy for data set 1 and data set 2 are given in Table 4.2 and Table 4.3, respectively. The results are given for four different parameter sets (rows of the table). The maximum target distance (300 km or 100 km) is used to only evaluate aircrafts that are closer than the max. target distance to the reference sensor. Due to the curvature of the earth and signal transmission parameters like center frequency and transmission power, ADS-B signals of aircrafts flying at $\approx 35000\,\text{ft}$ cannot be received at distances somewhat larger than 300 km. Only localization results of messages that were received by the minimum number of sensors parameter (5 or 10) are used in the tracking evaluation. The parameter minimum messages/target gives the number of messages of a single aircraft (identified by its ICAO address) that are at least used in the tracking process.
The localization results of the MLAT tracks compared to the ADS-B position information are given in the first column of the tables. The results using the RTRN as ground truth for the RMSE calculation are given in the second column of each table. Not for all aircrafts (identified by their ICAO address) corresponding RTRN tracks could be found. Thus, the number of evaluated messages for the RMSE of the MLAT

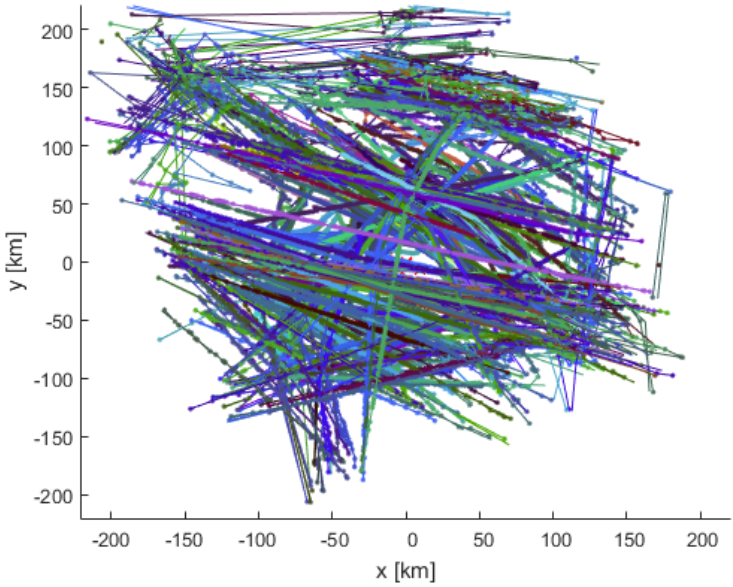

Figure 4.12: MLAT tracking results for data set 1.

tracks compared to the RTRN tracks is smaller than for ADS-B. Columns 3 to 5 give the mean difference of the tracks compared to the RTRN tracks in x-, y-, and z-direction.

The error distribution for the MLAT track compared to ADS-B and the RTRN tracks are depicted in Fig. 4.13. For better readability, outliers with errors larger than 4 km are not shown. The difference between MLAT track and ADS-B shows a significant bias. The results presented in Section 4.3.5 indicate that the ADS-B position information sent by the aircrafts is often not very precise. Throughout this thesis, we assume the RTRN accuracy to be higher than the ADS-B accuracy. This seems valid since ADS-B in its currently deployed configuration is known to cause high inaccuracies and is thus rarely used in critical airspace surveillance situations.
For both ground truths (ADS-B and RTRN), the altitude information is given as barometric pressure (see Section 3.3), the MLAT tracks use altitude information over geoid. This explains the distribution of the altitude difference around a mean value other than 0. The error distribution figures for the other parameter sets and data set 2 are omitted, because no significant difference in the error distribution is observed.

Max. Target Distance	300 km	300 km	100 km	100 km
Min. Number of Sensors	5	10	5	10
Min. Messages/Target	1	1	25	25
RMSE MLAT-ADS-B	2664 m	622 m	1537 m	584 m
Evaluated Messages	124830	4284	104764	4283
RMSE MLAT-RTRN	789 m	262 m	702 m	273 m
Evaluated Messages	57427	1653	48044	1209
$\mu_{\hat{x}}$ MLAT-RTRN	54 m	-13 m	30 m	-33 m
$\mu_{\hat{y}}$ MLAT-RTRN	134 m	13 m	59 m	8 m
$\mu_{\hat{z}}$ MLAT-RTRN	-229 m	-375 m	-253 m	-383 m

Table 4.2: Kalman filter multilateration track accuracy for data set 1.

When evaluating only messages that were received by all 10 sensor nodes, the RMSE compared to the RTRN tracks is in the range between 205 m and 273 m. Compared to the usual travel speed of aircrafts (around 850 km/h $\approx$ 236 m/s), this error is of the same magnitude than the distance the aircraft travels in 1 second.
Even for messages that were only received by 5 sensors, the RMSE is below 850 m, which is comparable to the distance the aircrafts travels in 3.5 seconds.

The difference in the altitude bias between data set 1 and data set 2 is probably due to changed weather/air pressure conditions. Data set 2 was recorded in the evening around 12 hours before data set 1.

Max. Target Distance	300 km	300 km	100 km	100 km
Min. Number of Sensors	5	10	5	10
Min. Messages/Target	1	1	25	25
RMSE MLAT-ADS-B	1625 m	398 m	874 m	399 m
Evaluated Messages	53634	2155	35194	2155
RMSE MLAT-RTRN	815 m	205 m	418 m	205 m
Evaluated Messages	19634	858	13707	832
$\mu_{\hat{x}}$ MLAT-RTRN	70 m	16 m	18 m	15 m
$\mu_{\hat{y}}$ MLAT-RTRN	120 m	24 m	90 m	24 m
$\mu_{\hat{z}}$ MLAT-RTRN	-189 m	-280 m	-172 m	-283 m

Table 4.3: Kalman filter multilateration track accuracy for data set 2.

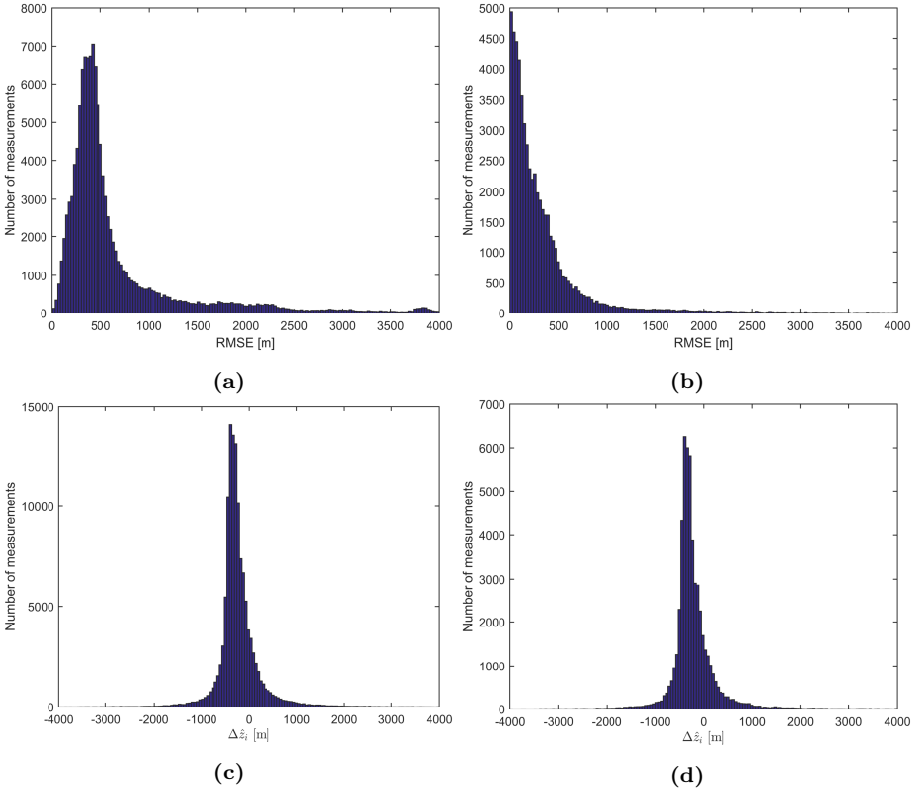

Figure 4.13: Kalman filtered MLAT track localization error distribution for data set 1: (a) MLAT compared to ADS-B, (b) MLAT compared to RTRN. Altitude difference between (c) MLAT and ADS-B (d) MLAT and RTRN. 300 km maximum distance between reference sensor and localization results, minimum 5 sensors used for position estimation, minimum 1 message/target. Outliers > 4 km are not shown.

4.3.4 Tracking of aircrafts flying at constant high altitudes

To show the tracking accuracy for aircrafts flying parallel to the sensor plane at high altitudes, the first 30 minutes of data set 2 are evaluated. Only MLAT tracks of aircrafts flying above 9000 m with at least 500 processed measurements are considered. To give a more readable image of the tracks, only aircrafts are used that have a maximum distance to the reference sensor in y-direction of 50 km giving a 100 km wide corridor in y-direction around the reference sensor. 8 aircrafts match these parameters resulting in 8608 processed messages. The results are depicted in Fig. 4.14. The sensor nodes are given as red "x". Fig. 4.14 (a) gives the horizontal view of the scenario, Fig. 4.14 (b) the altitude view, respectively. The RMSE of the tracking results using the RTRN as ground truth reference is depicted in Fig. 4.14 (c). The difference between MLAT and the RTRN altitude information is shown in Fig. 4.14 (d).

The numerical results are given in Table 4.4. The high mean difference between MLAT and RTRN tracks in z-direction again results from the difference between barometric pressure altitude and altitude over geoid.

Max. Target Distance	300 km
Min. Number of Sensors	5
Min. Messages/Target	1
Min. Altitude	9000 m
RMSE MLAT-ADS-B	586 m
Evaluated Messages	8608
RMSE MLAT-RTRN	344 m
Evaluated Messages	3033
$\mu_{\hat{x}}$ MLAT-RTRN	-67 m
$\mu_{\hat{y}}$ MLAT-RTRN	20 m
$\mu_{\hat{z}}$ MLAT-RTRN	-354 m

Table 4.4: Kalman filter multilateration track accuracy for aircrafts flying at constant high altitudes (first 30 minutes of data set 2).

As can be seen, the overall tracking accuracy is very precise. The altitude estimation degrades with higher distances to the sensor network. The best accuracy is achieved when aircrafts are flying in a parallel plane directly above the sensor network. This is

not unexpected, since the performance of TOA/TDOA based geolocation decreases outside the sensor networks geometry and the measurement errors induce much higher localization uncertainty at high distances. It was already observed in our previous work [KSR+12], that the altitude of aircrafts flying at a constant height parallel to the sensor plane can be tracked with high accuracy.

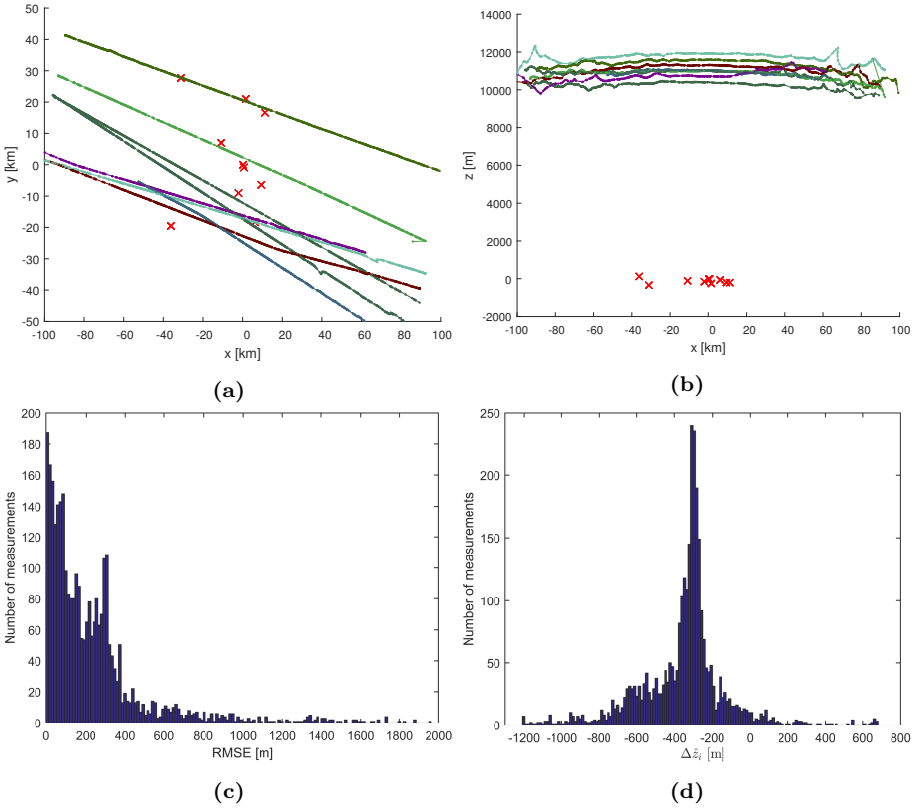

Figure 4.14: Kalman filtered MLAT track localization results (a) horizontal (b) altitude and the corresponding (c) RMSE and (d) altitude difference between MLAT and RTRN.

4.3.4.1 Comparison to the CRLB

To show the coverage and the corresponding achievable accuracy, the CRLB is plotted for the same area as was analyzed in the previous section. A TDOA measurement standard deviation of $\sigma_{\tau_{(a,b)}} = 19\,\text{m}$ (approximately 63 ns in time domain) for all sensor pairings (a, b) is used to calculate the CRLB on emitter localization accuracy according to Section 2.7.2. The bound is evaluated for a fixed altitude of 10 km. The results are given in Fig. 4.15. The sensor positions are marked by white x symbols. The localization standard deviation is given by a color distribution. It can be observed, that a very high accuracy is expected right above the sensor network. Even at distances of 100 km and more to the reference sensor in the origin of the coordinate system, a good position estimation performance is expected.

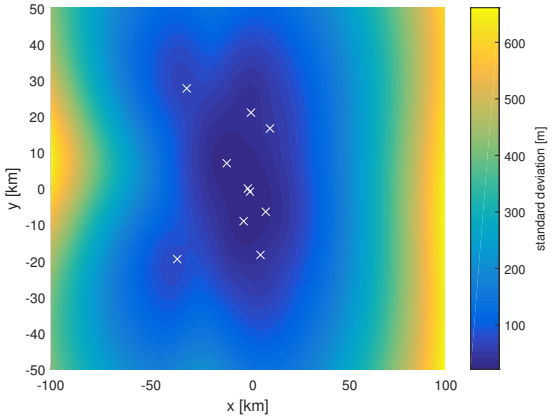

Figure 4.15: CRLB for the area of interest at 10 km altitude. Sensor positions are given by white x.

For the above calculation of the CRLB for the area of interest, it is assumed that all sensor nodes receive the signal. Therefore, all nodes are used in the localization process. Since this is usually not the case, a trajectory of an aircraft flying at a high altitude was selected from the data set and the localization performance of the sensor network is compared to the CRLB. The selected trajectory is depicted in Fig. 4.16. The aircraft is first observed in the south east and travels in north west direction. For each observation, namely each time, the sensor network received an ADS-B message of the aircraft at five or more sensors, a localization estimate is calculated as described in Section 4.3.2.2. The CRLB is calculated using the corresponding positions given

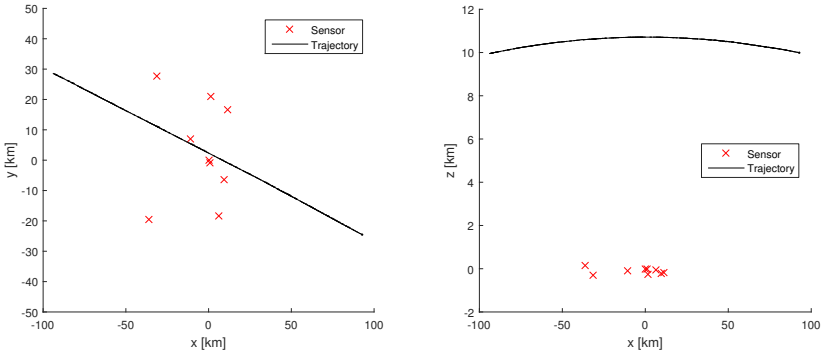

Figure 4.16: Trajectory used for the comparison of localization results and CRLB.

by the RTRN data set as ground truth. Only the sensor nodes, that received the signals are used for the calculation of the bound.

The localization accuracy of the sensor networks position estimates is compared to the CRLB. Fig. 4.17 shows this comparison. The localization errors are compared to the CRLB separately in x-, y-, z-direction and as 3D error. It can be observed, that the highest deviation between real data and CRLB is in z-direction. As already stated in the previous sections, this is probably due to the offset between the ground truth altitude given in barometric pressure (most likely QNE, see Section 3.3) and the sensor networks altitude information in WGS84. The localization results that are used here are taken individually and are not smoothed by using the Kalman filter, since the employed CRLB on TDOA based emitter localization applies to single position estimates only.

Additionally, a Monte-Carlo simulation was carried out for the same scenario. The true emitter positions obtained from the RTRN data set are used to calculate the true TOA values. To those values, zero-mean Gaussian noise with standard deviation $\sigma_{\tau_n} = \sqrt{\frac{\sigma^2_{\tau_{(a,b)}}}{2}}$, $\forall n \in N$ was added, where the TDOA standard deviation was set to $\sigma_{\tau_{(a,b)}} = 19\,\mathrm{m}$ as in the previous CRLB analysis. The RMSE of 2000 Monte-Carlo runs for each emitter position is calculated and compared to the corresponding CRLB value. The results are depicted in Fig. 4.18. The same emitter localization algorithm as for the evaluation of the field experiments data was used. It can be observed, that the algorithm reaches the CRLB for the selected aircraft trajectory.

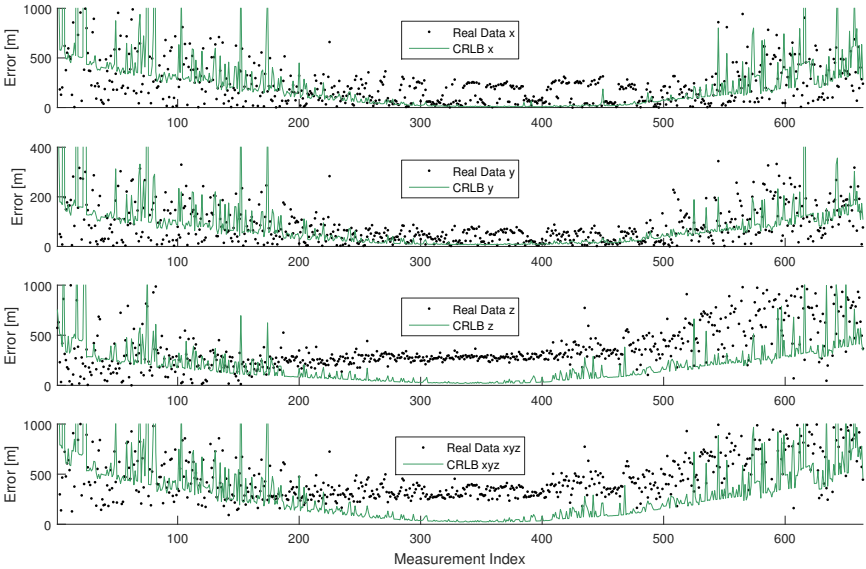

Figure 4.17: Results of the comparison of localization results and CRLB for the selected trajectory.

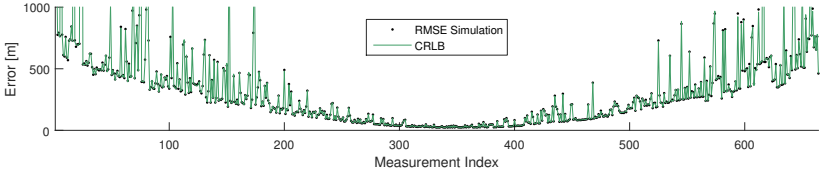

Figure 4.18: Results of 2000 Monte-Carlo runs compared to the CRLB.

4.3.5 Examples of aircrafts sending faulty ADS-B information

During the evaluation of the data sets, some multilateration tracks with noticeable localization bias were found. In this section, examples of aircrafts sending wrong ADS-B position information are given. To verify if the ADS-B or the calculated multilateration track is wrong, the localization results are compared to track data recorded by the RTRN. One example was chosen from each data set to give an impression of imprecise ADS-B position information. Furthermore, during the evaluation of the collected data sets, an aircraft attracted attention because all transmitted ADS-B positions were off by more than 100 km and were not even resulting in a connected or plausible track of any kind.

The ADS-B position errors of both example tracks seem to result from erroneous INS/GPS data since both tracks have noticeable errors during maneuvers. The employed ADS-B transponders are probably not connected directly to a GPS receiver but gain their position information from a flight computer which incorporates GPS and other INS navigation sensors into one location information.

4.3.5.1 Example 1

The first example shows an aircraft of the type Fokker F70 flying north of the sensor network, see Fig. 4.19 (a). The aircraft starts at Cologne-Bonn Airport (CGN) and flies in north-western direction. The plane is observed for a duration of 687 s and the corresponding RTRN track has a length of approximately 107 km. The zoomed area depicted in Fig. 4.19 (b) shows the deviation of the position information transmitted using ADS-B (blue line) compared to the RTRN (black dotted line) and to the MLAT (magenta line) tracks. The same tracks are depicted in Fig. 4.20 plotted in a georeferenced map. The aircraft is first observed after leaving the runway of the airport CGN in southern direction.

For the multilateration track (MLAT), the geolocation of the aircraft was determined for 528 received ADS-B messages. The resulting 528 TDOA based localization results were given as input to the Kalman filter. The RMSE of the MLAT track compared to the ADS-B track is 2153 m. It is very probable, that the ADS-B information is imprecise since the RTRN and MLAT tracks are very similar. The RMSE of the MLAT track compared to the RTRN track is 133 m. The 528 messages are received by an average of 6.2 sensors.

The error distributions are given in Fig. 4.21. Fig. 4.21 (a) depicts the error distribution of the multilateration localization results compared to the ADS-B position information. Fig. 4.21 (b) gives the error distribution of the multilateration results

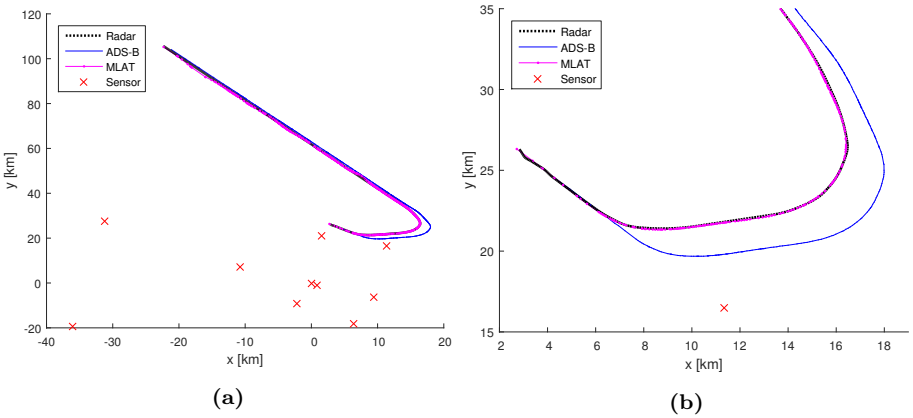

Figure 4.19: Example 1. Aircraft starting at CGN and flying in north-western direction.

compared to the corresponding RTRN track. A good multilateration localization accuracy can be observed whereas the ADS-B position information shows a large error, especially during the maneuver of the aircraft.

Figure 4.20: Example 1. Aircraft departing at CGN projected over satellite image. (Map Data: ©GeoBasis-DE/BKG 2016).

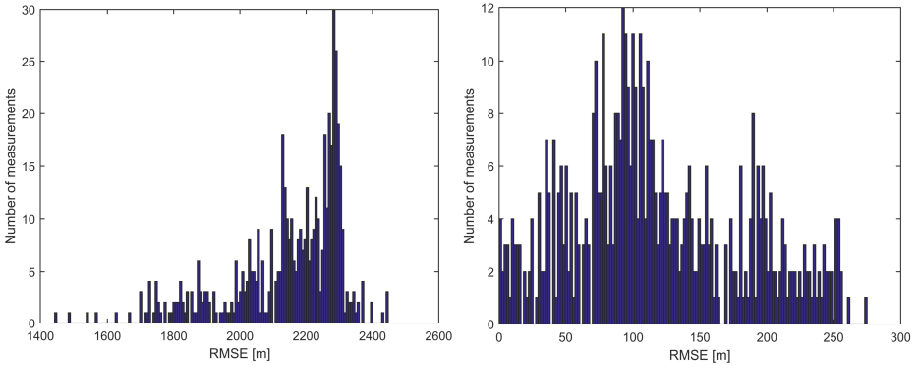

(a) **(b)**

Figure 4.21: Error distribution of Example 1: (a) MLAT compared to ADS-B (b) MLAT compared to RTRN.

4.3.5.2 Example 2

The second example was chosen from data set 2 (29.10.2015 21:30-22:30 UTC). A total of 247 ADS-B messages were received from a Boeing 757 aircraft. For each received telegram, the position is estimated based on TDOA. The MLAT track results from Kalman filtering those 247 localization results.

The aircraft is first observed at a distance of more than 100 km in the north east of the sensor network. It is then tracked until approximately 3 km before landing at CGN. The observation duration is 920 s and the length of the corresponding RTRN track is approximately 133 km. The whole track and an enlarged sector are depicted in Fig. 4.22. A constant bias between RTRN/MLAT and the ADS-B track can be observed. The RMSE of the MLAT track compared to the ADS-B positions is 1315 m. The RMSE of the MLAT track compared to the RTRN track is 514 m. The same sector as given in Fig. 4.22 (b) is plotted in a georeferenced map to show the aircraft approaching the runway of the airport CGN.

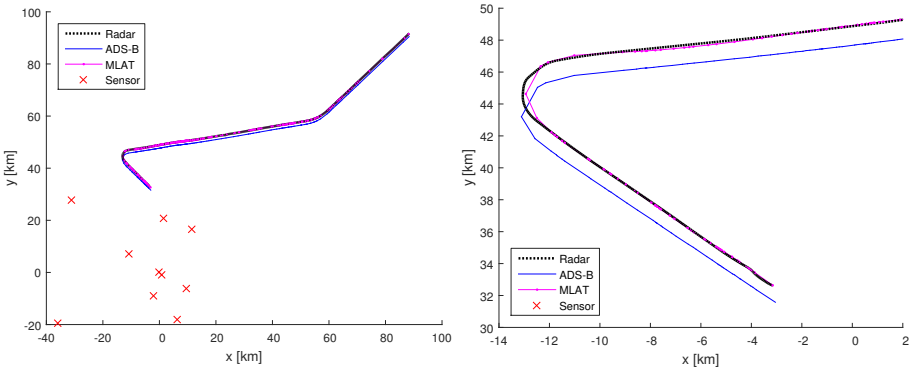

Figure 4.22: Example 2. Aircraft landing at CGN.

Due to the sensor network being located far in the south-east of the airport CGN, at very low altitudes, the ASD-B messages are not received by enough sensors to calculate a TDOA localization result for ground located aircrafts at the airport CGN. The higher localization error of this example compared to Example 1 is partly caused by less sensors receiving the messages and by the sensor to emitter geometry. For Example 1, the average number of sensors used for the TDOA localization is 6.2. For Example 2, on average, only measurements from 5.2 sensors are used for the

position estimation. This is caused by inferior line of sight conditions. The TDOA based geolocation estimation accuracy naturally decreases with less measurements. A better sensor network placement around the airport would allow for a tracking of the aircraft until touch-down with much higher accuracy than the one achieved for this example.

The localization error distribution compared to ADS-B is given in Fig. 4.23 (a). The error distribution compared to the RTRN tracks is depicted in Fig. 4.23 (b).

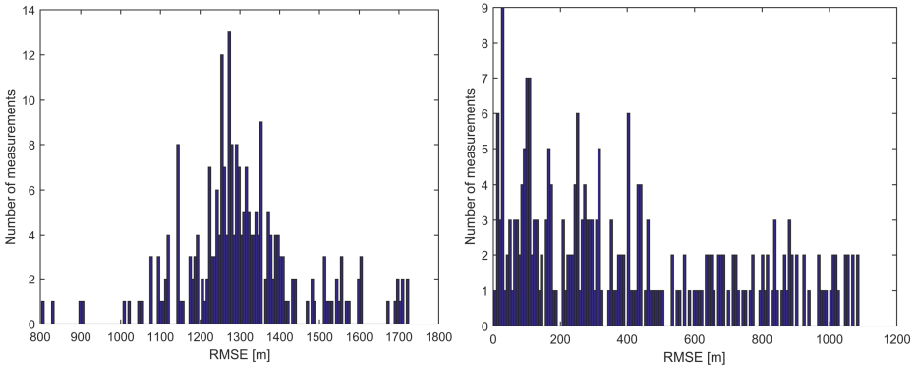

Figure 4.23: Error distribution of Example 2: (a) MLAT compared to ADS-B (b) MLAT compared to RTRN.

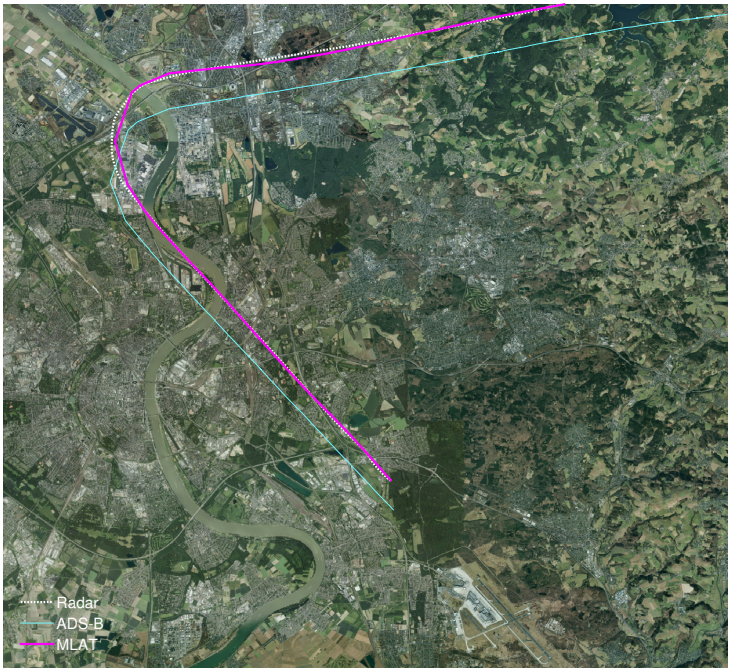

Figure 4.24: Example 2. Aircraft landing at CGN projected over satellite image. (Map Data: ©GeoBasis-DE/BKG 2016).

4.3.6 Comparison of TDOA and TOA based localization

As already stated in Section 2.7, the localization accuracy using TDOA and TOA should be very similar. Our results in [KSR+12] also tended towards this direction with a slightly worse precision of the used TOA estimator. In this section, the single localization results w.r.t. to the ADS-B position information (without applying a tracking filter) using TDOA and TOA localization are compared. The estimators are described in Section 4.3.2.2 and are initialized using the same position obtained by applying a closed form TDOA solution.

Data set 1 (as described in Section 4.3.1) is evaluated. Only localization results were selected where the results of both methods meet the filter parameters (like the maximum distance of the position estimate to the reference sensor), thus only considering localization results that are plausible for both methods. In this case, we only analyzed localization results that use the same parameters as the data given in

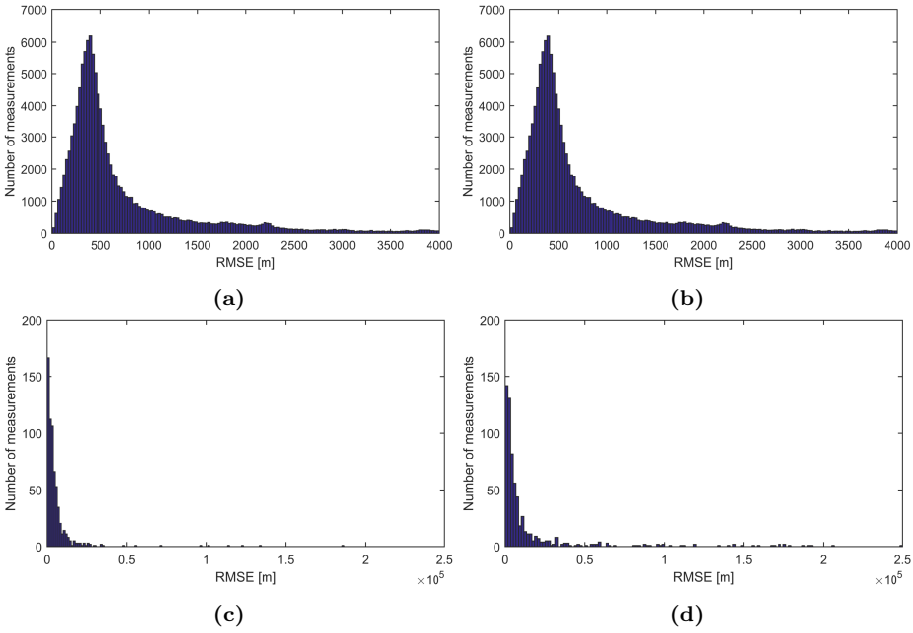

Figure 4.25: Error distribution of (a) TDOA and (b) TOA localization cut at 4 km. Error distribution of (c) TDOA and (d) TOA localization using only estimates where the error of TDOA and TOA differ by more than 10 m.

	All data	TDOA-TOA < 10 m	TDOA-TOA > 10 m
Evaluated Messages	123078	122428	650
RMSE TDOA-ADS-B	2687 m	2470 m	14775 m
RMSE TOA-ADS-B	3622 m	2470 m	36535 m

Table 4.5: Comparison of TDOA and TOA based localization using the field experiments data set 1.

the first result column of Table 4.2. The maximum target distance was set to 300 km, the minimum number of sensors used for a localization estimate was set to 5 and the minimum messages per target were set to 1. The error of the estimates is calculated w.r.t. the transmitted ADS-B position information. Results where the error of both methods differ by more than 10 m are examined in detail.

Fig. 4.25 shows the error distributions. The distribution for all evaluated position estimates is given in Fig. 4.25a and 4.25b. Errors larger than 4 km are not displayed. The error distribution of the position estimates where TDOA and TOA differ by more than 10 m are given in Fig. 4.25c and 4.25d. The results look very similar with some few larger outliers of the TOA estimator.

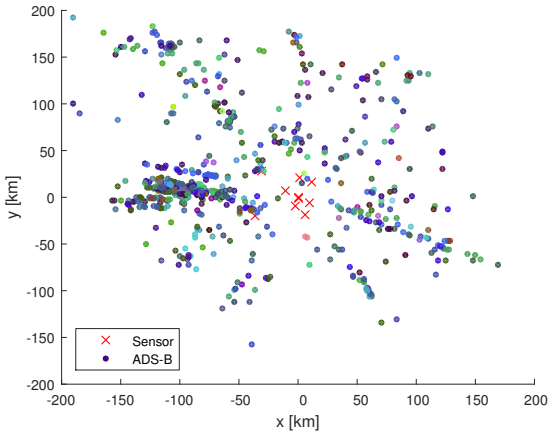

Figure 4.26: Emitter positions of localization results where TDOA and TOA localizer differ by more than 10 m.

The RMSE errors for all position estimates, only the position estimates for TDOA/ TOA difference less than 10 m and the localization results for TDOA/TOA difference larger than 10 m are given in Table 4.5. Less than 0.53 % of the TDOA and TOA localization differ by more than 10 m. For those outliers, the performance of the TDOA estimator with a RMSE of 14775 m is better than of the TOA estimator with 36535 m. However, this small number of outliers significantly downgrades the performance of the TOA estimator. This might give a false impression and possibly TOA might outperform TDOA in other scenarios with different sensor-emitter-geometries.

The position distribution of those outliers is depicted in Fig. 4.26. As was assumed by [SHM10,Kau12] the difference in localization accuracy of TDOA and TOA estimators is probably due to different nonlinearities of the interpretation of TDOA and TOA measurements. Clusters of emitter positions that show this behavior can for example be observed in the west of the sensor network. But this may also be due to flight corridors, since the aircrafts are not distributed uniformly over the area of interest.

4.4 Summary

In this chapter, the evaluation of a multilateration data set was presented. The data was collected during a period of one week (29.10.2015 - 05.11.2015) using a sensor network with 10 sensor nodes distributed over an area of approximately 50×50 km. Data from aircrafts sending ADS-B, Mode-S and Mode-A/C messages (operating at a center frequency of 1090 MHz) was collected.
First, an experimental analysis concerning the time synchronization and TOA timestamping accuracy for received ADS-B messages was presented in Section 4.2. The accuracy of the resulting TDOA measurements was in the range of 51 ns to 88 ns which is well suited for multilateration (MLAT) based emitter geolocation.

In Section 4.3, the experimental setup of the data collection as well as the evaluation of the data were given. The results with respect to the position estimation of the aircrafts sending ADS-B messages were presented in Section 4.3.3. These position estimates were obtained by applying TDOA based localization methods to messages received by multiple sensor nodes. The resulting position estimates were merged to a track using a Kalman filter. The obtained tracks were compared to the ADS-B position information transmitted by the aircrafts as well as to track data from a Reference Tracking Radar Network (RTRN) with up to 30 radars. A good localization performance of the multilateration sensor network was observed.
The reliability of the transmitted ADS-B position information however is questionable. For two selected examples, it was shown that the MLAT tracks were much more accurate compared to the RTRN tracks than the ADS-B (see Section 4.3.5).

The feasibility to track aircrafts based on TDOA measurements obtained by a sensor network (5 to 10 sensor nodes) from received ADS-B (Mode-S, Mode-A/C) data was shown. Using a sensor network distributed over an area of less than 50×50 km, an area of approximately 350×350 km could be observed with high localization accuracy. Using a sensor network with multilateration capability gives very promising results for complementary airspace surveillance.

The examples of aircrafts sending faulty ADS-B position information presented in Section 4.3.5.1 and Section 4.3.5.2 indicate that ADS-B in its currently deployed stage is not reliable enough to allow for example a safe airport approach under poor weather conditions or airspace separation in very densely used airspaces without additional information from PSR/SSR. Multilateration can fill this surveillance gap making use of the signals sent by aircrafts and giving reliable localization and tracking results which can help improving airspace surveillance in combination with the already existing systems like primary and secondary surveillance radars and ADS-B.

In Section 4.3.6, the localization accuracy using TDOA and TOA measurements is compared based on data set 1 of the field experiments. The position estimation error only differs by more than 10 meters in less than 0.53 % of the results. For this small number of outliers, TDOA seems to outperform TOA which also results in a higher RMSE over all results. However, this may give a false impression, since a small number of outliers downgrades the otherwise very similar performance of both estimators.

Future work should/could include the following topics. The field experiments concerning the timestamping and synchronization accuracy of the sensor network revealed only small errors. However, with further distance of the target to the sensor network, even small measurement errors have high impact on the precision of the localization estimate. Estimating and compensating clock drifts and clock biases of the sensors along with the emitter positions in a data fusion step would allow for even more accurate aircraft tracking.
Including Mode-S and Mode-A/C messages into the localization and tracking would give more position estimates which should result in even more precise MLAT tracks. Since the 1090 MHz data transmission does not use any channel access method, messages are not received correctly or fully due to overlaps. It is very unlikely, that the same message is incorrectly received at each sensor node. Thus, those partially received messages still carry information and can be used in the localization step once they are assigned to the corresponding fully received data from other sensors.
A safe airport approach could be realized using a MLAT sensor network with only a few sensor nodes. When placed at suitable positions near the airport, the received data can not only be used to calculate a MLAT track independent of the transmitted ADS-B position but already two sensor nodes may suffice to verify the plausibility of the transmitted ADS-B position which is an important information for the operator.

CHAPTER V

(Direct) Localization using a single moving sensor

The localization techniques presented in this chapter and the corresponding evaluation given in Chapter 6 are based on [Ste15, SO15] © 2015 IEEE and [SO16]. In the following, the introduced approaches are referred to as single sensor signal structure TDOA (S^4TDOA) localization.

5.1 Motivation

Passive emitter localization is a fundamental task encountered in various fields like wireless communication, radar, sonar, seismology, and radio astronomy. An airborne sensor platform is the preferable solution in many applications. The sensor is typically mounted e.g. on an aircraft, a helicopter, or an unmanned aerial vehicle (UAV). Airborne sensors provide in comparison to ground located sensors a far-ranging signal acquisition because of the extended radio horizon. Mostly for localization issues, sensors are installed under the fuselage or in the wings of the airborne sensor platform. In case of hard payload restrictions only compact sensors which preferably use only one small antenna come into consideration.

Passive emitter localization using a sensor consisting only of a single channel receiver and an omni-directional antenna may thus be of significant advantage when using small and light weight observer platforms. A TOA/TDOA based localization approach that makes use of specific knowledge of signal repetition intervals, encountered for example in mobile communication or radar systems, allows passive emitter localization using an omni-directional antenna and single-channel sensor hardware. Constraints concerning the emitted signal itself and a precise time synchronization or stable local clock of the observer need to be taken into account.

The current trend in emitter localization tends towards small UAV carried sensor systems that act the most covertly possible. Thus, wideband communication between observer platforms and ground control stations can be considered to be a significant strategic risk. In many military applications, knowledge of infrastructure locations like mobile communication base stations or radar systems is of great benefit. Using small platforms and reducing the amount of own signal emission makes reconnaissance flights harder to detect and can offer this strategic advantage. The presented localization schemes only require a narrowband communication channel to transmit the localization estimates to a GCS (Ground Control Station) or an operator. If the methods are used in a sensor network, S^4TDOA can be used as a TOA estimator and only the observer's position and the corresponding TOA obtained by S^4TDOA have to be transmitted.

Aspects of the two-dimensional and three-dimensional localization problem examined in the literature include numerous estimation algorithms, estimation accuracy, and target observability [Tor84, Bec01]. Typical localization systems of interest obtain measurements like direction of arrival (DOA), frequency difference of arrival (FDOA), time difference of arrival (TDOA) or combinations of the aforementioned measurements [KMK10].

Commonly, the desired source locations are determined in multiple steps: the signal processing step where the sensor data is computed from the raw signal data, and the sensor data fusion step where the localization and tracking task is performed. Alternatively, direct position determination (DPD) approaches have been proposed to compute the desired target parameters in a single step based on the raw signal data without explicitly computing intermediate measurements like DOA, FDOA, and TDOA [WA06, Wei04]. It has been shown that this kind of data processing offers a superior performance in scenarios with weak or closely-spaced sources but requires a higher computational burden in comparison to the standard multi-step processing. For example for TDOA based localization, a direct approach based on the raw signal data has been proposed in [WA06, AW09], and a standard approach based on TDOA/FDOA measurements has been proposed in [Ste81, Tor84], respectively. In [PF14], a localization approach based on the complex ambiguity function (CAF) has been introduced which turned out to be a compromise between localization performance and computational burden. Analysis of emitter localization using a single moving observer based on frequency measurements with context knowledge has been introduced in [Fow01]. The results show the advantage of using a priori knowledge concerning the emitter's altitude (either known or using a terrain model) on the performance of a localization system. In [Bec92], a method for single platform ge-

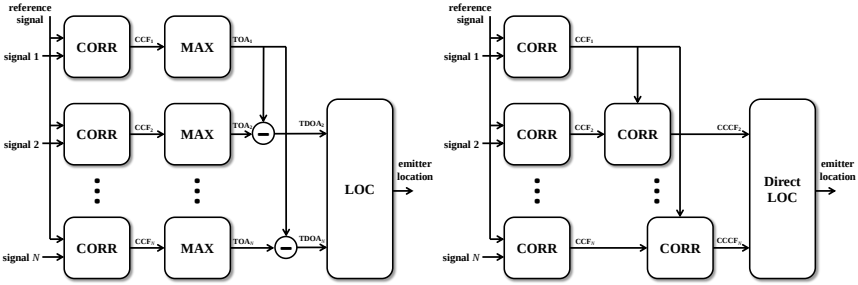

(a) S^{4}TDOA approach **(b)** DS^{4}TDOA approach

Figure 5.1: Comparison of non-direct and direct S^{4}TDOA approach. © 2015 IEEE.

olocation using joint Doppler and AOA measurements is proposed. The combination of these heterogeneous measurements can allow more accurate position estimation. More recently, research on the single receiver TOA/TDOA based localization using the periodicity of emitted signals has attracted attention. In [TBW14], the single observer geolocation dealing with oscillator instability is investigated. Experimental results using a moving observer and Kalman filters for the estimation of the local oscillator drift can be found in [MQT15, QMT15].

A DPD approach for a moving antenna array sensor was proposed in [ON10, Ois09]. Furthermore in [Ste15], we introduced a *single element* TDOA localization approach using just a single omni-directional antenna (Fig. 5.1a). Commonly, single-element approaches using a single directional antenna take the directions in which local maximum power is received to be the DOA estimates [SG93]. Since directional antennas cannot simultaneously scan in all directions, some transient signals can escape detection and fluctuations of the source signal strength and polarization during the sequential lobing process may have a significant impact on the DOA accuracy. However, these problems are circumvented by the technique proposed in [Ste15] which is applicable when information about the signal structure is known a priori (e.g. communication and radar emitters). The method does not require knowledge of the contents of the emitted signal. The information that is needed, is that the emitter sends message bursts at a known repetition frequency. For the example of GSM signals, the emitter sends data of a duration of $\approx 546.46\,\mu$s followed by a pause of $\approx 30.46\,\mu$s. The knowledge of this repeated pattern of signal transmissions and pauses is used for the single sensor signal structure TDOA approach. In this chapter, we assume the transmission on/off structure to be known but never assume the transmitted signal

itself to be known to the estimator during the simulations and real data evaluation.

In [SO15], the single-element TDOA localization approach is extended by the key-idea of direct emitter localization. For an airborne scenario with a single stationary source, we introduce a novel direct localization approach based on the cross correlation function (CCF). Our simulation and experimental measurement results demonstrate that the proposed approach considerably outperforms the standard single-element localization approach. This approach is named as direct S^4TDOA abbreviated with DS^4TDOA (Fig. 5.1b).

The block diagram given in Fig. 5.1 depicts the different approaches in the measurement/localization steps. For the non-direct S^4TDOA method, the signal received at each observation step is correlated with the reference signal. The maximum of this correlation yields the TOA of the signal. By differentiating TOAs of two observation steps, a TDOA measurement is obtained (first step: measurement step). These TDOA measurements are used in the localization step (2nd step). The direct method DS^4TDOA omits the TDOA estimation step and the correlation functions are input to the localization algorithm (Direct Position Determination, single step localization).

This chapter is based on the work presented in [SO15] where two slightly different (D)S^4TDOA are described. The newly introduced methods are called (D)S^4TDOA* and do not rely on the explicit representation of the signal structure using a reference signal. All four (D)S^4TDOA$^{(*)}$ approaches are compared using the Cramér-Rao Lower Bound CRLB and Monte-Carlo simulations. The results were also published in [SO16].

This section is organized as follows: In Section 5.2, the considered localization problem is stated which is a special case of the localization problem described in Chapter 2. The employed Cramér-Rao Lower Bounds on TDOA estimation and on TDOA based emitter localization are referred in Section 5.3. In Section 5.4, we briefly review the S^4TDOA localization approach based on the CAF [Ste15] as well as the direct version DS^4TDOA [SO15] and introduce the two novel (D)S^4TDOA* approaches [SO16]. Monte-Carlo simulations and the comparison to the Cramér-Rao Lower Bound are shown in Section 6.1. Simulation results for a real data scenario comparing S^4TDOA and DS^4TDOA approaches are presented in Section 6.2. In Section 6.3, the experimental measurement results proof the concept. Finally, the concept of (D)S^4TDOA$^{(*)}$ is compared to classic localization techniques (Section 6.4) and conclusions are given in Section 6.5.

The following notations are used throughout this chapter: $f[k]$ is a discrete version of

the function $f(t)$, $f^*[k]$ is the conjugate complex of the function $f[k]$, $f^{(\tau)}[k]$ denotes the sampled version of $f(t-\tau)$ and $(\cdot)^T$ denotes transpose.

5.2 Problem Formulation

We consider an omni-directional antenna sensor mounted on an airborne platform moving along an arbitrary but known sensor path observing a single stationary, ground-located source at position $\mathbf{x}$. The target emits a coherent signal $s(t)$ which is built up by times, where information is transmitted and pause intervals between those transmissions. The duration of each transmission and each pause intervals is assumed to be constant and known. For example in the case of a communication signals, the information is sent as bursts during the transmission time and the pause times are guard periods between consecutive bursts. The exact modulation method or the content of the transmission bursts doesn't need to be known as long as a certain level of signal-to-noise ratio results from the transmission.

A special case of the localization problem stated in Section 2.3 is investigated in this chapter. Since only one moving sensor node is considered that acquires measurements over time at different locations, only the index n is used for measurements at different locations and time steps. A slightly different notation is required for the method description, therefore the problem is described in its totality and changes compared to the localization problem in Section 2.3 are described. For example, the local sensor clock at the beginning of each signal acquisition is necessary to be known independently of the TOA of the signal. This demands for a slightly enhanced notation as is usually used for TOA/TDOA based localization.

During the movement, the sensor collects N signal data batches. The n-th received signal at some measurement point reads

$$z_n(t) = a_n\, s(t - t_{\mathrm{e},n} - t_n)\, \exp(\mathrm{j}\,\nu_n t) + w_n(t)\,, \tag{5.1}$$

where a_n denotes a path attenuation factor, $t_{\mathrm{e},n}$ denotes the unknown signal emission time of the n-th received signal, t_n denotes the time difference between signal emission and signal acquisition, ν_n is the signal Doppler shift induced by the movement of the own sensor platform, and w_n denotes some additional receiver noise, $n = 1, ..., N$. The transmitted signal $s(t)$ and the received signals $z_n(t)$ are assumed to be complex base-band signals.

In practice, the sensor collects data samples from the received signal. In the considered scenario, the sampling rate is assumed to be high enough that the sensor location p_n

is approximately constant for each collected data batch (Fig. 5.2). Then, t_n and ν_n are given by

$$t_n(\mathbf{x}) = \frac{||\triangle p_n(\mathbf{x})||}{c}\,, \tag{5.2}$$

$$\nu_n(\mathbf{x}) = \frac{\mathbf{v}_n^T \triangle p_n(\mathbf{x})}{||\triangle p_n(\mathbf{x})||}\,\frac{f_0}{c}\,, \tag{5.3}$$

respectively, where $\triangle p_n(\mathbf{x}) = \mathbf{x} - p_n$ denotes the relative vector between sensor and source, $\mathbf{v}_n$ is the sensor velocity vector, c is the signal propagation speed, and f_0 is the center frequency of the emitted signal.

Considering the time-discrete version of the received signal in (5.1), the k-th data sample of the n-th data batch is given by

$$z_n[k] = a_n\, s(k\triangle - \mathrm{clk}_n - \tau_n)\, \exp(\mathrm{j}\,\nu_n k\triangle) + w_n[k]\,, \tag{5.4}$$

where $\triangle$ is the sample interval, clk_n is the known sensor clock of the n-th measurement, τ_n is the signal time of arrival relative to the sensor clock. Please note that $\mathrm{clk}_n + \tau_n = t_{e,n} + t_n$ holds. The additional receiver noise w_n is assumed to be temporally uncorrelated and zero-mean Gaussian. When investigating this special case of TDOA based localization, the local sensor clock at the beginning of each signal acquisition is of high importance to the method and is taken into account in the measurement functions separately. The TOA in this and the following chapter therefore

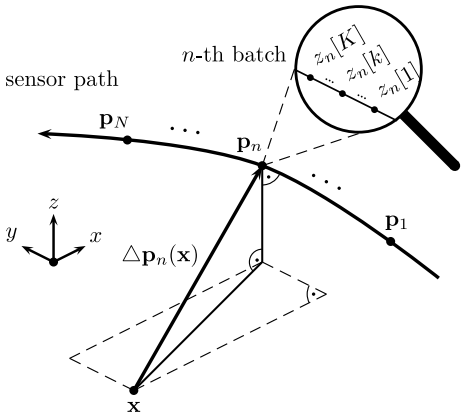

Figure 5.2: Three-dimensional localization scenario. © 2015 IEEE.

refers to the signal time of arrival relative to this sensor clock instead of the absolute time of arrival.

For the single sensor TDOA estimation, a reference signal $\tilde{s}[k]$ is used which characterizes the repetition pattern of the transmitted signal. For the ideal case, the emitted signal would be known and thus $\tilde{s}[k] = s[k]$. Since usually, the emitted signal is unknown for almost all applications, the reference signal we employ throughout this paper only characterizes the transmission on/off pattern of the emitted signal, which basically results in a comparison of the amplitudes of the received signal with the reference signal. If the emitted signal were known, much better localization performance could be achieved. Throughout this paper, we assume the transmission and guard interval periods to be known. The method doesn't require knowledge of the contents of the emitted signal and we never assume the signal to be known during the simulations or real data evaluation (where in fact, we don't know the emitted signal).

Finally, the localization problem is stated as follows: Estimate the source location $\mathbf{x}$ from the received signal data batches $\mathbf{z}_n = (z_n[1], ..., z_n[K])^T$, $n = 1, ..., N$.

5.3 Cramér-Rao Lower Bound

In the following, we state which Cramér-Rao Lower Bounds are used for the TDOA estimation as well as for the localization problem with respect to the investigated scenario.

CRLB on TDOA Estimation

In Section 2.6, bounds on TDOA estimation were described. For the evaluation of the investigated (D)S^{4}TDOA* methods, the bound presented in Section 2.6.2 based on [YA11] is used as measurement variance in the calculation of the CRLB on emitter localization.

CRLB on Emitter Localization

The CRLB on emitter localization was presented in Section 2.7. The localization approaches analyzed in this chapter use TDOA measurements that are spatially and temporally uncorrelated. Thus, addition of the Fisher Information of different measurement steps is possible. The bound that applies to this scenario is given in Section 2.7.1. The scenario described in Section 6.3.3 uses the full measurement set over all observation steps. Therefore, the bound given in Section 2.7.2 with the adaption to a 3-dimensional scenario with known emitter altitude is applied.

5.4 Localization Approaches

In this section, approaches for the stated localization problem are presented i.e. the localization of a source with periodic coherent emission using a single moving sensor. Four measurement approaches for the single observer scenario are considered.

Firstly, an approach S^{4}TDOA based on TOA measurements is presented (Section 5.4.1). Then, a derivation of this method called DS^{4}TDOA based on the CCF and direct position determination is presented in Section 5.4.2. For both methods, approaches without the use of a representation of the reference signal $\tilde{s}[k]$ are introduced in Section 5.4.4. Those methods are called S^{4}TDOA* and DS^{4}TDOA* respectively. For the sake of simplicity, only TOA/TDOA measurements are considered in following and the Doppler is neglected. Nevertheless, the following techniques could be generalized to full CAF.

5.4.1 Two-step S^4TDOA Approach [Ste15]

Step 1: Commonly for a sensor network, TDOA measurements are extracted from the cross correlation function

$$\mathrm{CCF}(\tau_{(1,2)}) = \sum_{k=1}^{K} z_1^*[k] z_2^{(-\tau_{(1,2)})}[k]\,, \tag{5.5}$$

i.e. from the correlation of the two signals $z_1[k]$ and $z_2[k]$ in time domain. The TDOA estimates are calculated by detecting the peak in the CCF:

$$\hat{\tau}_{(1,2)} = \arg\max_{\tau_{(1,2)}} \mathrm{CCF}(\tau_{(1,2)})\,. \tag{5.6}$$

However, since a single moving sensor is considered, the measurements are not taken simultaneously. Thus in the following, the signal processing for the single sensor case is presented (Fig. 5.1a). Due to the known signal structure, a quasi-TDOA measurement can be computed by considering the individual known sensor clock clk_n:

$$\hat{\tau}_n = \arg\max_{\tau_n} \mathrm{CCF}_n(\tau_n) \tag{5.7}$$

with

$$\mathrm{CCF}_n(\tau_n) = \sum_{k=1}^{K} z_n^*[k] \tilde{s}^{(-\mathrm{clk}_n - \tau_n)}[k]\,, \tag{5.8}$$

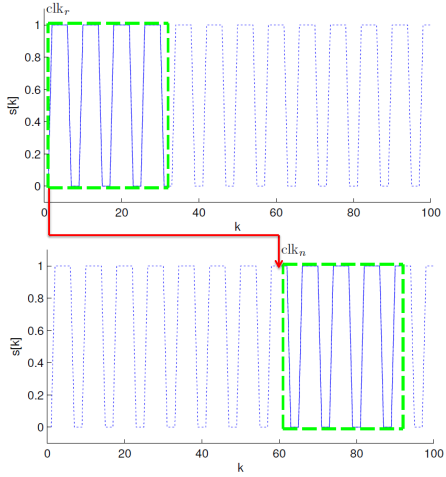

Figure 5.3: Schematic representation of the received signals at measurement step r and n. © 2015 IEEE.

where $\tilde{s}[k]$ denotes a reference signal introduced in (5.4). Then similar to (5.6), a quasi-TDOA measurement can be calculated by taking the clock differences (Fig. 5.3)

$$\triangle \mathrm{clk}_{(n,r)} = \left(\left\lceil \frac{\mathrm{clk}_n - \mathrm{clk}_r}{T} \right\rceil - \left\lfloor \frac{\mathrm{clk}_n - \mathrm{clk}_r}{T} \right\rfloor \right) T \tag{5.9}$$

into account, where the index r indicates some reference time. Then a quasi-TDOA measurement can be extracted from the TOA estimates by

$$\hat{\tau}_{(n,r)} = \hat{\tau}_n - (\hat{\tau}_r + \triangle \mathrm{clk}_{(n,r)}) \,, \tag{5.10}$$

i.e. by the difference of the individual estimated TOAs corrected by the clock difference. The correction of the clock difference is mandatory because the measurements are not taken simultaneously.

Step 2: The emitter localization problem can be solved by searching the emitter location that most likely explains the TDOA measurements calculated in (5.10). Therefore, the emitter location can be calculated by solving the following least-squares form:

$$\hat{\mathbf{x}} = \arg\min_{\mathbf{x}} \sum_{\substack{n=1 \\ n \neq r}}^{N} \frac{||\hat{\tau}_{(n,r)} - \tau_{(n,r)}(\mathbf{x})||^2}{\sigma^2_{\tau_{(n,r)}}} \,, \tag{5.11}$$

where $\tau_{(n,r)}(\mathbf{x})$ denotes the measurement function given analog to (5.10) by

$$\tau_{(n,r)}(\mathbf{x}) = t_n(\mathbf{x}) - (t_r(\mathbf{x}) + \triangle \mathrm{clk}_{(n,r)}) \,, \tag{5.12}$$

according to (5.2) and $\sigma^2_{\tau_{(n,r)}}$ denote the TDOA measurement variance, $n = 1, ..., N$. The solution in (5.11) can be geometrically interpreted as the intersection of the hyperbolae represented by the individual TDOA measurements.

At this point it is worth to mention that in practice, the measurement variances are unknown and vary during the time. Consequently, the measurement variance have to be estimated because otherwise one could use an estimator with a reduced performance.

5.4.2 One-step DS^4TDOA Approach [SO15]

The key-idea of direct localization approaches is to avoid the decision for one TOA/TDOA/AOA measurement in the first step of a localization algorithm. In the case of the S^{4}TDOA method as described in the previous section, this decision is represented by the process of maximum determination of the CCF. The choice will always fall on the highest peak of the CCF, but when taking into account all measurement batches, this peak might be wrong. In this case, f.e. the second highest peak of the CCF would correspond to the sensor emitter geometry and fit all other measurement batches. Thus, leaving this decision open, allows the implicit evaluation of multiple measurement hypotheses in one localization step.

The intention is to create a cost function that has to be optimized in the localization step, which takes into account all measurement batches at the same time without the explicit decision for TDOAs (Fig. 5.1b). By calculating the CCF of the CCF$_r$ (CCF of $\mathbf{z}_r$ and $\tilde{s}[k]$) and the CCF$_n$ (CCF of $\mathbf{z}_n$ and $\tilde{s}[k]$), the choice for an explicit TDOA can be postponed into the localization step. We call this approach direct single-sensor signal structure TDOA localization (DS^{4}TDOA).

The choice of this approach is motivated by the scheme used for the multi-sensor TDOA localization, where the TDOA is not explicitly chosen in the first step but the TDOA measurement function is directly used as input for the localization step [AW09, PF14]. Instead of a TDOA estimation from two received signals, DS^{4}TDOA obtains the TDOA from two TOA measurements. The equivalent DS^{4}TDOA then relies on the CCF of the TOA measurement functions, which are the CCFs of the received signals with the reference signal.

The proposed cost function (cross correlation of cross correlation functions) subject to the position $\mathbf{x}$ is defined as

$$\mathrm{CCCF}_{(n,r)}(\mathbf{x}) = \sum_{k=1}^{K} \mathrm{CCF}_n^*[k]\mathrm{CCF}_r^{(-\tau_{(n,r)}(\mathbf{x}))}[k]\,, \tag{5.13}$$

with the CCF given in (5.8). The localization problem is then stated by

$$\hat{\mathbf{x}} = \arg\max_{\mathbf{x}} \sum_{\substack{n=1 \\ n\neq r}}^{N} \mathrm{CCCF}_{(n,r)}(\mathbf{x})\,. \tag{5.14}$$

5.4.3 Discussion

The localization accuracy for both methods may degrade, if the distance between two observer positions is too big compared to the signal repetition duration T.

If $\tau_{(n,r)}(\mathbf{x}) \geq \frac{T}{2}$ the wrong peak may be chosen in the maximum determination of the CCFs in the case of S^{4}TDOA. This choice has a direct effect on the localization accuracy using S^{4}TDOA.

The influence on the localization for DS^{4}TDOA is smaller if $\tau_{(n,r)}(\mathbf{x}) < \frac{T}{2}$ for almost all n. If $\tau_{(n,r)}(\mathbf{x}) \geq \frac{T}{2}$ for a significant number of measurements , the optimization of the localization function (5.14) may run into the maximum that corresponds to the wrong time slots. However this is unlikely, because the ambiguities that are due to $\tau_{(n,r)}(\mathbf{x}) \geq \frac{T}{2}$ are unlike to join in the same spatial position unless more than one emitter is present.

5.4.4 (D)S^{4}TDOA without the use of $\tilde{s}[k]$ [SO16]

Both approaches described in the previous sections use an additional signal $\tilde{s}[k]$ representing the information on the signal structure. This allows data reduction for the localization step. If processing power and data storage capacity and - in case of the use of the methods with multiple sensors - communication bandwidth is not an issue, the received signals can be stored and used for the localization process. In this case, instead of using TOA estimates calculated using $\tilde{s}[k]$ for S^{4}TDOA and the CCCF for DS^{4}TDOA, the cross correlation function of two received signals is used to estimate the TDOA or in the cost function of the direct method respectively. An additional shift factor according to the signal repetition interval and the observation time span has to be taken into account. We call these methods S^{4}TDOA* and DS^{4}TDOA*.

S^{4}TDOA*:

The first step of the localization process of S^{4}TDOA* is to calculate the maximum of the cross correlation function of two received signals at different time steps n, r:

$$\mathrm{CCF}_{(n,r)}(\tau_{(n,r)}) = \sum_{k=1}^{K} z_n^*[k] z_r^{(-\tau_{(n,r)})}[k]\,. \tag{5.15}$$

The TDOA measurement is then given by

$$\hat{\tau}_{n,r} = \arg\max_{\tau_{(n,r)}} \mathrm{CCF}_{(n,r)}(\tau_{(n,r)})\,. \tag{5.16}$$

In the second step, the emitter position is estimated by solving (5.11).

DS^{4}TDOA*:

Similar to (5.13), the cost function for DS^{4}TDOA* is given by

$$\mathrm{CCF}_{(n,r)}(\mathbf{x}) = \sum_{k=1}^{K} z_n^*[k] z_r^{(-\tau_{(n,r)}(\mathbf{x}))}[k]. \tag{5.17}$$

The localization problem is then stated by

$$\hat{\mathbf{x}} = \arg\max_{\mathbf{x}} \sum_{\substack{n=1 \\ n\neq r}}^{N} \mathrm{CCF}_{(n,r)}(\mathbf{x})\,. \tag{5.18}$$

For the evaluation of the real measurement data in this thesis (Chapter 6), S^{4}TDOA* and DS^{4}TDOA* are not applicable since processing power and storage capacity were limited. In the theoretical simulation and the CRLB evaluation (see Section 6.1), all four (D)S^{4}TDOA$^{(*)}$ methods are compared.

CHAPTER VI

(Direct) Localization using a single moving sensor - Evaluation

6.1 Localization Accuracy Evaluation

6.1.1 Simulation Setup

To evaluate the four presented (D)S^{4}TDOA$^{(*)}$ localization approaches, Monte-Carlo simulations and CRLB analyses are conducted. A 2-dimensional scenario is investigated where one observer moves along a trajectory from west to east as depicted in Fig. 6.1. For each observation time step $n \in \{1, ..., 12\}$, a signal $s_n[k]$ that is emitted from the target is simulated. We assume free space path loss

$$\mathrm{FSPL_{dB}} = 10\log_{10}\left(\frac{4\pi||\triangle \mathrm{p_n}(\mathbf{x})||}{\lambda}\right)^2 \tag{6.1}$$

and, by taking the receiver sensitivity $\mathrm{S_{dB}}$ into account, calculate the corresponding SNR

$$\mathrm{SNR_{dB}(n)} = (\mathrm{P_E} + \mathrm{G_E} + \mathrm{G_R} - \mathrm{FSPL_{dB}}) - \mathrm{S_{dB}}\,, \tag{6.2}$$

where λ is the wavelength of the signal, $\mathrm{P_E}$ is the transmitter power, $\mathrm{G_E}$ and $\mathrm{G_R}$ are antenna gain of the emitter and receiver antennas. The received signal is delayed by the time $t_n(\mathbf{x})$ the signal took to travel from the emitter to the observer according to (5.2).

The signals for each observation step are simulated as complex valued base-band signals at a sample rate of $f_s = 400\,\mathrm{kHz}$ using the following parameters. The duration of each observed signal is $\mathrm{T} = 1\,\mathrm{ms}$ composed of repeated data transmission

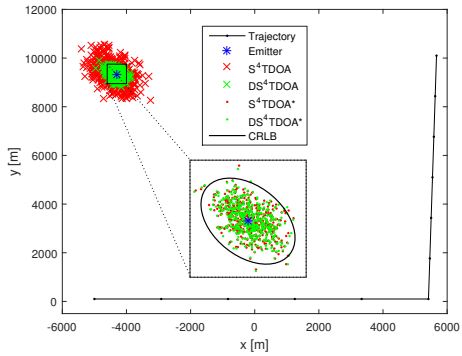

Figure 6.1: Scenario used for localization accuracy analysis including results of (D)S^{4}TDOA. Zoom of target area shows only (D)S^{4}TDOA* results. Transmission power $P_E = 30\,\text{dBm}$. CRLB is depicted as 3σ ellipse.

$T_{data} = 50\,\mu s$ and guard periods with duration $T_{guard} = 10\,\mu s$. During the time of data transmission, the emitted signal consists of a chirp signal with bandwidth $B = 200\,\text{kHz}$. During the guard periods, no data is transmitted. White Gaussian noise is then added to the signal according to the SNR calculated using (6.2). The noise power is determined over the whole observation bandwidth of 400 kHz. The parameters for the path loss calculation are $G_E = 3\,\text{dB}$, $G_R = 0\,\text{dB}$, $S_{dB} = -90\,\text{dBm}$ at a center frequency of 1800 MHz. The transmission power P_E is varied for different evaluations. The received signal is then given by $z_n[k]$.

The reference signal $\tilde{s}[k]$ which is used by (D)S^{4}TDOA has the same duration as the simulated received signal. The data transmission period starts with the first sample of $\tilde{s}[k]$ and the same reference signal is used at each time step. Since the TDOA and position estimation using (D)S^{4}TDOA in this special realization rely on the amplitude comparison by correlating the received signals z_n with the reference signal $\tilde{s}$, the reference signal can be modeled as a real valued signal with $\tilde{s}[k] = 1$ during data transmission periods and $\tilde{s}[k] = 0$ during guard periods.

TDOA measurements are taken between consecutive observation steps resulting in a total of $N/2$ TDOA measurements. The measurement set for each measurement index $m \in \{1, ..., N/2\}$ is given by $\{\hat{\tau}_{(1,2)}, ..., \hat{\tau}_{(2m-1,2m)}\}$.

The cost functions of (D)S^{4}TDOA$^{(*)}$ are maximized using Nelder Mead simplex optimization under the assumption of constant TDOA measurement variance. The initial position estimate for the optimization process is calculated by evaluating the

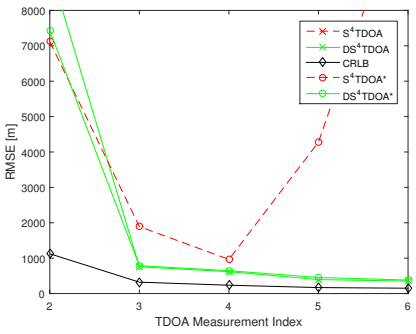

(a) Comparison of localization approaches to CRLB (transmission power $P_E = 18\,\text{dBm}$).

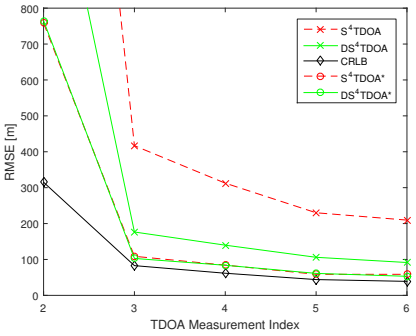

(b) Comparison of localization approaches to CRLB (transmission power $P_E = 30\,\text{dBm}$).

Figure 6.2: Comparison of localization approaches to CRLB for different transmission powers.

cost functions on a grid of possible emitter positions. The grid points are spaced by $500 \times 500\,\text{m}$. For the first TDOA measurement, no position estimate is given, since the emitter location is not observable with only one TDOA measurement.

Simulations with 500 Monte-Carlo runs are conducted. For each run, the emitter position is chosen uniformly at random from an area of interest ($AOI_x = -5000, ..., 5000\,\text{m}$, $AOI_y = 1000, ..., 8000\,\text{m}$). The position is estimated using all four (D)S^{4}TDOA$^{(*)}$ methods and the corresponding localization CRLB is calculated according to 5.3 and Eq. (2.47).

6.1.2 Results

The simulations are carried out for different transmission powers. Fig. 6.2a shows the results for $P_E = 18\,\text{dBm}$. For many emitter positions throughout the area of interest, this results in low SNR values. Both direct localization approaches are more robust against low SNR, since ambiguities in the cross correlation functions have less effect on the localization. The two step localization methods need to chose one TDOA measurement in the first step independently of all other observation steps whereas the direct technique postpones this decision into the localization step, where all measurements are incorporated (see also Section 5.4.3). The similar accuracy of DS^{4}TDOA and DS^{4}TDOA* is due to the high repetition rate of transmission and guard periods. The correlation of the reference signal, having very high SNR, and the received

signal with low SNR, still shows good cross correlation characteristics. The position estimation accuracy of S^{4}TDOA is out of the scale of Fig. 6.2a. The performance of S^{4}TDOA* improves until measurement index 4 and then degrades again. This is due to the fact that the mean SNR for the given trajectory and randomized emitter positions from the area of interest is often lower at the last observation points and thus the probability of choosing a wrong peak of the CCF increases.

By increasing the signal transmission power to $P_E = 30\,\text{dBm}$ and thus having higher SNR, the performance of S^{4}TDOA* is very similar to DS^{4}TDOA* for all measurement steps. The results are depicted in Fig. 6.2b. Again, DS^{4}TDOA outperforms S^{4}TDOA, which shows the lowest localization accuracy.

To show the distribution of the position estimates of all four (D)S^{4}TDOA$^{(*)}$ methods, a fixed emitter position is chosen. For this scenario, again 500 Monte-Carlo runs are conducted. The results of TDOA measurement index 6 are depicted in Fig. 6.1. The zoomed area shows only the estimates of S^{4}TDOA* and DS^{4}TDOA*. The CRLB is given by a 3σ error ellipse.

The advantages of (D)S^{4}TDOA compared to (D)S^{4}TDOA* are given by less need for storage space and a reduction of processing power (and communication requirements). A trade-off between localization accuracy and sensor requirements is possible using (D)S^{4}TDOA.

6.2 Simulation Using Real Data Scenario

The proposed localization approaches performances are evaluated in Monte-Carlo simulations for a given scenario. GSM base stations are chosen as emitter with recurring signal structure. In this section, only S^{4}TDOA and DS^{4}TDOA algorithms are evaluated.

6.2.1 Simulation Setup

The desired signal is sent on the broadcast channel of a GSM base station and is divided into time slots. Each time slot has a duration of $576.92\,\mu\text{s}$. A time slot is divided into data transmission time and guard period during which no transmission takes place. This time slot signal structure is represented by the reference signal $\tilde{s}[k]$ introduced in Section 5.2.

The sensor trajectory remains the same over all Monte-Carlo runs. The position of the emitter is chosen uniformly at random from a given area of interest. The

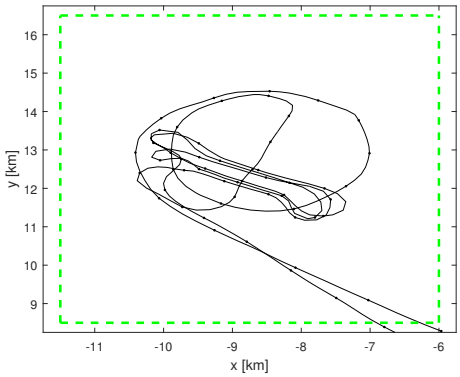

Figure 6.3: Simulation Scenario: Sensor trajectory and area of interest (green box).

localization accuracy is also evaluated w.r.t. the signal-to-noise ratio (SNR). A sensor trajectory that is similar to the one of the field experiments (Section 6.3) is used for the simulations. Fig. 6.3 shows the trajectory as well as the area of interest in which possible emitters are located.

We use the following definition of SNR for the simulations:

$$\mathrm{SNR}_{[\mathrm{dB}]} = 10\log_{10}\frac{\mathrm{P_s}}{\mathrm{P_n}} \tag{6.3}$$

with $\mathrm{P_s}$ being the mean signal power and $\mathrm{P_n}$ the mean noise power. A total of 250 Monte-Carlo runs were performed. Each Monte-Carlo run consists of the following:

1. An emitter position is chosen at random from the area of interest.
2. A random start drift of the broadcast signal is generated.
3. Signal noise for each sensor is generated.
4. For the given observer trajectory and emitter position and time of measurement, corresponding TOAs are calculated.
5. The broadcast signal is embedded into noise in accordance to the respective TOAs and scaled to meet given SNR value.
6. Localization results are calculated using both estimation methods
   a) The initialization is done by evaluating a grid of the respective cost functions for the area of interest.

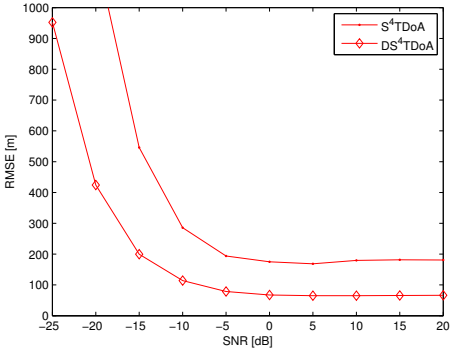

Figure 6.4: Simulation results: Localization RMSE over SNR for DS^{4}TDOA (red diamonds) and S^{4}TDOA (red dots). © 2015 IEEE.

b) The position is estimated using Nelder Mead simplex optimization.

7. Points 5 to 6 are repeated for all SNR values in question.

6.2.2 Position Estimation

The position estimation for the S^{4}TDOA method is divided into two main steps. In the first step, the received signal is correlated with the stored reference signal. The maximum of this correlation function yields the TOA of each measurement. TOAs of two observation steps form one TDOA measurement. In the second step, the emitter position is estimated based on a set of TDOA measurements.

For the DS^{4}TDOA localization, from the two observation steps that form the TDOA measurement in the above described case, cross correlate the cross correlation functions of the respective received signals and the reference signal. Estimate the emitter position from a set of those cross correlation functions.

For both methods, the respective cost functions are minimized using Nelder/Mead simplex optimization. The initialization problem is solved by evaluating the cost functions of each method for a grid over the area of interest. For the simulations, the grid points were spaced by 100×100 m.

6.2.3 Results

Fig. 6.4 depicts the results of the simulations. For each SNR value, the RMSE of the position estimation over all 250 simulation runs is calculated. The red line with red

dots shows the RMSE using the S^4TDOA, DS^4TDOA is plotted using red diamonds. The accuracy of the DS^4TDOA localization approach outperforms the S^4TDOA localization method.

6.3 Experimental Results

6.3.1 Experimental Setup

Field experiments were conducted to verify the presented method for real data. A GPS time-synchronized sensor node was used to gather data from a GSM mobile station. The sensors receiving antenna was mounted under the wing of an aircraft. The sensor itself and a PC for data processing were installed inside the aircraft. Every five seconds, data from the broadcast channel of the GSM base station was recorded at a sample rate of $f_s = 1$ MHz.

Along with the signal data, corresponding timestamps $\mathrm{clk_n}$ and position information from the GPS receiver of the sensor are recorded. For each observation time step n, the received signals are filtered and the CCF is calculated. From this CCF the TOA $\hat{\tau}_n$ of the signal is estimated as described in Section 5.4. The CCF, the estimated TOA, the sensors position and time are used in the localization step. The localization estimates for both methods are calculated using the same initialization for the optimization algorithm.

A 3-dimensional localization scenario is investigated. Fig. 6.5 depicts the sensors trajectory, the position of the GSM base station as well as the localization results using the presented S^{4}TDOA and DS^{4}TDOA method. The presented localization approach is evaluated for different levels of signal strength. Here, a threshold P_t is applied to the measurements. If the mean received signal strength $\mathrm{P_{z_n[k]}}$ is below the threshold, the measurement is not used in the localization step. The mean signal

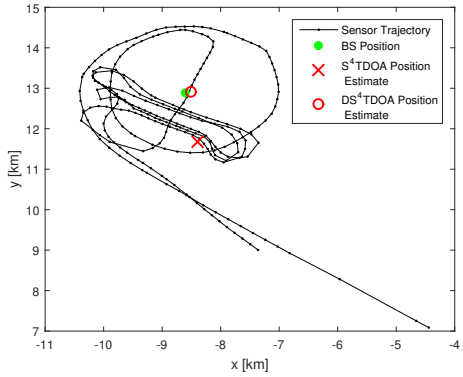

Figure 6.5: Scenario of field experiments. Sensor trajectory and localization results.

strength of a signal $z_n[k]$ is defined as

$$P_{z_n[k]} = \frac{z_n^*[k] z_n[k]}{K} \tag{6.4}$$

with K being the total number of samples.

6.3.2 Results

Fig. 6.6a to Fig. 6.6d show the localization cost functions Eq. (5.11) and Eq. (5.14) evaluated for a grid of possible emitter positions. The black line indicates the flight trajectory where the black dots indicate the measurements that are taken into account in the localization step according to the received signal strength threshold. The true position of the emitter is marked by a green dot. The position estimate of the S^{4}TDOA method is shown by a yellow x, the respective DS^{4}TDOA estimate by a red circle. The achieved localization accuracy is given in Table 6.1.

RSS	S^{4}TDOA	DS^{4}TDOA	RSS	S^{4}TDOA	DS^{4}TDOA
-80	4049	385	-69	1003	129
-79	889	257	-68	2026	82
-78	681	449	-67	1542	190
-77	842	223	-66	186	166
-76	1203	50	-65	161	179
-75	1424	451	-64	170	268
-74	1272	89	-63	312	141
-73	1374	145	-62	458	404
-72	1623	116	-61	258	66
-71	1546	112	-60	199	119
-70	901	332			

Table 6.1: Localization accuracy in [m] of field experiments data.

As can be seen in Fig. 6.6a, the minimum of the cost function of the S^{4}TDOA for a received signal strength threshold level of $P_\mathrm{t} = -74\,\mathrm{dBm}$ is not located at the true emitter position due to the choice of one or more faulty TOA values (maximum peaks of the CCF). This results in a larger localization error. Here, the advantage of the DS^{4}TDOA approach can be seen. Fig. 6.6b depicts the cost function of the DS^{4}TDOA method for the same scenario. As can be observed, the minimum of the cost function is located near the true emitter position and the localization result is more accurate. For this scenario with a received signal strength threshold of $P_\mathrm{t} = -74\,\mathrm{dBm}$, the 3-D localization error of the S^{4}TDOA is 1272 m. Using the DS^{4}TDOA localization algorithm, the position estimation error is 89 m.

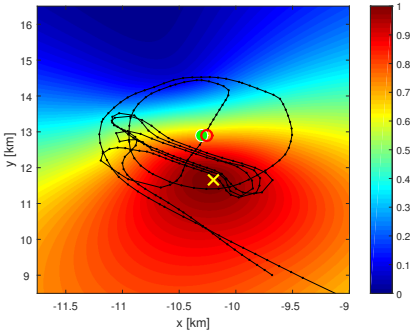

(a) Normalized cost function for S^{4}TDOA (signal threshold -74 dBm).

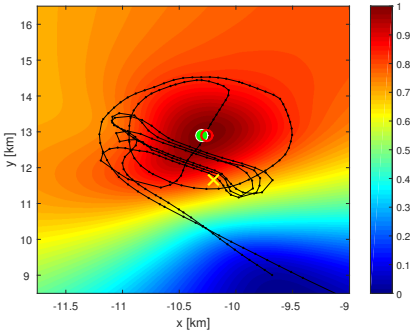

(b) Normalized cost function for DS^{4}TDOA (signal threshold -74 dBm).

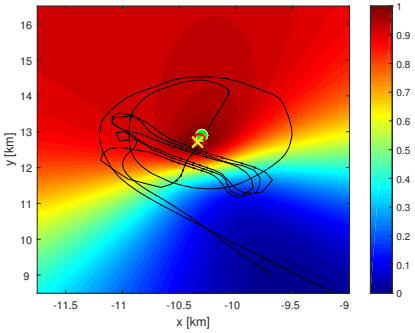

(c) Normalized cost function for S^{4}TDOA (signal threshold -60 dBm).

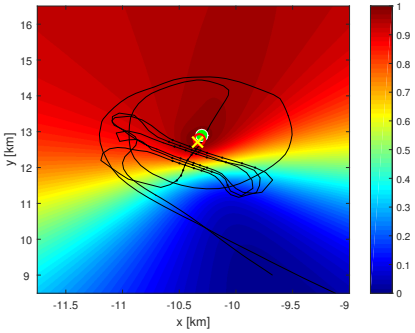

(d) Normalized cost function for DS^{4}TDOA (signal threshold -60 dBm).

Figure 6.6: Comparison of the cost functions of S^{4}TDOA and DS^{4}TDOA for different signal thresholds.

The cost function of the S^{4}TDOA and a received signal strength threshold of $P_\mathrm{t} = -60\,\mathrm{dBm}$ is shown in Fig. 6.6c. Less measurements are used to localize the emitter, but due to the higher signal level, the choice of the peak of the CCF as TOA value tends towards the correct peak. With more accurate TDOA estimation, the localization result becomes more accurate. The cost function using the direct localization method (Fig. 6.6d) is very similar to the afore mentioned, also the localization results are nearly the same.

The localization accuracy for the S^{4}TDOA improves from 1272 m ($P_\mathrm{t} = -74\,\mathrm{dBm}$)

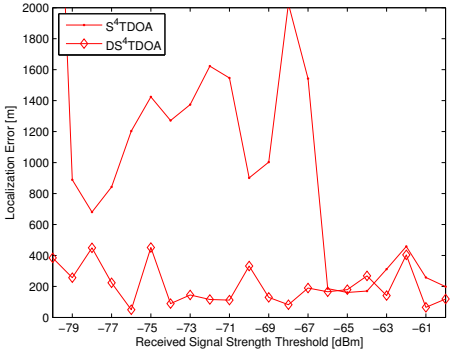

Figure 6.7: Localization accuracy for different received signal strength thresholds of field experiment data. © 2015 IEEE.

to 199 m ($P_\mathrm{t} = -60\,\mathrm{dBm}$). For the DS^{4}TDOA location estimation method, a slight degradation of accuracy from 89 m ($P_\mathrm{t} = -74\,\mathrm{dBm}$) to 119 m ($P_\mathrm{t} = -60\,\mathrm{dBm}$) is noticed.

Fig. 6.7 shows the comparison of the localization errors of both methods over different signal strength levels. It can be observed, that the DS^{4}TDOA method is more robust to smaller received signal strength and outperforms the S^{4}TDOA based method. As the TOA estimation using the signal structure information relies on the amplitude of the signal, with lower SNR, the TOA estimation becomes more and more noisy until peaks that do not correspond to the signal are chosen as TOA. Since the DS^{4}TDOA method does not require choosing one peak of the CCF, the localization results remain more stable for lower signal level values.

6.3.3 Experimental Setup 2

A second field experiment was conducted to demonstrate the feasibility of localizing an emitter using S^{4}TDOA in real-time. A GPS synchronized software defined radio receiver was installed in a car alongside a computer for signal processing and position estimation. A small onmi-directional antenna was mounted on the roof of the car. The observer position is determined using a GPS receiver. Since the installed receiver system has limited processing power, only S^{4}TDOA is used for the TDOA measurements and the localization. The signal processing of the received raw data and the position estimation run in real-time.

A signal generator using an external GPS receiver as 10 MHz frequency standard was deployed. The emitter sends a signal with known repetition structure. The signal is built up by times with transmission $T_{data} = 450\,\mu s$ and guard periods between the transmissions with $T_{guard} = 50\,\mu s$. A chirp signal with a bandwidth of 700 kHz was used. The received signal is digitized by the sensor node. This results in a complex base-band signal with a duration of 1 second for each measurement step with a sample rate of 1 MS/S. The target position is also determined using a GPS receiver for the evaluation of the position estimation.

The sensor processes a measurement each second, resulting in one TOA estimate using S^{4}TDOA. For the evaluation given in this thesis, a measurement rate of 10 s is used for better readability (the ELS processes a measurement each second in real-time), thus discarding 9 out of 10 measurements. 41 measurement steps are evaluated. At each measurement step, we use the full TDOA measurement set obtained by the

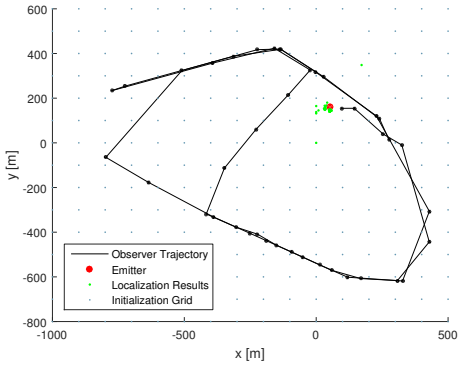

Figure 6.8: Scenario of the 2nd field experiment.

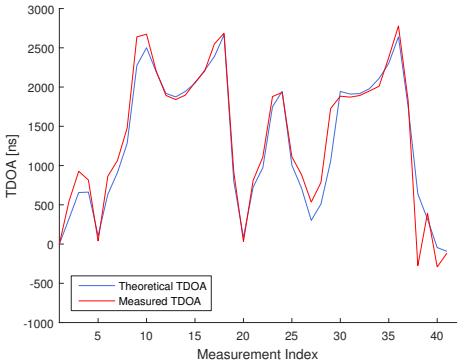

Figure 6.9: Comparison the measured TDOA and the theoretical TDOA given by the observer-target geometry.

current and all previous observation steps (see Eq. 2.7) which results in correlated measurement errors. In contrast to the previous field experiment described in Section 6.3.1, the altitude of the emitter state is assumed to be known.

6.3.4 Results of the 2nd field experiment

The observer trajectory as well as the emitter position are depicted in Fig. 6.8 . The black dots indicate the measurement positions. The same S^4TDOA estimator as described in the previous sections is used with the full TDOA measurement set. The estimator is initialized by evaluating the cost function over a grid of positions in the area of interest ($\mathrm{AOI_x} = -2000, ..., 2000\,\mathrm{m}$, $\mathrm{AOI_y} = -2000, ..., 2000\,\mathrm{m}$). The grid points are depicted by blue dots and were spaced by 100×100 m. The position estimates are plotted as green dots.

The results of the field experiment are compared to the CRLB and to Monte-Carlo simulations. Even though the altitude is assumed to be known, different altitudes still affect the CRLB. A 2×2 FIM for x- and y-coordinates similar as described in Section 2.7.2 is calculated. However, since a 3D scenario with known altitude is considered, the elements of the FIM are slightly different. The known z-value is taken into account in the range between emitter and observer, which is determined based on all three coordinates, and thus influences the CRLB. The covariance matrix of the TDOA measurements remains the same.

The variance of the TDOA measurements is determined by calculating the TDOAs

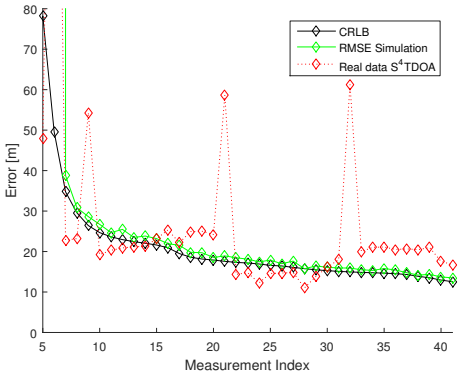

Figure 6.10: Comparison of the localization error of the field experiments, the RMSE of the Monte-Carlo simulation and the CRLB.

that result from the observer-emitter geometry and subtracting the measured TDOAs. The theoretical TDOA given by the geometry and the measured TDOA are depicted in Fig. 6.9. The RMSE of the resulting data yields the standard deviation $\sigma_{\tau_{(M)}}$. We assume equal error induced by each TOA measurement and thus the standard deviation of the TOA measurement is given by $\sigma_{\tau_N} = \sqrt{\sigma^2_{\tau_{(M)}}/2}$.

1000 Monte-Carlo runs are conducted for each observation step. By using the observer and target position, the true TOAs are calculated. To those TOAs, zero-mean Gaussian noise with standard deviation σ_{τ_N} is added. From the resulting TOAs, the TDOA measurement set is determined. The same localization algorithm with the same initialization as for the field experiment data is used. The RMSE over all simulation runs is calculated for each observation step.

The position estimation error of the field experiment data is compared to the results of the Monte-Carlo simulation and the CRLB. Fig. 6.10 depicts the comparison. As can be observed, the Monte-Carlo simulations are close to the CRLB. The localization accuracy of the field experiment data is near the CRLB. After all 41 observation steps, a localization accuracy of 16.8 m could be achieved. The RMSE of the simulations is 13.5 m and the CRLB reads 12.6 m.

6.3.5 Discussion

A large amount of localization error of a real world TDOA system can be caused by time and position inaccuracies of the sensors and by multipath signal propagation.

In our experiments, we used GPS to determine the observers position during the flight. Especially the elevation estimation of a GPS receiver is known to be imprecise. Although we employed GPS disciplined oscillators, the time synchronization error might be the largest cause of the localization error. In the case of stationary observers, a synchronization to UTC in the range of 20 ns is achievable. For in-flight use, the accuracy of the local clock can degrade up to 200 ns. Even though an exact time stamp is not necessary for the (D)S^{4}TDOA$^{(*)}$ methods, the employed experimental system allows only processing of one second of signal each five seconds. If continuous streaming of data is possible, a stable oscillator without exact time information is sufficient (the accuracy issue remains the same). Another real world error lies in the clock accuracy of the emitter which needs to be stable enough for all (D)S^{4}TDOA$^{(*)}$ methods to be applicable. It also has to be mentioned that the emitter position is also determined using a GPS receiver and is therefore also error prone. However, the accuracy can be assumed to be higher, since the emitter is stationary and the position is determined using a longer integration time.

6.4 Comparison to classic localization techniques

Like all passive emitter localization techniques, (D)S^{4}TDOA* clearly has its advantages and drawbacks. The main advantage, namely the possibility to use light weight single sensor hardware, is closely related to the main requirement: All (D)S^{4}TDOA* approaches are only applicable to signals with known repetition intervals which are emitted by a target with a sufficiently stable clock like radars or mobile communication infrastructure. Another key advantage is the very reduced requirement on the communication channel of the observer network compared to classic TDOA based localization where raw signal data has to be transmitted to other sensor nodes or a data fusion center. Like for AOA based localization, only the localization result itself or the measurements (pseudo-TDOA, TOA, AOA) are transmitted to other platforms or a GCS. Similar to all time based localization approaches, precise time synchronization or stable local clocks are required. The combination of TOA/TDOA/(D)S^{4}TDOA* with AOA based localization methods and thus the fusion of these heterogeneous sensor data allows the best coverage and performance as well as position estimates after only a few observation time steps.

(D)S^{4}TDOA* can also be used in a sensor network to distribute pseudo-TDOA/TOA measurements to other sensor nodes or a data fusion center [Ste15]. Only a narrow band communication channel is required. Instead of using measurements taken by a single sensor over time, measurements of multiple sensors taken at the same time step oder over time can be fused into position estimates. When using wide band

communication between multiple observer platforms, a (D)S^{4}TDOA* sensor system can always be used as a classic TDOA sensor node.

6.5 Summary

In this chapter, the evaluation of four (direct) localization approaches for the use with a single moving sensor was presented. The methods are based on the S^{4}TDOA found in [Ste15]. The direct localization solution DS^{4}TDOA firstly introduced in [SO15] is derived in Section 5.4.2. The performance in means of emitter localization accuracy of S^{4}TDOA and DS^{4}TDOA are evaluated in simulations (Section 6.2). Field experiments dealing with the localization of GSM base stations using a single airborne sensor are presented in Section 6.3. A second field experiment using a sensor node installed in a car again confirms the results. Additionally, the two methods (D)S^{4}TDOA* [SO16] that do not require the explicit representation of the signal structure are introduced in Section 5.4.4. All four approaches are evaluated in Monte-Carlo simulations and compared to the CRLB (Section 6.1).

All presented methods allow emitter localization with a light weight and small sensor node. Only one reception channel combined with an omni-directional antenna is needed. The requirements on the communication channel bandwidth between sensor and situation display system are small. Even if the position estimate is not determined at the sensor node but is calculated at a control station on ground, for (D)S^{4}TDOA only a subset of the CCF and corresponding time and position information needs to be transmitted. Classic TDOA approaches require the transmission of raw signal data to a reference sensor or control station, thus having higher demands on the communication channel.

If processing power and storage capacity is not a limiting factor, direct localization using DS^{4}TDOA* is shown in simulations to give the best localization results.

The feasibility of determining the position of an emitter using (D)S^{4}TDOA$^{(*)}$ is shown. The proposed DS^{4}TDOA$^{(*)}$ direct localization is more robust to smaller SNR and outperforms the S^{4}TDOA$^{(*)}$ localization in both simulations and field experiments.

CHAPTER VII

Conclusions and Future Work

This thesis is divided into two key aspects of passive emitter localization using signal structure information. Each topic is separated into theoretical considerations and the evaluation of the presented methods in field experiments, simulations and the comparison to the corresponding Cramér-Rao lower bounds. The introduced novel approaches open new possibilities in passive emitter localization.

7.1 Conclusions

Wide Area Multilateration

The first investigated topic is the passive localization of civil aircrafts to enhance airspace surveillance. In Chapter 3 the basics of ADS-B and SSR are introduced. A novel technique for the estimation of precise TOAs using the known signal modulation of the considered transponder signals is proposed. The introduced method for TOA estimation reduces the communication requirements of the sensor network drastically compared to classic TDOA based localization techniques where the raw signal data needs to be transmitted. Therefore, applying classic TDOA estimation schemes without the use of signal structure information to this use case is not recommendable and would also result in a much higher computational burden at the information fusion center.

The feasibility to localize and track aircrafts using a distributed sensor network is investigated in Chapter 4. Field experiments are described and the evaluation of the obtained data is given. TDOA and TOA based emitter localization with unknown time of signal emission are compared. The localization results are compared to the

position information that aircrafts transmit using ADS-B and to radar data obtained from the RTRN. A good localization performance using TDOA based emitter localization and Kalman filter tracking is observed. As was already suspected, ADS-B position information can be subject to large errors. The use of a multilateration sensor network can close the surveillance gap and enhance air traffic management and high coverage of the area of interest.

(Direct) Localization using a single moving sensor

The second examined topic deals with passive emitter localization using only one small (airborne) observer. TDOA measurements are usually estimated for a signal received simultaneously by two or more sensor nodes. We introduce a novel technique to estimate TDOAs over time using one moving sensor node thus shifting the commonly only spatial into a spatial and temporal problem named single sensor signal structure TDOA S^{4}TDOA method in Chapter 5. It makes use of recurring signal structure that is for example found in mobile communication or radar signals. The direct position determination scheme is applied to S^{4}TDOA. For both non-direct and direct localization, two approaches are introduced.

In Chapter 6, the (D)S^{4}TDOA$^{(*)}$ approaches are evaluated in simulations, field experiments and compared to the CRLB. The feasibility to accurately localize emitters sending signals with recurring structure is shown for all four techniques. These approaches offer the capability to localize emitters using TDOA measurements of only one moving observer. S^{4}TDOA can also be applied in sensor networks where, similar to the first topic, the requirements on the communication channel between sensor nodes and data fusion center can be significantly reduced.

Summary

The contributions of this thesis can be summarized by the following conclusions.

- A novel technique for the TOA estimation of ADS-B/Mode-S transponder signals was derived.
- Algorithms for wide area airspace surveillance based on the previously mentioned TOA estimation were developed and evaluated in a field experiment of high informative value.
- Novel approaches for single sensor TDOA based emitter localization were introduced.

- The known scheme of DPD was extended to single sensor signal structure TDOA.
- The validity of the presented (D)S^{4}TDOA$^{(*)}$ methods was assessed in field experiments and simulations.

7.2 Future Work

Wide Area Multilateration

Deploying a sensor network in the proximity of an airport would be likely to allow safe landing approach under bad weather conditions. If the sensor network is built up around the airport, higher confidence in the position of the aircraft will lead to better airspace security. The detection of aircrafts sending faulty ADS-B position information can also be achieved using only a small number of sensor nodes. The sensor network would not need to estimate the position but only compare the measured TDOAs to the ones resulting from the sensor-emitter geometry derived from received ADS-B messages. Aircrafts with high deviations can thus be detected and the attention of the air traffic controller can be drawn to this particular aircraft to avoid dangerous situations as early as possible.

The compensation of clock offsets and drifts would allow even more accurate TDOA estimation. As was indicated by the results given in Section 4.2, the TDOA measurements tend to be subject to offsets which most probably result from the time synchronization. Since many measurements of different targets are taken almost simultaneously or at least in short time spans, the clock offsets can be estimated. Higher TDOA measurement accuracy could be the outcome.

In the case of GPS loss, the local clocks of the sensor nodes would no longer be synchronized thus also resulting in measurement errors. Using stationary reference transponders at known positions could enable sensor clock synchronization in case of GPS loss.

(Direct) Localization using a single moving sensor

The approach of localizing emitters using only one moving observer was currently strictly focused on TDOA estimation. The movement of the sensor however induces a Doppler shift, which on the one hand decreases the TDOA measurement accuracy and on the other hand carries information on the emitter location. The TDOA measurement accuracy is strongly dependent on the FDOA. Therefore, addressing this

issue would allow for more accurate TDOA estimation and thus more precise position estimation. The fusion of TDOA and FDOA measurements can also improve the localization performance of the ELS.

So far, the signal repetition pattern was assumed to be known. This is valid for some applications like mobile communication. Other use cases with unknown signal repetition pattern require the estimation of the frequency of signal repetition. The approach of single sensor signal structure TDOA can be extended to more applications by estimating the signal repetition pattern alongside with the TDOA/FDOA or in a separate step.

Another problem that can be addressed is the imprecision of the emitters local clock-/oscillator. In many applications, the local clock of the emitter will not be synchronized and will thus underlie a certain drift. Estimating and compensating this drift will result in more precise measurements and better localization performance.

The fusion of heterogeneous sensor data (S4TDOA/FDOA/AOA) either on the same observer platform or using a sensor network can result in better surveillance coverage, higher localization precision and position estimates after fewer observation steps.

CHAPTER VIII

Appendix

8.1 Radarcape Data Format

The data obtained by the Radarcape sensor network is organized as follows. Each sensor node continuously collects data from aircrafts. The received telegrams are stored along with the GPS NMEA (National Marine Electronics Association) information from the sensors GPS receiver on a removable storage device (direct message transmission via TCP/IP is also possible). Using a software developed by Fraunhofer FKIE, this information is stored in two separate files. Every five minutes, new files are generated.

The filenames are composed of the sensor name and the date and time of data reception. The files with the extension `.bin` hold the binary received message data and with the extension `.gps` the corresponding GPGGA (time, position, and fix related data) NMEA strings of the sensors GPS receiver. For example, the file

`radarcape_S0_2015-10-30-1000.bin`

comprises received information recorded by sensor $S0$ on 30th of October 2015 during 10:00-10:05 UTC.

The Radarcape data output format according to [Rada] is:

```
<esc> "1" : 6 byte MLAT timestamp, 1 byte signal
    level, 2 byte Mode-AC
<esc> "2" : 6 byte MLAT timestamp, 1 byte signal
    level, 7 byte Mode-S short frame
```

```
<esc> "3" : 6 byte MLAT timestamp, 1 byte signal
    level, 14 byte Mode-S long frame
<esc> "4" : 6 byte MLAT timestamp, status data, DIP
    switch configuration settings
<esc><esc>: true 0x1a
<esc> is 0x1a, and "1", "2" and "3" are 0x31, 0x32
    and 0x33
```

The first 18 bits of the 6 byte MLAT timestamp give the UTC seconds of the current day since midnight. The bits 19-48 hold the nanoseconds of the current second elapsed since the last 1PPS signal of the GPS receiver.

The data used for the evaluation described in Chapter 4 was recorded by 10 sensor nodes for the duration of one week starting on 29.10.2015, ending on 05.11.2015. Due to technical reasons, one sensor node (S8) only collected data from 29.10.2015 16:45 UTC till 31.10.2015 20:15 UTC.

8.2 The Kalman Filter

In this section, an overview of the Kalman filter that is used for aircraft position tracking is given. More details on Kalman filtering can for example be found in [Koc14, Kay93]. In general, filtering techniques incorporate target observations that were taken at different observation steps. A target state filter makes use of the fact, that for a target state that was observed or given by the state estimate $\mathbf{x}_k$ at time step k, the target state space at an observation step $k+1$ is limited by the targets velocity and acceleration capabilities. The state space of the position estimates is given by $\mathbf{x}$. The measurement at time step k reads $\mathbf{z}_k$. For the tracking algorithm used in Chapter 4, the state space is 6 dimensional with $\mathbf{x} = (x, y, z, \dot{x}, \dot{y}, \dot{z})^T$. The measurements $\mathbf{z}$ are the TDOA localization estimates which are 3 dimensional positions. A standard Kalman filter can thus be used, since the state and measurement space are linear.

The prediction step of the state estimate $\mathbf{x}$ and the state covariance $\mathbf{P}$ is given by

$$\mathbf{x}_{k|k-1} = \mathbf{F}_{k|k-1}\mathbf{x}_{k-1|k-1} \tag{8.1}$$

$$\mathbf{P}_{k|k-1} = \mathbf{F}_{k|k-1}\mathbf{P}_{k-1|k-1}\mathbf{F}^T_{k|k-1} + \mathbf{Q}_{k|k-1}\,. \tag{8.2}$$

The measurement and covariance residuals (innovation) are given by

$$y_k = \mathbf{z}_k - \mathbf{H}_k x_{k|k-1} \tag{8.3}$$
$$\mathbf{S}_{k|k-1} = \mathbf{H}_k \mathbf{P}_{k|k-1} \mathbf{H}_k^T + \mathbf{R}_k \,. \tag{8.4}$$

The Kalman gain matrix is

$$\mathbf{K}_{k|k-1} = \mathbf{P}_{k|k-1} \mathbf{H}_k^T \mathbf{S}_{k|k-1}^{-1} \,. \tag{8.5}$$

$$\mathbf{x}_{k|k} = x_{k|k-1} + \mathbf{K}_{k|k-1} \left(z_k - \mathbf{H}_k \mathbf{x}_{k|k-1} \right) \tag{8.6}$$
$$\mathbf{P}_{k|k} = \left(I - \mathbf{K}_{k|k-1} \mathbf{H}_k \right) \mathbf{P}_{k|k-1} \,. \tag{8.7}$$

The retrodiction of the state estimate and covariance is

$$\mathbf{x}_{l|k} = \mathbf{x}_{l|l} + \mathbf{K}_{l|l+1} (\mathbf{x}_{l+1|k} - \mathbf{x}_{l+1|l}) \tag{8.8}$$
$$\mathbf{P}_{l|k} = \mathbf{P}_{l|l} + \mathbf{K}_{l|l+1} (\mathbf{P}_{l+1|k} - \mathbf{P}_{l+1|l}) \mathbf{K}_{l|l+1}^T \tag{8.9}$$
$$\mathbf{K}_{l|l+1} = \mathbf{P}_{l|l} \mathbf{F}_{l+1|l}^T \mathbf{P}_{l+1|l}^{-1} \,. \tag{8.10}$$

List of Figures

List of Tables

List of Abbreviations

ADS-B ..... Automatic Dependent Surveillance-Broadcast

AGL ..... Above Ground Level

AOA ..... Angle of Arrival

APM ..... Airborne Position Message

ATM ..... Air Traffic Management

CAF ..... Complex Ambiguity Function

CCF ..... Cross Correlation Function

CPR ..... Compact Position Reporting

CRC ..... Cyclic Redundancy Check

CRLB ..... Cramér-Rao Lower Bound

DPD ..... Direction Position Determination

ECEF ..... Earth-Centered Earth-Fixed (Coordinate System)

ELS ..... Emitter Location System

ENU ..... East North Up (Coordinate System)

FDOA ..... Frequency Difference of Arrival

FOA ..... Frequency of Arrival

FIM ..... Fisher Information Matrix

FL ..... Flight Level

FSPL ..... Free Space Path Loss

GCS ..... Ground Control Station

GPS ..... Global Positioning System

ICAO ..... International Civil Aviation Organization

MLAT ..... Multilateration

MSL ..... Mean Sea Level

NLOS ..... Non-Line of Sight

NM ..... Nautical Mile

OCXO ..... Oven Controlled Crystal Oscillator

PET ..... Passive Emitter Tracking

PPM ..... Pulse Position Modulation

PSR ..... Primary Surveillance Radar

LOS ..... Line of Sight

RF ..... Radio Frequency

RMS ..... Root Mean Square

RMSE ..... Root Mean Square Error

RTRN ..... Reference Tracking Radar Network

SNR ..... Signal-to-noise ratio

SSR ..... Secondary Surveillance Radar

TCXO ..... Temperature Compensated Crystal Oscillator

TDOA ..... Time Difference of Arrival

TOA ..... Time of Arrival

UAS ..... Unmanned Aerial System

UTC ..... Coordinated Universal Time

WGS84 ..... World Geodetic System 1984 (Coordinate System)

WSS ..... Wide-sense Stationary

Bibliography

[AOS+15] B. S. Ali, W. Y. Ochieng, W. Schuster, A. Majumdar, and T. K. Chiew. A safety assessment framework for the automatic dependent surveillance broadcast (ADS-B) system. *Safety Science*, 78:91–100, October 2015.

[ASG01] Y. I. Abramovich, N. K. Spencer, and A. Y. Gorokhov. Detection-estimation of more uncorrelated gaussian sources than sensors in nonuniform linear antenna arrays – part i: Fully augmentable arrays. *IEEE Trans. Signal Processing*, 49:959–971, May 2001.

[AW09] A. Amar and A. J. Weiss. Direct geolocation of stationary wideband radio signal based on time delays and doppler shifts. In *Proc. 15th Workshop on Statistical Signal Processing*, pages 101–104, Cardiff, Wales, September 2009.

[Bec92] K. Becker. An efficient method of passive emitter location. *IEEE Trans. Aerosp. Electron. Syst.*, 28:1091–1104, October 1992.

[Bec01] K. Becker. Target Motion Analysis (TMA). In S. Stergioulos, editor, *Advanced Signal Processing Handbook*, chapter 9, pages 284–301. CRC Press, New York, NY, 2001.

[BHB+16] J. Baek, E. Hableel, Y. J. Byon, D. S. Wong, K. Jang, and H. Yeo. How to Protect ADS-B: Confidentiality Framework and Efficient Realization Based on Staged Identity-Based Encryption. *IEEE Transactions on Intelligent Transportation Systems*, (99), August 2016.

[CH94] Y.T. Chan and K.C. Ho. A simple and efficient estimator for hyperbolic location. *Trans. Sig. Proc.*, 42(8):1905–1915, August 1994.

[Coo15] E. Cook. ADS-B, Friend or Foe: ADS-B Message Authentication for

NextGen Aircraft. In *2015 IEEE 17th International Conference on High Performance Computing and Communications (HPCC), 2015 IEEE 7th International Symposium on Cyberspace Safety and Security (CSS), 2015 IEEE 12th International Conference on Embedded Software and Systems (ICESS)*, pages 1256–1261, August 2015.

[DK10] M. Daun and R. Kaune. Gaussian mixture initialization in passive tracking applications. In *Proc. ISIF 13th International Conference on Information Fusion*, Edinburgh, UK, July 2010.

[DM03] A. Daskalakis and P. Martone. A technical assessment of ADS-B and multilateration technology in the Gulf of Mexico. In *Proc. of the 2003 IEEE Radar Conference*, pages 370–378, May 2003.

[DM12] J. P. Delmas and Y. Meurisse. On the cramer rao bound and maximum likelihood in passive time delay estimation for complex signals. In *IEEE International Conference on Acoustics, Speech and Signal Processing (ICASSP)*, pages 3541–3544, March 2012.

[FH08] M. L. Fowler and X. Hu. Signal models for TDOA/FDOA estimation. *IEEE Trans. Aerosp. Electron. Syst.*, 44(4):1543–1550, October 2008.

[Fow00] M. L. Fowler. Exploiting rms time-frequency structure for data compression in emitter location systems. In *Proceedings of the IEEE 2000 National Aerospace and Electronics Conference, NAECON 2000*, pages 227–234, October 2000.

[Fow01] M. L. Fowler. Analysis of single-platform passive emitter location with terrain data. *IEEE Trans. Aerosp. Electron. Syst.*, 37(2):495–507, April 2001.

[Fri84] B. Friedlander. On the cramer- rao bound for time delay and doppler estimation (corresp.). *IEEE Trans. Inform. Theory*, 30(3):575–580, May 1984.

[Fri87] B. Friedlander. A passive localization algorithm and its accuracy analysis. *IEEE Journal of Oceanic Engineering*, 12(1):234–245, January 1987.

[GS08] M. D. Gillette and H. F. Silverman. A Linear Closed-Form Algorithm for Source Localization From Time-Differences of Arrival. In *IEEE Signal Processing Letters*, volume 15, pages 1–4, 2008.

[HC93] K. Ho and Y. Chan. Solution and performance analysis of geolocation by

TDOA. *IEEE Trans. Aerosp. Electron. Syst.*, 29(4):1311–1322, October 1993.

[HLK07] K. C. Ho, X. Lu, and L. Kovavisaruch. Source localization using tdoa and fdoa measurements in the presence of receiver location errors: Analysis and solution. *IEEE Trans. Signal Processing*, 55(2):684–696, February 2007.

[Int13] International Civil Aviation Organisation - South American Regional Office. *Guide on Technical and Operational Considerations for the Implementation of ADS-B in the SAM Region, Version 1.2.* Lima, Peru, May 2013.

[Int14] International Civil Aviation Organisation. *ICAO Annex 10 on the Convention on International Civil Aviation. Aeronautical Telecommunications. Volume IV: Surveillance and Collision Avoidance Systems*, 5th edition, July 2014.

[JNB12] J. Johnson, H. Neufeldt, and J. Beyer. Wide area multilateration and ADS-B proves resilient in Afghanistan. In *Integrated Communications, Navigation and Surveillance Conference (ICNS)*, April 2012.

[Kau12] Regina Kaune. Accuracy Studies for TDOA and TOA Localization. In *Proc. ISIF 15th International Conference on Information Fusion*, Singapore, July 2012.

[Kay93] S. M. Kay. *Fundamentals of statistical signal processing.* Prentice Hall, 1993.

[KC76] C. Knapp and G. Carter. The generalized correlation method for estimation of time delay. *IEEE Trans. Acoust., Speech, Signal Processing*, 24(4):320–327, August 1976.

[KHK11] Regina Kaune, Julian Hörst, and Wolfgang Koch. Accuracy analysis for tdoa localization in sensor networks. In *Proc. ISIF 14th International Conference on Information Fusion*, Chicago, IL, USA, July 2011.

[KMK10] R. Kaune, D. Musicki, and W. Koch. On passive emitter tracking in sensor networks. In C. Thomas, editor, *Sensor Fusion and its Applications*, chapter 13, pages 293–318. InTech, 2010.

[Koc14] W. Koch. *Tracking and Sensor Data Fusion – Methodological Framework and Selected Applications.* Springer, 2014.

[KV13] S. Kay and N. Vankayalapati. Improvement of TDOA position fixing using the likelihood curvature. *IEEE Trans. Signal Processing*, 61(8):1910–1914, April 2013.

[Lee75a] H. B. Lee. Accuracy limitations of hyperbolic multilateration systems. *IEEE Trans. Aerosp. Electron. Syst.*, AES-11(1):16–29, January 1975.

[Lee75b] H. B. Lee. A novel procedure for assessing the accuracy of hyperbolic multilateration systems. *IEEE Trans. Aerosp. Electron. Syst.*, AES-11(1):2–15, January 1975.

[LS15] Y. Lin and S. Saripalli. Sense and avoid for Unmanned Aerial Vehicles using ADS-B. In *2015 IEEE International Conference on Robotics and Automation (ICRA)*, pages 6402–6407, May 2015.

[Lük92] H.D. Lüke. *Korrelationssignale*. Springer, 1992.

[MBK+15a] M. Monteiro, A. Barreto, T. Kacem, J. Carvalho, D. Wijesekera, and P. Costa. Detecting malicious ADS-B broadcasts using wide area multilateration. In *IEEE/AIAA 34th Digital Avionics Systems Conference (DASC)*, October 2015.

[MBK+15b] M. Monteiro, A. Barreto, T. Kacem, D. Wijesekera, and P. Costa. Detecting malicious ADS-B transmitters using a low-bandwidth sensor network. In *18th International Conference On Information Fusion (FUSION)*, pages 1696–1701, Washington, D.C., USA, July 2015.

[Mey16] Lisa Meyer. Passive Emitterlokalisierung zur flächendeckenden Luftraumüberwachung. Master's thesis, Hoschule Trier, Umwelt-Campus Birkenfeld, May 2016.

[MH95] Philip Moser and Patricia Hasenfang. Experimental results of time synchronization between two aircraft using gps. In *Proceedings of the National Technical Meeting "Navigating The 90's: Technology, Applications and Policy"*, 1995.

[MKK10] D. Musicki, R. Kaune, and W. Koch. Mobile Emitter Geolocation and Tracking Using TDOA and FDOA Measurements. *IEEE Trans. Signal Processing*, 58(3):1863–1874, March 2010.

[MQT15] Z. Madadi, F. Quitin, and W. P. Tay. Periodic rf transmitter geolocation using a mobile receiver. In *Proc. IEEE International Conference on*

Acoustics, Speech and Signal Processing (ICASSP), pages 2584–2588, South Brisbane, QLD, Australia, April 2015.

[NAK+16] Y. Nijsure, M. F. A. Ahmed, G. Kaddoum, G. Gagnon, and F. Gagnon. WSN-UAV Monitoring System with Collaborative Beamforming and ADS-B Based Multilateration. In *IEEE 83rd Vehicular Technology Conference (VTC Spring)*, May 2016.

[NKGG16] Y. Nijsure, G. Kaddoum, G. Gagnon, and F. Gagnon;. Adaptive Air-to-Ground Secure Communication System Based on ADS-B and Wide-Area Multilateration. *IEEE Transactions on Vehicular Technology*, 65(5):3150–3165, May 2016.

[NM65] J. A. Nelder and R. Mead. A simplex method for function minimization. *Computer Journal*, 7:308–313, January 1965.

[OBB12] J. Overfield, Z. Biskaduros, and R. M. Buehrer. Geolocation of MIMO signals using the cross ambiguity function and TDOA/FDOA. In *2012 IEEE International Conference on Communications (ICC)*, pages 3648–3653, June 2012.

[Ois09] M. Oispuu. Direct state determination of multiple sources with intermittent emission. In *Proc. 17th European Signal Processing Conference*, pages 1948–1952, Glasgow, Scotland, August 2009.

[OL02] J.R. Ohm and H.D. Lüke. *Signalübertragung*. Springer, 2002.

[ON10] M. Oispuu and U. Nickel. Direct detection and position determination of multiple sources with intermittent emission. *Signal Processing*, 90:3056–3064, December 2010.

[PF11] M. Pourhomayoun and M. L. Fowler. Exploiting cross ambiguity function properties for data compression in emitter location systems. In *45th Annual Conference on Information Sciences and Systems (CISS)*, March 2011.

[PF14] M. Pourhomayoun and M. L. Fowler. Distributed computation for direct position determination emitter location. *IEEE Trans. Aerosp. Electron. Syst.*, 50:2878–2889, October 2014.

[PMH11] K. Pourvoyeur, A. Mathias, and R. Heidger. Investigation of measurement characteristics of MLAT / WAM and ADS-B. In *2011 Tyrrhenian International Workshop on Digital Communications - Enhanced Surveil-*

lance of Aircraft and Vehicles (TIWDC/ESAV), pages 203–206, September 2011.

[PZJ15] S. Poursheikhali and H. Zamiri-Jafarian. Tdoa based target localization in inhomogenous underwater wireless sensor network. In *5th International Conference on Computer and Knowledge Engineering (ICCKE)*, October 2015.

[QMT15] F. Quitin, Z. Madadi, and W. P. Tay. Rf transmitter geolocation based on signal periodicity: Concept and implementation. In *Proc. IEEE International Conference on Communications (ICC)*, pages 4593–4598, London, England, June 2015.

[Qua81] A. Quazi. An overview on the time delay estimate in active and passive systems for target localization. *IEEE Trans. Acoust., Speech, Signal Processing*, 29(3):527–533, June 1981.

[Rada] Radarcape Data Output Format. http://wiki.modesbeast.com/Mode-S_Beast:Data_Output_Formats. Accessed: 2016-03-07.

[Radb] Radio Technical Commisson for Aeronautics. Minimum Operational Performance Standards for 1090MHz Extended Squitter Automatic Dependent Surveillance-Broadcast (ADS-B) and Traffic Information Services-Broadcast (TIS-B), Working Paper 1090-WP30-18 as Draft Version 4.2 of DO-282B.

[RBSS09] C. Reck, U. Berold, J. Schur, and L. P. Schmidt. Direction of arrival sensor calibration based on ADS-B airborne position telegrams. In *European Radar Conference, 2009. EuRAD*, pages 77–80, October 2009.

[Rek14] C. Rekkas. Status of WAM, ADS-B out and ATSAW deployment in Europe. In *2014 Tyrrhenian International Workshop on Digital Communications - Enhanced Surveillance of Aircraft and Vehicles (TIWDC/ESAV)*, September 2014.

[RRJS11] C. Reck, M. S. Reuther, A. Jasch, and L. P. Schmidt. Independent surveillance broadcast - ADS-B receivers with DOA estimation. In *2011 Tyrrhenian International Workshop on Digital Communications - Enhanced Surveillance of Aircraft and Vehicles (TIWDC/ESAV)*, pages 219–222, September 2011.

[SA87] J. Smith and J. Abel. Closed-form least-squares source location estima-

tion from range-difference measurements. *IEEE Transactions on Acoustics, Speech, and Signal Processing*, 35(12):1661–1669, December 1987.

[SG93] S. V. Schell and W. A. Gardner. High-resolution direction finding. In N. K. Bose and C. R. Rao, editors, *Handbook of Statistics, Signal Processing and its Applications*, volume 10, chapter 18, pages 755–817. Elsevier, 1993.

[SHM10] T. Sathyan, M. Hedley, and M. Mallick. An analysis of the error characteristics of two time of arrival localization techniques. In *Proc. ISIF 13th International Conference on Information Fusion*, pages 4593–4598, Edinburgh, UK, July 2010.

[SMV11] A. Soto, P. Merino, and J. Valle. ADS-B integration in the SESAR surface surveillance architecture. In *2011 Tyrrhenian International Workshop on Digital Communications - Enhanced Surveillance of Aircraft and Vehicles (TIWDC/ESAV)*, pages 13–18, September 2011.

[SSL+14] M. Schäfer, M. Strohmeier, V. Lenders, I. Martinovic, and M. Wilhelm. Bringing up OpenSky: A large-scale ADS-B sensor network for research. In *Proc. IPSN-14 of the 13th International Symposium on Information Processing in Sensor Networks*, pages 83–94, April 2014.

[Ste81] S. Stein. Algorithms for ambiguity function processing. *IEEE Trans. Acoust., Speech, Signal Processing*, 29:588–599, June 1981.

[Ste93] S. Stein. Differential delay/doppler ml estimation with unknown signals. *IEEE Trans. Signal Processing*, 41(8):2717–2719, August 1993.

[TBW14] E. Tzoreff, B. Z. Bobrovsky, and A. J. Weiss. Single receiver emitter geolocation based on signal periodicity with oscillator instability. *IEEE Trans. Signal Processing*, 62(6):1377–1385, February 2014.

[Tor84] D. J. Torrieri. Statistical theory of passive location systems. *IEEE Trans. Aerosp. Electron. Syst.*, 20:183–198, March 1984.

[TX15] Z. Tao and T. Xiaoming. High-accuracy radar calibration based on ADS-B. In *IET International Radar Conference*, October 2015.

[UG99] R. Ulman and E. Geraniotis. Wideband tdoa/fdoa processing using summation of short-time caf's. *IEEE Trans. Signal Processing*, 47(12):3193–3200, December 1999.

[VB16] R. M. Vaghefi and R. M. Buehrer. On the crlb of tdoa/fdoa estimation from mimo signals. In *IEEE/ION Position, Location and Navigation Symposium (PLANS)*, pages 772–778, April 2016.

[VGS10] R. M. Vaghefi, M. R. Gholami, and E. G. Ström. Bearing-only target localization with uncertainties in observer position. In *IEEE 21st International Symposium on Personal, Indoor and Mobile Radio Communications Workshops (PIMRC Workshops)*, pages 238–242, September 2010.

[VKD14] N. Vankayalapati, S. Kay, and Q. Ding. TDOA based direct positioning maximum likelihood estimator and the cramer-rao bound. *IEEE Trans. Aerosp. Electron. Syst.*, 50(3):1616–1635, July 2014.

[WA06] A. J. Weiss and A. Amar. Direct position determination of multiple radio transmitters. In S. Chandran, editor, *Advances in Direction-of-Arrival Estimation*, chapter 11, pages 213–239. Artech House, Norwood, MA, 2006.

[Wax82] M. Wax. The joint estimation of differential delay, doppler, and phase (corresp.). *IEEE Trans. Inform. Theory*, 28(5):817–820, September 1982.

[Wei04] A. J. Weiss. Direct position determination of narrowband radio frequency transmitters. *IEEE Signal Processing Lett.*, 11:513–516, May 2004.

[YA11] A. Yeredor and E. Angel. Joint tdoa and fdoa estimation: A conditional bound and its use for optimally weighted localization. *IEEE Trans. Signal Processing*, 59(4):1612–1623, April 2011.

[Yer10] A. Yeredor. A signal-specific bound for joint tdoa and fdoa estimation and its use in combining multiple segments. In *ICASSP*, pages 3874–3877. IEEE, 2010.

[YLX05] G. Yao, Z. Liu, and Y. Xu. Tdoa/fdoa joint estimation in a correlated noise environment. In *IEEE International Symposium on Microwave, Antenna, Propagation and EMC Technologies for Wireless Communications*, pages 831–834, August 2005.

[ZWLZ16] T. Zhang, R. Wu, R. Lai, and Z. Zhang. Probability hypothesis density filter for radar systematic bias estimation aided by ADS-B. *Signal Processing*, 120:280–287, March 2016.

[ZZL15] Y. Zhang, W. Zhang, and H. Long. Application of ADS-B for unmanned aerial systems: Case study and practical approach. In *2015 IEEE 6th International Symposium on Microwave, Antenna, Propagation, and EMC Technologies (MAPE)*, pages 712–716, October 2015.

Own References

[KSR+12] Regina Kaune, Christian Steffes, Sven Rau, Wolfgang Konle, and Jürgen Pagel. Wide Area Multilateration using ADS-B Transponder Signals. In *15th International Conference on Information Fusion*, Singapore, July 2012.

[SKR11] Christian Steffes, Regina Kaune, and Sven Rau. Determining Times of Arrival of Transponder Signals in a Sensor Network using GPS Time Synchronization. In *Informatik 2011 - 6th Workshop Sensor Data Fusion: Trends, Solutions, Applications*, Berlin, Germany, October 2011.

[SM13] Christian Steffes and Lisa Meyer. Evaluation of a TDoA based Acoustic Localization System. In *8th Workshop Sensor Data Fusion: Trends, Solutions, Applications (SDF 2013)*, Bonn, Germany, September 2013.

[SM16] Christian Steffes and Lisa Meyer. Generierung von Multilaterationsdaten für Evaluationszwecke, Wide Area Multilateration using ADS-B Transponder Signals. Internal Project Report, Fraunhofer FKIE, March 2016.

[SO15] Christian Steffes and Marc Oispuu. Direct Single Sensor TDOA Localization Using Signal Structure Information. In *18th International Conference On Information Fusion (FUSION)*, pages 767–773, Washington, D.C., USA, July 2015.

[SO16] Christian Steffes and Marc Oispuu. Direct Position Determination for TDOA-based Single Sensor Localization. *Journal of Advances in Information Fusion*, 11(2):250–261, December 2016.

[SR12a] Christian Steffes and Sven Rau. FDOA Determination of ADS-B

Transponder Signals. In *7th Workshop Sensor Data Fusion: Trends, Solutions, Applications (SDF 2012)*, Bonn, Germany, September 2012.

[SR12b] Christian Steffes and Sven Rau. Multipath Detection in TDOA Localization Scenarios. In *7th Workshop Sensor Data Fusion: Trends, Solutions, Applications (SDF 2012)*, Bonn, Germany, September 2012.

[Ste14] Christian Steffes. Field Experiments for TDoA-based Localization of GSM Base Stations. In *9th Workshop Sensor Data Fusion: Trends, Solutions, Applications (SDF 2014)*, Bonn, Germany, October 2014.

[Ste15] Christian Steffes. Novel TDoA-based Single Sensor Localization Approach Using Signal Structure Information. In *12th Workshop on Positioning, Navigation And Communication (WPNC)*, Dresden, Germany, March 2015.